DEVELOPMENT OF VELOCITY DEPENDENT ICE FLEXURAL FAILURE MODEL AND APPLICATION TO SAFE SPEED METHODOLOGY FOR POLAR SHIPS

By

© Mahmud Sharif Sazidy

A thesis submitted to the School of Graduate Studies

in partial fulfillment of the requirement for the degree of

Doctor of Philosophy

Faculty of Engineering and Applied Science

Memorial University of Newfoundland

April, 2015

St. John's, Newfoundland, Canada

ABSTRACT

The main focus of this research work is to develop a velocity dependent ice flexural failure model through numerical investigation of ship icebreaking process. In addition, the present work involves development of Excel-VBA software using this flexural failure model to determine ice impact load, minimum plate thickness, frame dimensions and safe speed methodology for Polar ships.

First of all, individual material models of ice crushing, ice flexure and water foundation are developed using the FEM software package LS DYNA. Two different material models of ice are used to represent the ice crushing and ice flexure. The input parameters of these ice material models are selected from numerically conducted ice crushing test and four point bending test. The water foundation effect is modeled using a simple linear elastic material. The material models are incorporated into the numerical models of ship icebreaking. Two collision scenarios are considered for the ship icebreaking models; a head-on collision with a flat inclined ship face and a shoulder collision with an R-Class ship. In these models, the rigid ship impacts a cantilever ice wedge. The ice wedge rests on the water surface. Both collision scenarios are investigated with and without considering radial cracks in the level ice.

The ice impact force and wedge breaking length are extracted from these numerical models of ship ice wedge breaking. Results indicate that the ship velocity, normal ship frame angle, ice wedge angle, ice thickness and radial crack significantly affect the breaking process. At higher ship velocities, the bending crack location shifts toward the

ice crushing zone and results in a higher impact force. Higher impact force is produced for thicker ice, higher wedge angle and lower ship normal frame angle at a particular ship velocity. The existence of radial cracks reduces the magnitude of impact force and influences the breaking patterns.

A methodology is presented to estimate the dynamic ice failure load using existing static failure models and dynamic amplification factors. The comparative study with these dynamic failure loads indicates that the developed numerical model results are in good agreement.

A flexural failure model is developed based on validated numerical model results. The model provides velocity dependent force required to break an ice wedge in flexure. The developed model is validated with full scale test data and with non-linear finite element based dynamic bending model results. Application of this model is demonstrated to estimate the limit bow impact load and design ice load parameters.

Finally, the Excel-VBA software “Safe Speed Check for Polar Ships” is developed using the velocity dependent flexural failure model and Polar Rules based limit state equations. This software and the velocity dependent flexural failure model are believed to help in establishing a rational basis for safe speed methodology as well as in improving ship structural standards and assessing ice management capability.

ACKNOWLEDGEMENT

First and foremost, all praise to God, the most gracious and merciful who gave me the opportunity and patience to carry out this research work.

I would like to express my sincerest gratitude to my academic supervisors, Dr. Claude Daley, Dr. Bruce Colbourne and Dr. Amgad Hussein for their invaluable guidance, supervisions and constant encouragement throughout this research work. Working with them was a great learning experience and indeed without their assistance and support, this thesis would not have been completed.

Sincere thanks to Sakib Mahmood, John Dolny, Bruce Quinton and Jungyong Wang for their valuable suggestions and help during this work. I also greatly appreciate the immeasurable co-operation and support from all the members of Sustainable Technology for Polar Ships and Structures (STePS^2) Research Project, Memorial University.

This investigation has been funded by Atlantic Canada Opportunities Agency, Research and Development Corporation (RDC), American Bureau of Shipping (ABS), BMT Fleet Technology, Husky Energy, Rolls-Royce Marine, Samsung Heavy Industries and the National Research Council of Canada. I am grateful to them for their financial support.

I would like to extend my gratitude to my parents, wife, son, sisters and brothers for their inspiration and motivation in my higher study.

TABLE OF CONTENTS

LIST OF TABLES

LIST OF FIGURES

LIST OF SYMBOLS

A_f	Flange area
A_o	Minimum web area
A_n	Nominal contact area
A_w	Web area
AR_i	Load patch aspect ratio
b	Patch load height
C_b	Ship block coefficient
$C_{f,l,v..}$	Empirical parameters
C_m	Ship mid-ship coefficient
C_{pw}	Ship water plane coefficient
CF_c	Crushing class factor
CF_D	Patch class factor
CF_{DIS}	Displacement class factor
D	Ship displacement
E	Young modulus of ice
Ep	Plastic hardening modulus
E_w	Young modulus of water
ex	Exponent in pressure-area relationship
f_a	Shape coefficient
F_c	Ice crushing load
F_{df}	Dynamic ice load in flexural failure

$F_{f/flex}$ Flexural failure load of ice

F_i Bow impact load

F_l Limiting ice failure load

F_n Normal ice impact load

F_{nd} Dynamic normal impact load

F_{vd} Vertical component of dynamic ice load

FN_d Dynamic Froude number

FNs Static Froude number

Fr Froude Number

h Ice thickness

k_v Dynamic factor

k_w Flange factor

KE_e Effective kinetic energy

l Frame span

L_b Breaking length of ice

l_c Characteristic length of ice

M Ship mass

M_e Effective mass

P_{avg} Average contact pressure

P_f Bending failure load in Kashteljan's model

P_{hs} Hydrostatic pressure

P_i Load patch pressure

P_{limit}	Limit load for framing
P_o	Nominal strength of ice
Q_i	Line load
s	Frame spacing
t	Plate thickness
V	Velocity
v_n^{rel}	Relative normal velocity between ship and ice
x	Impact location
Z_p	Plastic modulus
α	Waterline angles
β'	Normal ship frame angles
θ	Wedge angle of ice
ρ	Density of ice
ρ_w	Density of water
ϑ	Vertical deflection of ice wedge
υ	Poisson's ratio
ζ_n	Normal indentation
Ω	Smallest angle between waterline and framing
σ_c	Compressive strength of ice
σ_c^o	Initial compressive strength
σ_f	Flexural strength of ice
σ_{mc}	Compressive mean stress

σ_{mt} Tensile mean stress

σ_t^o Initial tensile strength

σ_y Yield stress

ϵ_f Effective plastic failure strain

ϵ_p Effective plastic strain

Chapter 1

Introduction

1.1 Research Background

The Polar Regions, particularly the Arctic is believed to have vast amount of natural resources. Industries are becoming more interested, and have increased their activities in these regions. However, safe transportation of these resources in the Arctic is still a big challenge. The heavy multi-year ice to thin first year ice poses a great risk to the ships operating in these regions. In addition, these regions contain fish, wildlife and indigenous people. Any accident in these regions could result a great economic loss and do potential harm to the sensitive environment. Therefore, safety and sustainability are crucial for the resource development and marine activities in these regions. Design of Ice Class ships is an essential element in achieving this safety and sustainability. Historically, speed effects have not been incorporated into calculations of structural loading from ice. The flexural failure load model in the current IACS Polar Rules does not consider the velocity effects.

However, there is evidence that the ice failure load is influenced by the ship velocity due to the presence of water foundation and ice inertia. Therefore, the flexural failure load model could be improved to account for the velocity effects. In addition, the effect of ship hull shape and ice condition on the icebreaking process needs to be considered.

At present, the idea of safe ship speed for operations in ice (Safe Speed Criterion) is a topic of high priority at the International Maritime Organization (IMO) and with many classification societies. Implicit in this interest is an understanding that ice loads are speed dependent and that safe speed criteria can be a valuable tool for improving safety as a methodology to provide an operational guidance to the Polar ships for safe navigation through different ice conditions.

The development of a safe speed methodology requires structural limit state analysis and ice impact load prediction that incorporates the effect of speed in the ice loading/failure model. The structural limit state analysis is necessary to evaluate the strength of ship structural components such as plates, frames etc. The IACS Polar Rules has well established procedures and guidelines to determine these structural limit states. The most challenging part of developing a safe speed methodology is a reliable prediction of ice impact load. Physical model tests are of limited value in properly characterizing the local ice impact forces. Model ice is normally aimed at replicating overall ice resistance rather than the local contact pressures and forces. A good numerical or mathematical model can focus on the local contact mechanics and be beneficial for this purpose.

However, development of an ice impact load model is complex. It requires adequate knowledge of ship icebreaking process under dynamic loading conditions. To investigate the ship icebreaking process; ice edge crushing, ice flexural failure and water foundation effects need to be considered. Currently, there are few ice impact force models available that can accurately describe all these aspects.

Proper numerical techniques and material properties of ice and water foundation are important for modeling the ship icebreaking process. The ice is strain rate sensitive, and responds differently in tension and compression. Hence, modeling of ice material is difficult. It requires estimation of several physical and mechanical properties of ice. Individual material properties are needed for the ice crushing and ice flexure behavior. In addition, a material model of water is required to simulate the hydrodynamic force of water foundation.

In level ice flexure, the formation of circumferential crack limits the maximum ice impact force. Modeling of this crack initiation and propagation is difficult, and perhaps computationally expensive. An efficient numerical technique needs to be introduced for this purpose. In addition, the effect of radial cracks need to be considered in the modeling of ship icebreaking.

This research work is intended to develop a velocity dependent ice flexural failure model through the numerical investigation so that the model can be utilized to determine the design ice load parameters, minimum plate thickness, frame dimensions, and safe speed methodology for the Polar ships.

1.2 Research Objectives and Scopes

The primary objective of this research work is to develop a velocity dependent ice flexural failure model in order to improve understanding of the effects of ship speed in the load associated with icebreaking. This can provide a foundation to improve Polar ship design practice and develop a safe speed methodology. Special emphasis is placed on understanding and modeling aspects of the ship icebreaking and ice failure process to accomplish this objective. Influencing factors such as ship velocity, ship hull shape, ice conditions and water foundation are investigated in the present research. The Polar ship structural limit state conditions have been reviewed and analyzed to establish the safe speed methodology for the Polar ships. The objectives and scopes of this work can be categorized as:

- Review fundamental theories and modeling efforts of ship-ice interaction process in order to identify the critical issues which are important to model and investigate the ship icebreaking process.

- Review Polar ship design practice and the current status of safe speed methodology focusing on the bow impact load prediction, design ice load parameter estimation, structural requirements, and safe speed methodology formulation.

- Develop numerical material models for ice crushing, ice flexure and water foundation that incorporate the speed-dependent characteristics, based on independent models of each process.

- Develop a numerical model for the ship icebreaking to predict the ice flexural failure by combining the individual process and material models. Investigate dynamic ice flexural failure load models from existing static or quasi-static ice load models and dynamic factor models. Validate numerical models using dynamic flexural failure model.

- Exercise the new model under various level icebreaking conditions to determine the validity of the model and the assumptions of icebreaking mode. Use the model to study ship velocity, hull shape, ice condition and water foundation effects on the icebreaking process load in two different collision scenarios.

- Formulate a velocity dependent ice flexural failure model based on numerical model results. Validate the model using full scale test data and non-linear finite element based dynamic bending model results.

- Develop improved design ice load parameters, to design optimum plate and frame dimensions, and to analyze the safe speed methodology based on application of the velocity dependent ice flexural failure model.

- Develop a convenient software tool to allow simple estimation of limit bow load, design load parameters, minimum plate thickness, frame dimensions as well as analysis of safe speed methodology for the Polar ships based on the analysis from the velocity dependent ice flexural failure model.

1.3 Thesis Organization

The whole research work is organized in seven chapters. The first chapter addresses the general background, objectives and scopes of the proposed research work.

Chapter 2 presents an overview of the existing literature which contributes to the current research work. This includes review of current understanding in the ice failure and ship-ice interaction process, ship-ice interaction modeling approaches, Polar ship design practice and current status of safe speed criteria. At the end of this chapter, a literature summary is presented to describe the motivation and methodology of this research work.

Chapter 3 addresses the development of material models for the ice crushing, ice flexural failure and water foundation. A brief discussion on ice failure modes and water foundation effect in the ship icebreaking process is also presented.

Chapter 4 presents the numerical models of ship icebreaking process considering two collision scenarios and different breaking conditions. The effect of ship velocity over icebreaking process is investigated for different ship hull shapes and ice conditions. A methodology is also introduced in this chapter to develop the dynamic ice load models of flexural failure from the existing analytical and semi-empirical models. Finally, the numerical model results are validated against the developed dynamic ice load models.

Chapter 5 demonstrates a velocity dependent ice flexural failure model which is developed based on the numerical model results. The model is validated against full scale

test data and non-linear finite element based dynamic bending model results. Application of the model to investigate the ship velocity effect on bow impact load is illustrated with an example Polar ship type (PC 1). A comparative study with respect to the IACS Polar Rules is also presented for this investigation.

Chapter 6 involves the analysis of safe speed methodology for the Polar ships using the velocity dependent flexural failure model. A brief overview on the design ice load model formulation and structural requirements in the Polar Rules is presented. Examples are illustrated for the Polar ships PC 5, PC 6 and PC 7 to determine the limit bow load, design load patch parameters, minimum plate thickness, frame dimensions, and to examine the safe speed capabilities in different ice conditions. Finally, the Excel-VBA software is presented which allows the easy prediction of ice load, investigation of ship velocity effect on ice load, optimum design of plate and frame, and analysis of safe speed methodology for the Polar ships.

Chapter 7 summarizes and concludes the findings and limitations of the present work. This chapter also includes the original contributions of this thesis along with some guidelines for future work.

Chapter 2

Literature Review

2.1 Introduction

Historically, Arctic shipping was mainly limited to summer operation in ice free water or light ice conditions. However increased marine activities in the region and decreasing ice conditions are increasing the likliehood of year-round shipping operations through ice-covered waters. According to the Arctic Council [1], year-round operation in ice-covered water has been maintained since 1978/79 through the Northern Sea Route. The Council reported that approximately 6000 vessels operated in the Arctic during a survey year 2004. More shipping activities are expected in the near future with increasing Arctic natural resource development. However, the presence of ice is a major concern along with other unique challenges for safe ship operation in this region.

The impact force from ice poses a risk to ships operating in the Arctic. A large number of ships are damaged due to impact with ice. These impact events commonly result in denting, deformation or fracture to the ship hull. Kubat and Timco [2] reviewed historical data of ship damage in the Canadian Arctic since 1978 and presented a histogram (Figure 2.1) in 2003 indicating the damage events and damage severity due to impact with the first year ice and multi-year ice. Likhomanov et al. [3] also reported high level of hull structural damages during operation in the Northern Sea Route. Generally, these damage events cause operational delays and lead to economic loss. In addition, the consequence of such damage events is a major threat to the Arctic environment. For example, an oil spill incident due to a ship impact with ice may potentially affect the local people, animals and environment. For this reason, well informed ice capable ship design is essential to ensure safety in Polar waters.

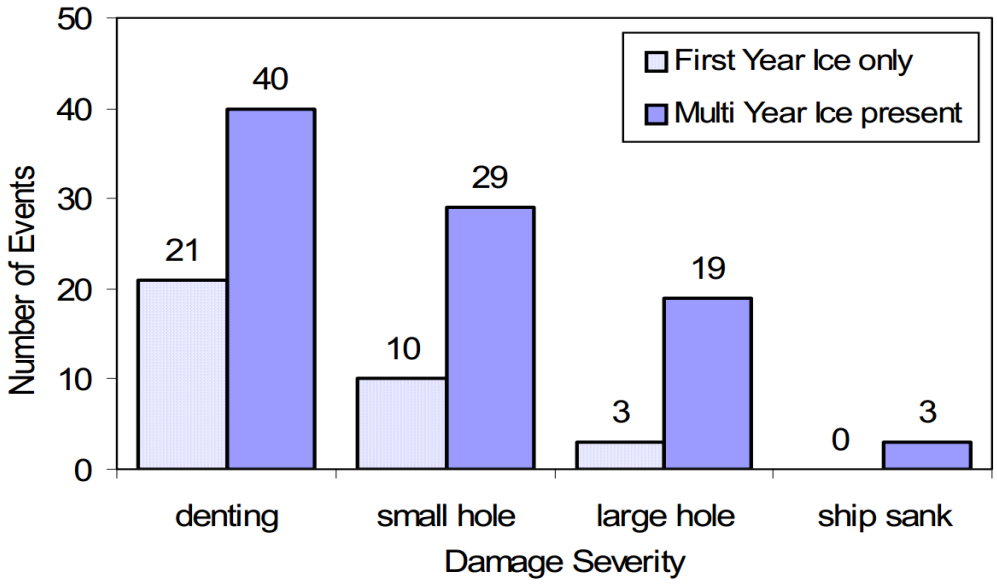

Figure 2.1 Damage events and damage severity in Canadian Arctic [2]

Polar ships or ice capable ships are designed to withstand ice loads without structural failure. Hull structures are locally strengthened against high intensity ice pressure to prevent the structural failure [3]. In general, this design or strengthening process involves the determination of local impact load. This requires a clear understanding of the ship-ice interaction process as well as the local contact mechanism between ship and ice. Understanding the complete ship-ice interaction process is important to estimate the global ice load, and hence to evaluate the overall performance of a ship in ice [4, 5]. On the other hand, the local contact mechanism of ship icebreaking provides the local ice load, and dictates the structural strengthening [4-6]. Therefore, the current understanding of ship-ice interaction process focusing on the local contact mechanisms of ship icebreaking is discussed in Section 2.2.

The International Maritime Organization (IMO), International Association of Classification Societies Ltd. (IACS) and different classification societies have been actively involved in developing rules and guidelines to design Polar ships and other ice capable ships. Among these, the IACS Polar Rules (Polar UR) represent the latest standard for Polar ship design [7]. In the Polar Rules, a glancing collision between the ship and ice wedge is considered the design scenario to determine ice load parameters [7-10]. This idealized glancing collision scenario involves a combination of ice crushing and flexural failure modes [7-11]. The Polar Rules provide two individual ice failure models to represent these ice crushing and ice flexural failure modes. The limiting bow impact load from these two failure models is used to formulate the design ice load model [7, 9-

11]. The ice crushing failure model has been widely utilized to investigate the ship-ice interaction at thicker ice or slow ship velocity operation [7, 12]. On the other hand, the ice flexural failure model is a simple function of hull shape and ice conditions [7, 8, 10-12]. Many researchers have pointed out that the Polar Rules based flexural failure model ignores any velocity effects [7, 12]. Several studies indicate that ice inertia and the effect of the water foundation make the ice flexural failure process strongly velocity dependent [12-14]. This makes it difficult to extrapolate the PC design process to the cases of thinner ice and higher ship velocity interaction. Surprisingly, few research studies have been performed to improve this flexural failure model. For this reason, the present study is focused on exploring the velocity dependency of ice flexural failure during the ship-ice interaction. At present, analytical and numerical models are commonly utilized to investigate this velocity dependency of ice flexural failure. A brief literature review is presented in Section 2.3 to identify different modeling related issues to study the ship-ice interaction process and velocity dependency of ice flexural failure.

The IACS Polar UR Rules provide a methodology to estimate the bow impact load [9, 10]. This impact load cannot be applied directly to the hull structure to evaluate the structural strength [7, 8, 11]. The Polar Rules have specific formulas to transform this bow impact load into a rectangular load patch which can be applied to the structure [7]. In addition, the Polar Rules contain limit state equations for ship plating and framing. Both the load patch formulation and limit state equations are important for the Polar ship design. Therefore, an overview on the Polar ship design practice is given in Section 2.4.

A Polar ship design or ice capable ship design does not ensure the safe ship operation in the Arctic. Hull damage may take place in an ice class ship due to an accidental event or an extreme operational condition [15, 16]. Figures 2.2a and 2.2b are the indication of such damages to the ice class ships operated in the Arctic.

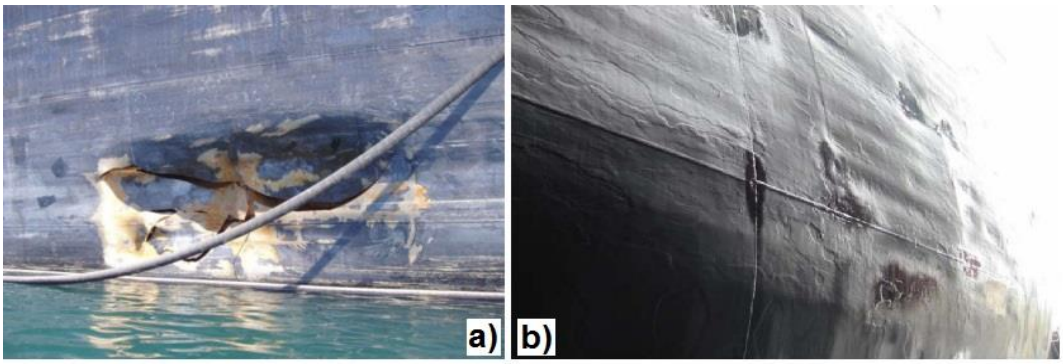

Figure 2.2 Ice class ship damage a) Side damage of a tanker operated in Iqaluit, Nunavut in 2004 [15]; b) Dents in the bow area of a chemical tanker operated in Arctic Waters [17]

Abraham [16] mentioned that the ice load acting on an Arctic ship is not constant and may exceed the design limit. Ship velocity or interaction velocity greatly influences this ice load [3]. For example, the peak ice load on a ship for a particular ice condition may not be the same for slow velocity interaction and high velocity interaction. For the same ship and ice condition, the slow velocity operation may be safe whereas the high velocity operation may be unsafe. This implies that safe operation in the Arctic can be controlled by regulating the ship velocity [7, 12]. A safe speed methodology can be an effective way to regulate ship velocity in different ice conditions [7, 12]. Researchers and scientists utilize several approaches and techniques to develop the safe speed methodology. Some of these approaches and techniques are discussed in Section 2.5.

Based on the above discussion, the following four topics are identified as important in developing a velocity dependent ice flexural failure model and safe speed methodology for Polar ships:

- Fundamentals of ship-ice interaction (Section 2.2)
- Modeling efforts in ship-ice interaction (Section 2.3)
- Polar ship design practice (Section 2.4)
- Current status of safe speed methodology (Section 2.5)

Finally in Section 2.6, key information from the above topics is extracted and summarized to explain the motivation and methodology of the present work.

2.2 Fundamentals of Ship-Ice Interaction

Designing an ice capable ship or developing a safe speed methodology for Polar ships requires a clear understanding of the ship-ice interaction process. Significant effort has been made to explore this complicated process [13, 14, 18]. Ship-ice interaction is a complex process which involves several mechanisms and phases. Most studies idealize these mechanisms and phases, and study each individually for complete understanding of the interaction process. A schematic diagram of ship-ice interaction process is presented in Figure 2.3 to illustrate these phases and mechanisms. In general, a localized interaction process involves the breaking of an ice piece, rotation of the ice piece and sliding of the ice piece etc. [13, 18-20].

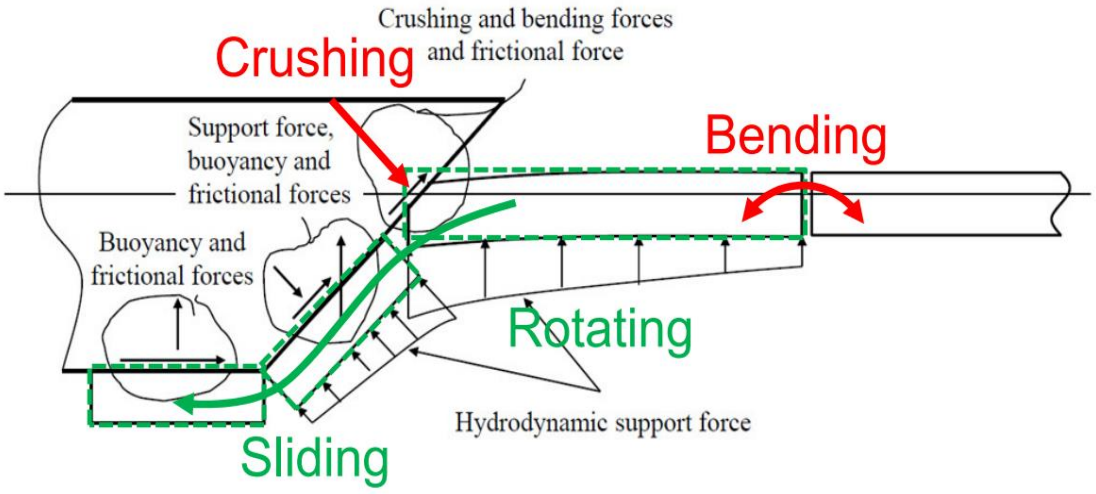

Figure 2.3 Fundamental of ship-ice interaction indicating several mechanisms [19, 20]

The breaking phase initiates when the ship interacts with a part of the level ice sheet and breaks off an ice piece. This breaking phase is associated with deformation, crushing, bending and fracture of ice. In a second phase, the broken ice piece is rotated or turned until it is parallel to the ship hull [18]. Finally, the rotated ice piece slides along the hull and clears out from the ship path. Detailed description of the interaction process can be found in Liu [21], Aksens [18], Daley and Colbourne [6] and Su et al. [14].

During ship-ice interaction, ice loads acting on the ship can be categorized as global ice load and local ice load as shown in Figure 2.4. Each and every individual local ice interaction mechanism contributes to the global ice load. Individual phases of the interaction process provide the local ice loads. Several approaches and approximations are made to determine the global ice load and local ice load. In general, local load

components from individual phases and mechanisms are integrated to obtain the global ice load and ice resistance. Su et al. [14] presented an idealized time history of the ice force from each mechanism, and provided definition of the ice resistance or global ice force as shown in Figure 2.5.

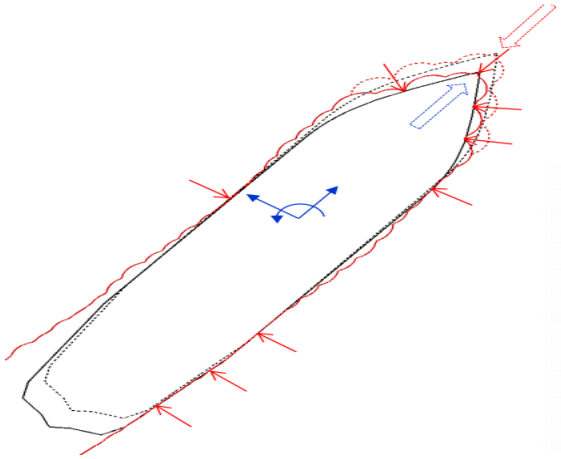

Figure 2.4 Local and global ice force on ice going ships [19]

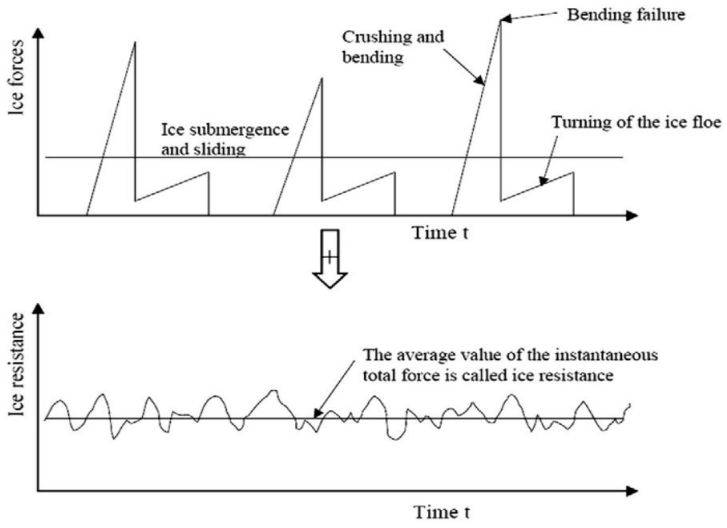

Figure 2.5 Ice force time history along with ice resistance [14]

The above figure indicates that the local ice load reaches at a maximum value in the breaking phase when the ice fails in flexure or bending. Similarly the global load fluctuates as the sum and average of the local loads rise and fall. Thus both the local and global maximum ice load is higher than the corresponding average value. The ice resistance and global ice load are important for evaluating the overall performance of ship in ice but do not generally pose structural risk [4, 12]. Structural risk arises from the local peak loads. Therefore, it is essential to investigate the local contact mechanism involved in the ship icebreaking phase to predict this peak load.

Most of the existing literature focuses on the determination of the resistance force and the maneuvering forces [13, 14, 18, 20-25]. In those cases, only the critical information is extracted which is relevant to the icebreaking phase. The following discussions will focus on the icebreaking pattern during ship-ice interaction.

During the ship-ice interaction, the resulting icebreaking pattern is irregular and difficult to predict [21]. According to Liu [21], non-uniformity of the mechanical properties of ice is the main reason for this irregular behavior. Significant effort has been made to study this irregular icebreaking pattern through model tests and field trials. Figure 2.6 is the example of such icebreaking patterns from model tests and field trials. The figure indicates the formation of several ice wedges. These ice wedges are the result of radial and circumferential cracks in the ice sheet. Several factors such as ship geometry, ship velocity, and ice condition affect this crack initiation and propagation process, and hence influence the icebreaking pattern. Myland and Ehlers [26] have investigated the effect of

such influencing factors. Figures 2.7 to 2.9 indicate how ship velocity, ship hull shape and ice condition affect the icebreaking pattern.

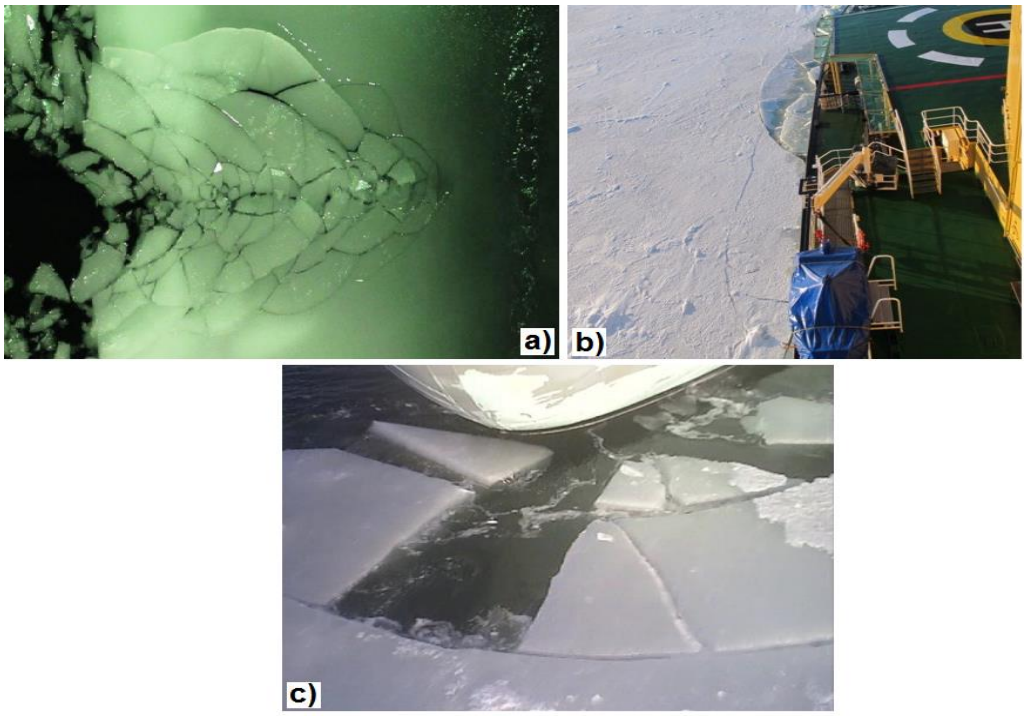

Figure 2.6 Icebreaking pattern from a) Model test in Aalto ice tank [27]; b) Field observation of YMER [27, 28] and c) Field observation of KV Svalbard [13]

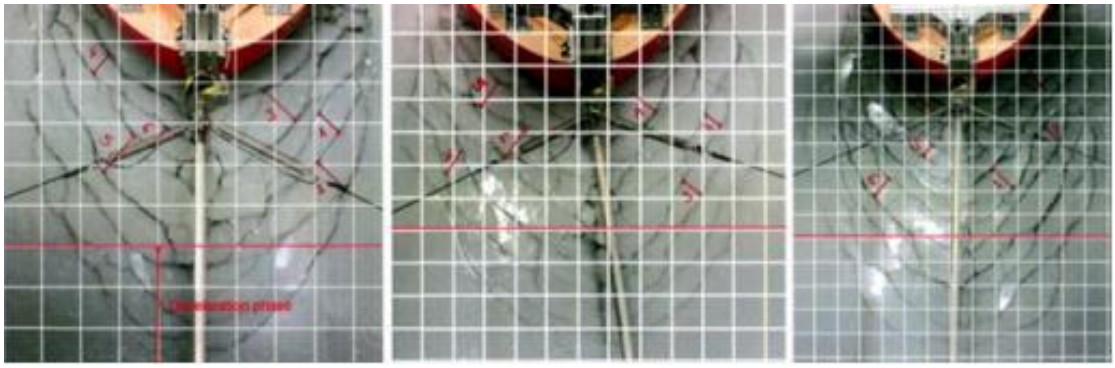

Figure 2.7 Icebreaking pattern at three different ship speed [26]

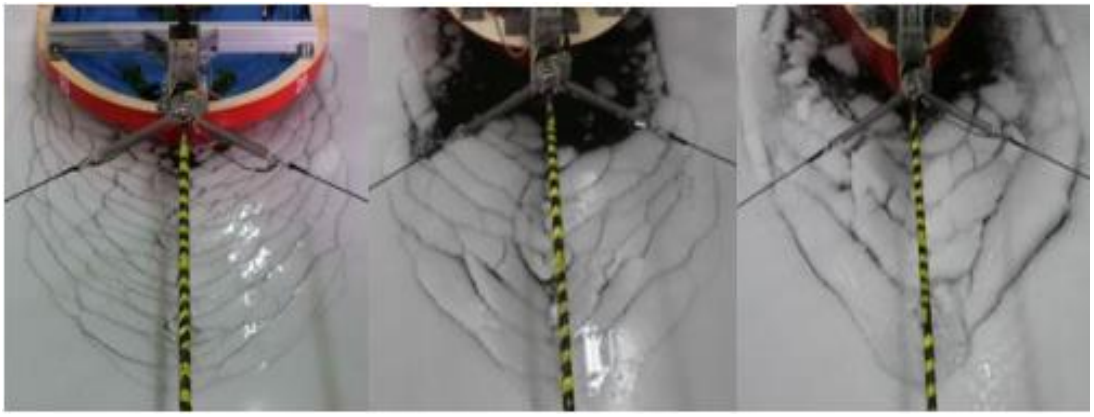

Figure 2.8 Icebreaking pattern from three different ship models indicating effect of hull shape [26]

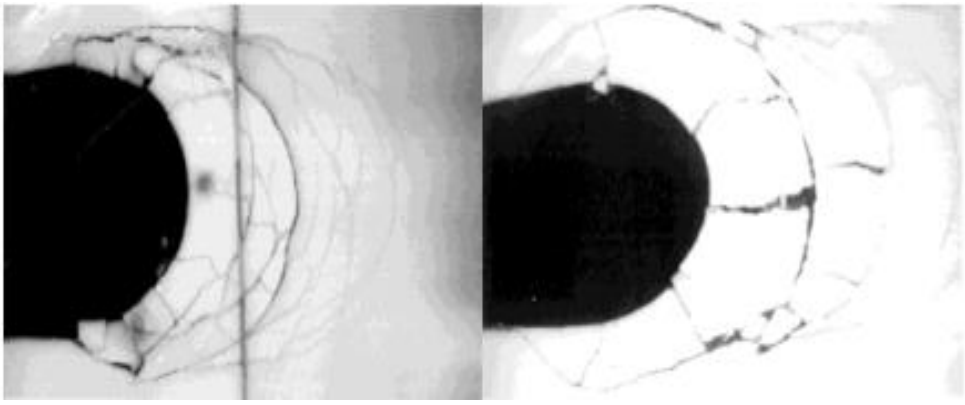

Figure 2.9 Icebreaking pattern in thin ice (left) and thick ice (right) [26]

The above study and observation are not sufficient to characterize the icebreaking process. Liu [21] mentioned that there is no universally accepted icebreaking model available due to the complexity involved in the process. However, many researchers idealize the icebreaking process based on field observation or model scale tests. Some of the idealized icebreaking patterns are shown in Figure 2.10.

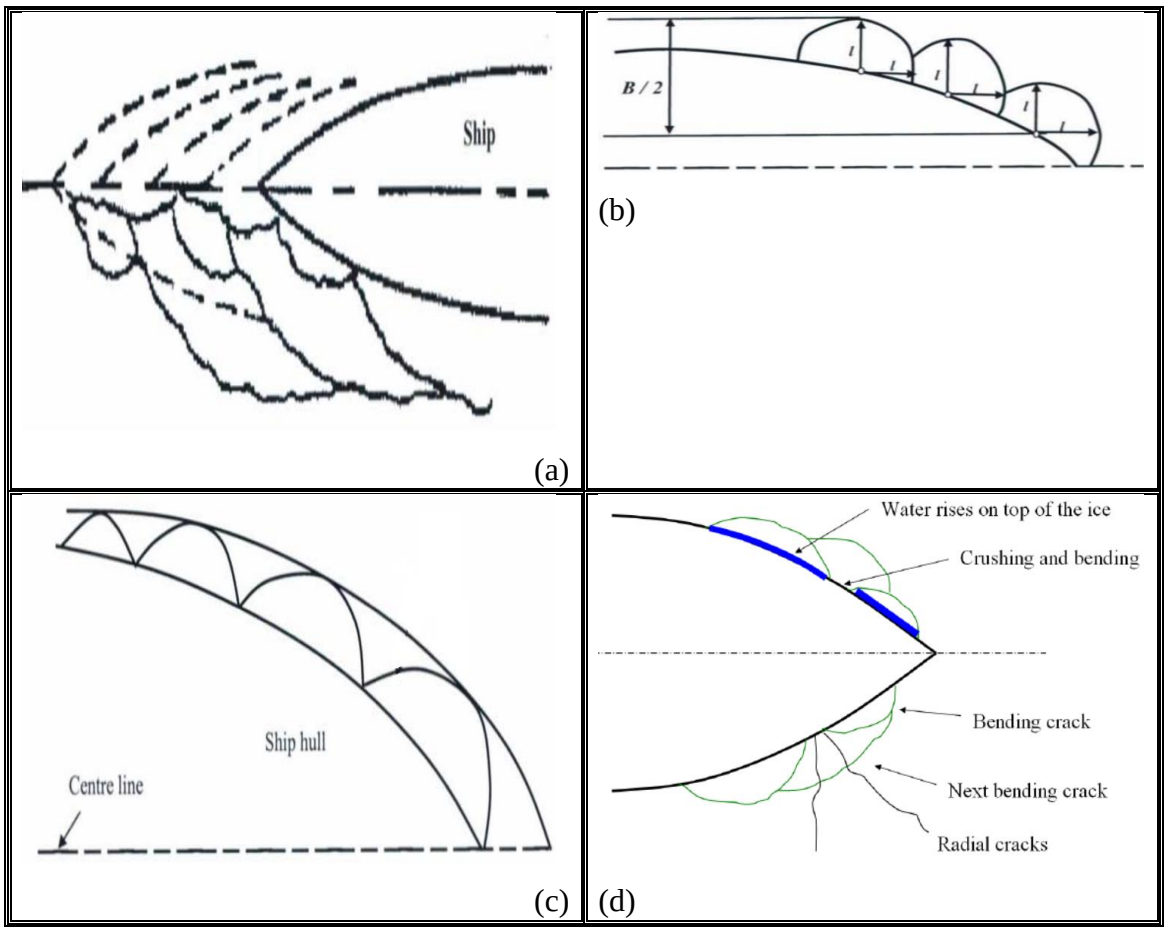

Figure 2.10 Different icebreaking patterns idealized by a) Kashteljan [29]; b) Enkvist [29]; c) Kotras [31] and d) Riska [20]

The above idealized breaking patterns are the indication of ice wedge formation as well. Lu et al. [33] mentioned that the radial cracks appear first and separate the ice sheet into several wedges during the ship-ice interaction. The ice wedges finally fail circumferentially in flexure. According to Lubbad and Loset [13], 3 to 5 ice wedges form during this interaction process. Therefore, many researchers have investigated the breaking process of simple ice wedge instead of full ice sheet [13, 33-35].

Simple ship ice wedge breaking analysis is sufficient to extract the local contact force. This type of analysis is simple but provides information regarding the local contact mechanism. In the IACS Polar Rules, the design ice load parameters are also estimated based on the ship and ice wedge (150 deg) breaking [7-9, 12]. It is important to consider both the ice edge crushing and ice flexural behavior in the ice wedge breaking analysis. Daley and Colbourne [6] mentioned that the ice edge must first be crushed in order to develop enough force to achieve this flexural failure. The influence of edge crushing on the ice load is illustrated in Figure 2.11. Without edge crushing the magnitude of maximum ice force may not be changed but it will influence the load duration and average force value [6]. Perhaps, the edge crushing can be ignored in the analytical or mathematical analysis if appropriate idealizations and assumptions are made. For example, Aksnes [18] assumed that the ice sheet bent and deflected until the flexural failure occurred for an analytical model of moored ship and ice interaction. Crushing was not considered in that model. However, the edge crushing needs to be considered for physical or numerical modeling in order to simulate the proper bending response. Su et al. [14] and Tan et al. [28] emphasized on the importance of considering edge crushing in the ship-ice interaction modeling.

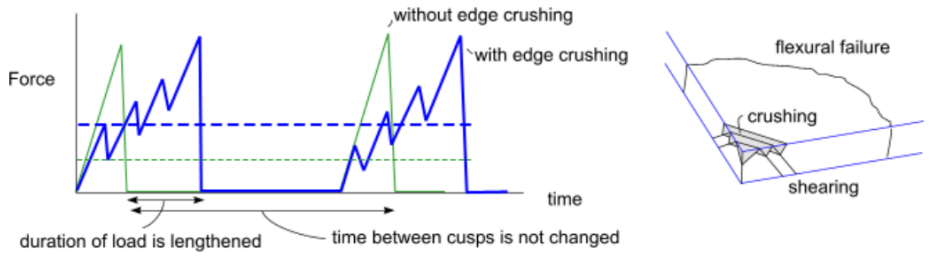

Figure 2.11 Influence of edge crushing on icebreaking process [6, 36]

In the ship ice wedge breaking analysis, impact force and wedge breaking length are evaluated to achieve the proper bending response. This impact force and breaking length strongly depend on the hull geometry, ice conditions, ship velocity and the presence of the elastic water foundation [13, 18, 26, 36]. For low velocity interactions, such as a moored ship or an offshore structure, the velocity effect or dynamic effect can be neglected [13, 18]. However, both the velocity and water foundation effects are significant for a ship with normal or high operating velocity. Daley and Colbourne [6] explained the velocity dependency of icebreaking process. The ice wedge is accelerated and the hydrodynamic force from the water foundation is changed, as the ship advances. Figure 2.12 indicates a velocity dependency in the icebreaking process due to the water foundation and ice inertia.

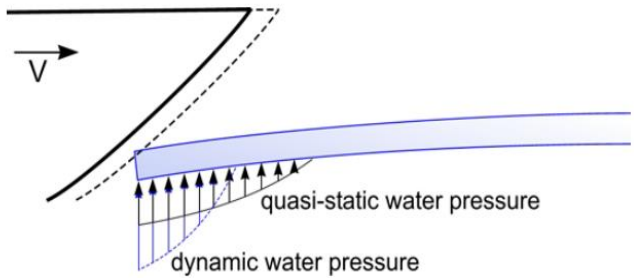

Figure 2.12 Influence of ship velocity and water foundation on icebreaking process [6]

2.3 Modeling Efforts in Ship-Ice Interaction

Model scale and full scale tests are thought to be the most accurate and acceptable methods for investigating the ship-ice interaction process. These provide useful information about the phenomena observed during ship-ice interaction [37]. The major

challenge of model and full scale tests is that they cannot explain all the complexities involved in the interaction process. Moreover, model scale tests are expensive and imperfect, while full scale tests are even more expensive and uncontrolled [6]. Nowadays, numerical modeling is preferred over the model and full scale tests to investigate the ship-ice interaction process. Numerical modeling is cost-effective and provides detailed information that cannot be obtained from those tests, for example pressure distribution, stress states etc. [5, 37].

Ship-ice interaction models can be studied analytically or numerically. These models are developed based on the observation of ship-ice interaction process and ice failure process [38]. Different characterizations and idealizations of the processes have been made in the recent past to obtain a reliable ship-ice interaction model, yet no universally accepted analytical or numerical model is found in the literature [39]. This is due to the complexities associated with the ship-ice interaction and uncertainties involved in the ice failure process [39, 40].

In this study, the considered ship-ice interaction models are categorized based on their formulation methods. The first category includes models based on analytical or semi-empirical approaches. The second category consists of models with advanced numerical techniques such as Finite Element Method (FEM), Discrete Element Method (DEM), Cohesive Element Method (CEM) etc. Discussions on each and individual modeling aspect of both categories are out of scope for the present study. General discussions on

existing models are presented in Sub-sections 2.3.1 and 2.3.2. However, the following critical areas are emphasized:

- Contact between ship and ice, pressure-area relationship
- Interaction between ice and water foundation
- Icebreaking pattern, breaking force and breaking length
- Ice behavior and failure process
- Influencing parameters of ship icebreaking process
- Dynamic effect of ice inertia and water foundation
- Modeling techniques and approaches
- Material models of ice and water foundation

2.3.1 Models using Analytical/Semi-Empirical Approaches

Modeling of the ship-ice interaction or ice-structure interaction is not new. According to Jones [41], the first scientific article on icebreakers was published by Runeberg [42] in 1888/89, which was the only published article in 19th Century. The article provided several expressions for continuous icebreaking to calculate the vertical pressure at the bow, the broken ice thickness and total elevation at the fore-end. Runeberg's [42] work recognized the importance of hull-ice friction effect on the ice resistance and stem angle effect on the bow. The work suggested that the vertical force component should be as large as possible to break the ice. This is still maintained in modern icebreaker design by sloping the bow at the waterline [41].

The vast majority of the work on ship performance in ice has been carried out since the 1960s. In 1968, Kashteljan et al. [29] analyzed the details of level ice resistance [21, 29, 41]. In their analysis, the total ice resistance was divided into four components; resistance due to icebreaking, resistance due to forces related with submersion of broken ice, turning of broken ice, change in position of icebreaker and dry friction, resistance due to passage through broken ice, and resistance due to water friction and wave making [29, 41]. Kashteljan's work established a platform based on dividing the problem into mechnasms or components for further research on different aspects of ship ice resistance and ship-ice interaction process.

The strategy of Kashteljan et al. [29] has been followed by many researchers in which the total resistance force is a summation of several force components. In most of these cases, individual phases and mechanisms of the ship-ice interaction process are investigated separately and incorporated into a final resistance formula. For example, Lewis and Edwards [43] gave an ice resistance formula in 1970 through detailed analysis of full-scale and model scale data for the icebreaker Wind-class, Raritan, M-9 and M-15. The formula consisted of individual force components to represent the icebreaking and friction, ice buoyancy, and momentum change between the ship and broken ice [41]. In the same year, White [44] provided a purely analytical method to investigate the bow performance in continuous icebreaking, ramming and testing extraction ability. Based on this investigation, a blunter bow form was recommended for the Polar ship which was used in the design of the MV Manhattan for its operation in the Arctic [41]. Later in

1972, Enkvist [30] made a significant contribution in the literature of ship-ice interaction. A semi-empirical ice resistance formula was derived from the combination of analytical analysis, non-dimensional analysis, model scale test and limited full scale test data [30, 41]. The velocity dependent term and the ice submergence term in the formula were isolated through model tests and pre-sawn tests, respectively [41].

In 1973, Milano [45] provided a purely analytical model to evaluate the ice resistance based on energy needed for a ship to move through the level ice [41]. Milano [45] also followed a non-dimensional approach, similar to Lewis and Edwards [43], to develop a design chart which was further utilized to predict the total ice resistance for different icebreakers.

One of the earliest ice interaction models is the Kheisin's extrusion model [46]. The model was developed in 1975 based on a drop test of steel ball on ice cover. The concept of pulverized layer formation at the ice-sphere contact interface was introduced into the model (Figure 2.13). The pulverized layer of uniform thickness must have to be extruded when the ice is crushed. The pulverized layer thickness was assumed as proportional to the local pressure. This assumption enabled the model to predict the ice pressure, ice force and indenter velocity which were unmeasurable previously [6, 38]. This simplified model has been used as a crushing model for many years [6]. The model cannot explain all the aspects of the interaction process.

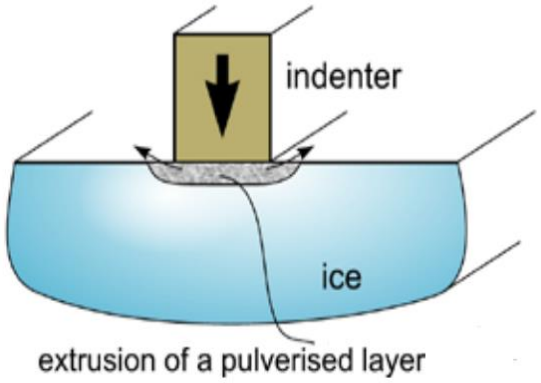

Figure 2.13 Kheisin extrusion model for ice-sphere interaction [6, 46]

In 1983, Varsta [47] adopted Kheisin's extrusion model into his ice load model to explain the wet contact between the ship and ice [38]. For the dry contact, Varsta [47] developed a new model using the finite element analysis and the Tsa-Wu failure criteria [38].

In 1989, Lindqvist's [36] ice resistance model considered three individual mechanisms; ice crushing at the stem, ice bending over the whole bow and ice submergence along the ship hull [6, 21]. The force components from each individual mechanism were derived analytically. These force components were combined to obtain the total ice resistance on a ship. This model also accounted for the velocity effect on the ice resistance through empirical formulas. According to Liu [21], these empirical formulas are over simplified and need further refinement. Nevertheless, the model is helpful to understand the interaction process, and can be useful in the early ship design process. The Lindqvist's model has been used to predict the ice resistance for several icebreakers such as Jelppari, Otso, Vladivostok, Mergus, Ware, Valpas and Silma etc. [21].

The early models mentioned above are purely analytical or semi-empirical, and are applicable to either static problems or simple contact geometry cases. Most of these models may not capture the entire phenomenon of ship-ice interaction process, yet each has a contribution to the current state of interaction modeling practice. Some of these models are still being used. For example, Valanto [48] utilized Lindqvist's [36] semi-empirical model for the underwater components, and combined it with a 3D numerical model of ship icebreaking for the prediction of ice resistance. A number of numerical models were developed in the recent past using these analytical or semi-empirical approaches for the real time simulation of continuous ship icebreaking. Most of these models utilize the analytical or semi-empirical formulas which were numerically integrated [13, 14, 21]. Liu's [21, 49] ice-hull interaction model is an example of this approach for the real-time simulation of ship maneuvering in level ice. Liu [21, 49] utilized Kotras's [31] idealized icebreaking pattern mentioned in Figure 2.10c to determine the depth and width of ice cusps. The model consisted of breaking, buoyancy and clearing phases. The breaking phase was comprised of ice crushing and bending failure. In ice crushing failure, the impact load (F_n) normal to the contact interface was related to the compressive strength (σ_c) of ice and the nominal contact area (A_n) with the following formula:

$$F_n = \sigma_c A_n \tag{2.1}$$

This crushing formula had been widely utilized in many crushing related studies [14, 24, 27, 28]. In Liu's model, the compressive strength or pressure was assumed as constant

over the contact area, which is a simplification of the real case. There is much evidence that the pressure changes with the contact area, and significantly affects the crushing force component [4, 50].

The bending failure load (P_f) was calculated using Kashteljan's semi-empirical formula given in Kerr [51]. The formula was based on the bearing capacity of a floating ice sheet subjected to the static or quasi-static load. This failure load was expressed as a simple function of the ice flexural strength (σ_f), ice wedge angle (θ) and ice thickness (h) as shown below:

$$P_f = C_f \left(\frac{\theta}{\pi}\right)^2 \sigma_f h \tag{2.2}$$

The empirical parameter (C_f) in the equation can be tuned to match experimental results. This bending formula does not account for any dynamic effect in the interaction, and is suited for the static loading conditions only. Additionally, it does not incorporate information regarding the hull geometry effect on the bending load. However, this bending model is commonly used by many researchers because few alternative bending formulas [5, 14, 24, 27, 28, 52] are available.

Lubbad and Loset [13] developed another numerical model for real time simulation of ship-ice interaction. Equations of motion for a rigid ship in three degree of freedom (DOF) were integrated over time. The ice was assumed a homogeneous, isotropic elastic-brittle material. Their work included investigation of radial crack initiation as well as the

circumferential crack formation. For anticipating the radial crack initiation, a closed form analytical solution of bending stress was derived based on the idealized semi-infinite plate resting on an elastic foundation which was subjected to a uniformly distributed load. This idealized semi-infinite plate was replaced with the adjacent wedge-shaped ice beam to predict the wedge failure and the formation of the circumferential crack. Nevel [60] provided power series solution was used for this prediction. Figure 2.14 indicates these two idealizations of an ice sheet resting on a water foundation.

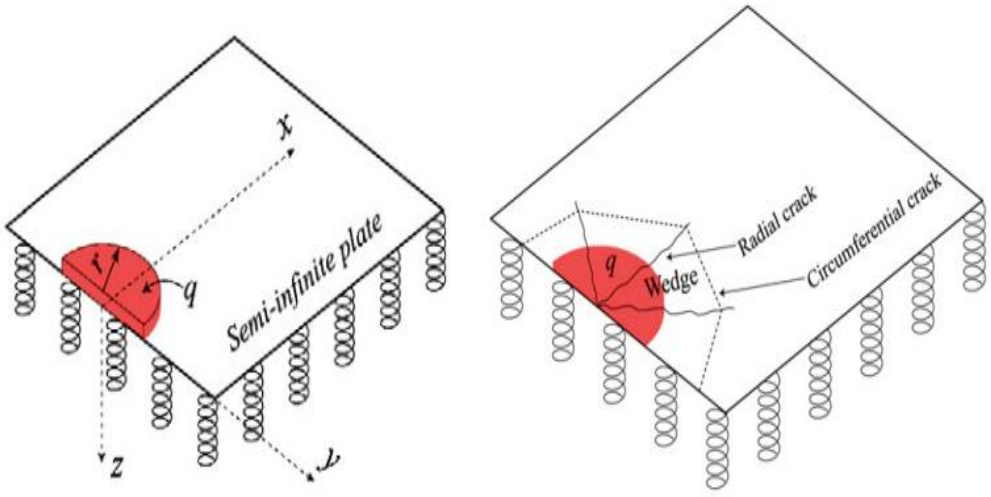

Figure 2.14 Idealized level ice sheet on elastic foundation [13] a) semi-infinite plate for radial crack initiation and b) adjacent wedge-shaped beam for circumferential crack formation

Lubbad and Loset's [13] model ignored the edge crushing and considered only the bending failure for icebreaking phase. The authors discussed the dynamic effect of ice inertia and water foundation on the breaking force and the breaking length. However, the dynamic effect was not considered in the model.

Sawamura et al. [5] developed a numerical model for the repetitive ship icebreaking pattern. The model considered the breaking phase, consisting of crushing and bending of an ice beam as shown in Figure 2.15. The model ignored the rotation and sliding phases as these are not important for the breaking force estimation. A circular contact detection technique was applied to determine the contact point between the ship and ice edge (Figure 2.16). The crushing formula given in Eq. (2.1) was used in the model. The compressive strength was constant in the model. The model adopted two different contact areas based on the crushing edge geometry as shown in Figure 2.17. The triangular contact area was generated because of the crushing on the top corner of the ice edge. Whereas, a rectangular contact area resulted when the crushing reached the bottom corner of the ice edge. Sawamura et al. [5] derived contact area formulas based on these contact geometries. Later Sawamura et al. [35] adopted FEM results from the fluid-ice interaction analysis into the model to represent the dynamic bending failure of ice sheet. The fluid-ice interaction analysis assumed that the bending failure occurs when the maximum bending stress exceeds the flexural strength of ice.

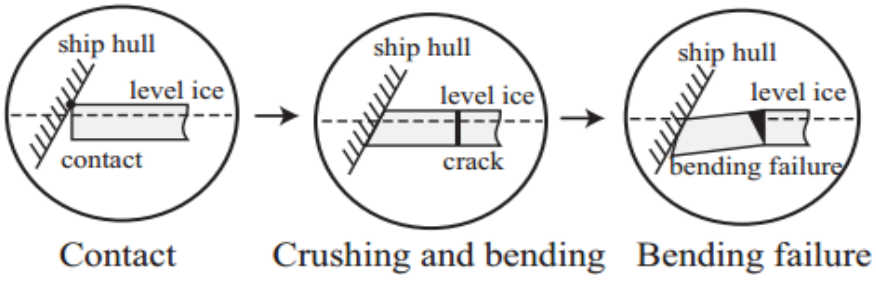

Figure 2.15 Breaking phase in ship icebreaking model [5]

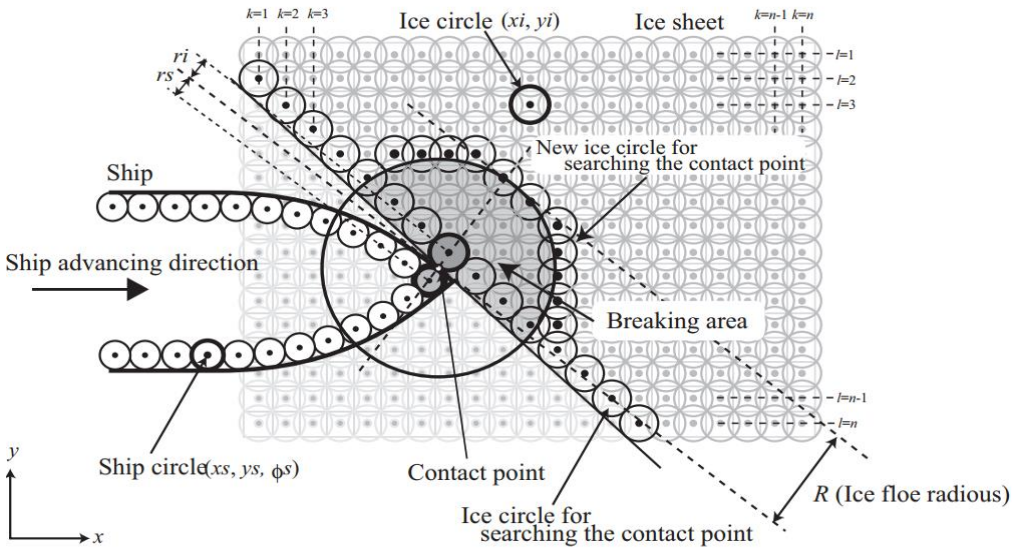

Figure 2.16 Circular contact detection technique in Sawamura's models [5]

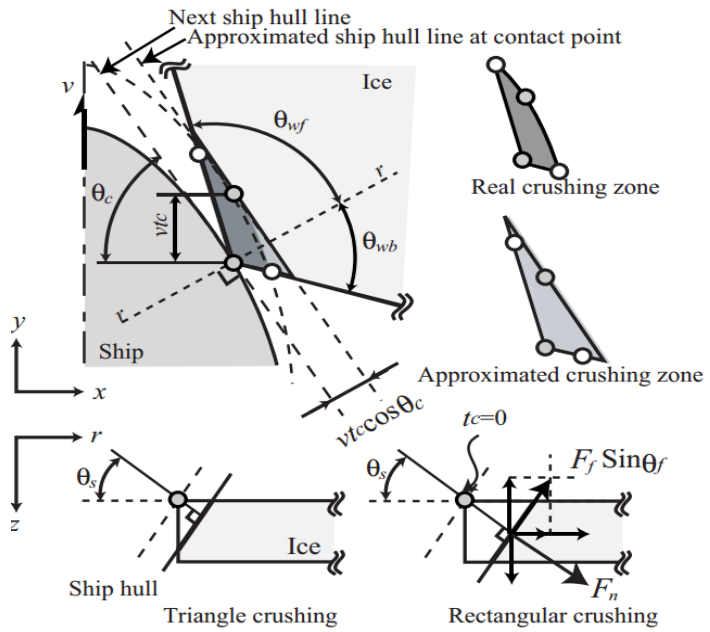

Figure 2.17 Contact geometries due to ice edge crushing in Sawamura's models [5]

The ship icebreaking model of Sawamura et al. [5] was extended in Sawamura et al. [53] for the ship maneuvering application in the level ice. The model considered 3 DOF rigid body motions of ship in surge sway and yaw directions. The crushing force component was modified by including a friction force component. The breaking pattern of the ice cusp was assumed as a circular arc. Sawamura et al.'s [5, 53] models identified the basic mechanisms which are crucial to model the dynamic ship icebreaking process. However, these simplified models need further improvement to determine more accurate crushing and bending force components.

Su et al. [14] introduced another numerical model for ship maneuvering in level ice. Equations of motion in surge, sway and yaw directions were numerically integrated. The icebreaking phase of this model considered crushing and bending failure but different contact detection and contact area calculation methods were employed. The ship hull and ice edge were discretized into a number of nodes to detect the contact point between the ship hull and ice wedge (Figure 2.18). The model assumed formation of ice wedges due to the bending crack. This bending crack was determined using an icebreaking radius. The model utilized a semi-empirical expression for the icebreaking radius:

$$R = C_l l(1.0 + C_v v_n^{rel}) \tag{2.3}$$

Where v_n^{rel} is the relative normal velocity between ship and ice, l is the characteristic length of ice, and C_l and C_v are the empirical parameters which were tuned to match experimental results. The icebreaking radius derived from the first and last contact points was used to idealize the ice wedge. The contact zone between the ship hull and ice wedge

was further discretized into a number of triangles for calculating the contact area. Figure 2.19 indicates the ice wedge idealization and contact zone discretization process. This model also considered two ice edge crushing scenarios (Figure 2.20) to derive the contact area equations.

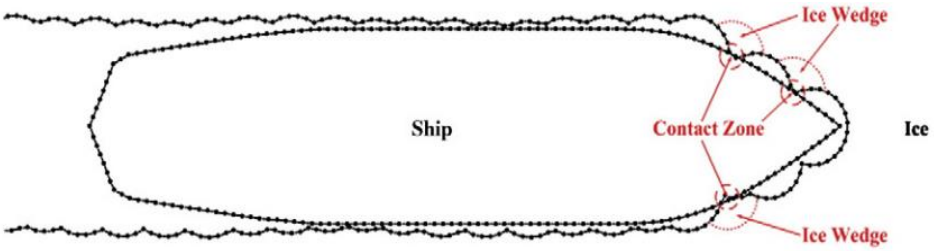

Figure 2.18 Contact detection technique in Su's model [14]

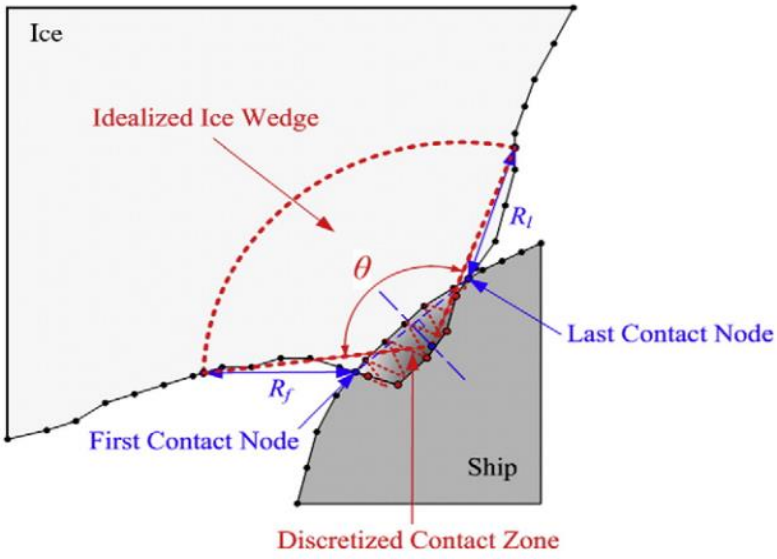

Figure 2.19 Ice wedge idealization and contact zone discretization [14]

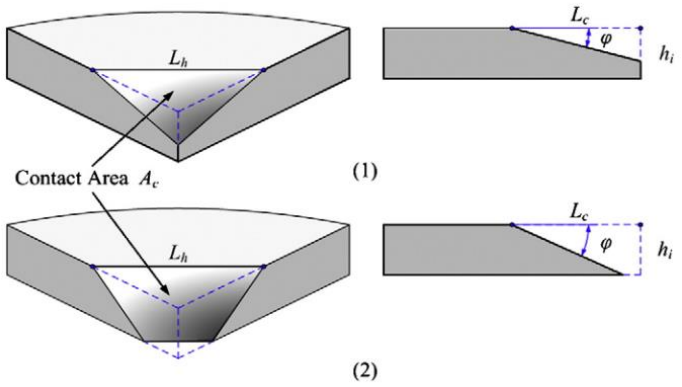

Figure 2.20 Geometries considered in contact area calculation [14]

The normal contact force in Su et al.'s [14] model accounted for the friction and ship velocity. The contact force was further resolved into horizontal and vertical components. The vertical component of contact force caused the bending failure of the ice wedge. This model used Kashteljan's model, mentioned in Eq. (2.2), to predict the flexural failure which ignores the dynamic effect.

Su et al.'s [14] modeling approach was followed by Zhou et al. [52], and was improved by Tan et al. [24, 27, 28] for several ship-ice interaction problems. Zhou et al. [52] utilized Su et al.'s numerical approach for modeling the dynamic ice force on a moored icebreaking tanker. Tan et al. [24] extended Su et al.'s model from the 3 DOF to 6 DOF ship motions. One of the major drawbacks with these models is the assumption of constant contact pressure. Tan et al. [28] improved the model by introducing the pressure-area relationship in the local contact force calculation. The model was further improved by Tan et al. [27] to include the dynamic effect in flexural failure. For this purpose, Kashteljan's bending model was modified with a semi-empirical dynamic

factor. The dynamic factor is a function of normal ship velocity (v), and was established based on finite element analysis results and physical tests. This allowed investigation of velocity effect on the icebreaking process. The dynamic bending failure model used by Tan et al. [27] can be written in SI units:

$$P_f = (1.65 + 2.47v^{0.4})\sigma_f h^2 \left(\frac{\theta}{\pi}\right)^2 \tag{2.4}$$

Aksnes [18] presented a simple one-dimensional (1D) numerical model to analyze the interaction between a moored ship and drifting level ice. The ship motion in the surge direction was considered, and the ice properties were sampled from probability distributions. The total force on the ship was taken as the sum of the hydrodynamic force, mooring force and ice force. The ice force was divided into a penetration dependent breaking term and a velocity dependent term. Again, the breaking term was associated with the icebreaking, rotation and sliding phases. The breaking force was derived based on the semi-infinite plate on elastic foundation, but neglected the dynamic effects of beam and foundation. A deflection based failure criteria was assigned to the breaking phase, and ignored any edge crushing. The velocity effect was accounted by considering the damping from ice as a function of relative velocity between the ship and ice. The model is applicable to the low ice drift velocity interaction problems and limited to moored ships only.

The above mentioned numerical models are helpful to understand the ship icebreaking process. These are beneficial to predict the global ice force or ice resistance for the continuous icebreaking and ship maneuvering. Most of these are applicable to simplified

cases and avoid many important features. These models are not capable of simulating the bending crack initiation and propagation effectively.

2.3.2 Models using Advanced Numerical Techniques

With the advancement of computational technology, several numerical methods and techniques, such as Finite Element Method (FEM) with several integration schemes, Element Erosion Method (EEM), Discrete Element Method (DEM), Cohesive Element Method (CEM), Extended Finite Element Method (XFEM), and Element Free Gelerkin Method (EFGM) are available for ship-ice interaction modeling [33, 35, 54-59]. These methods are well suited to investigate the non-linear problems as they allow modeling of material failure process or simulating transition from continua to discontinua [33]. These methods are effectively employed to simulate ice behavior under dynamic conditions and to capture the ice bending crack initiation-propagation [33, 57, 59]. Several, software packages such as ABAQUS/Explicit, LS DYNA, ANSYS, DECICE, DYTRAN etc. are able to implement most of the numerical methods listed above. Proper software package and numerical methods are selected based on problem nature, desired computational efficiency and desired accuracy of results.

Lu et al. [33], and Daiyan and Sand [59] examined several numerical methods, such as the element erosion method, the cohesive element method, the discrete element method, and the extended finite element method, for ice bending models. These numerical methods were used to simulate an ice wedge-conical structure interaction scenario using

the ABAQUS/Explicit. In general, a failure criterion is assigned in the element erosion method to produce a bending crack. When a particular element reaches that failure criterion, the element is deleted from the model. For the cohesive method, cohesive elements are inserted at the inter-element interfaces of bulk ice. The failure of these cohesive elements is governed by the cohesive law. The discrete element method and the extended finite element method also utilize cohesive elements for crack initiation and propagation. Model results from Lu et al. [33] indicate that all of these methods can simulate bending crack initiation and propagation as shown in Figure 2.21. However, the element erosion method is the most efficient one for modeling ice bending failure.

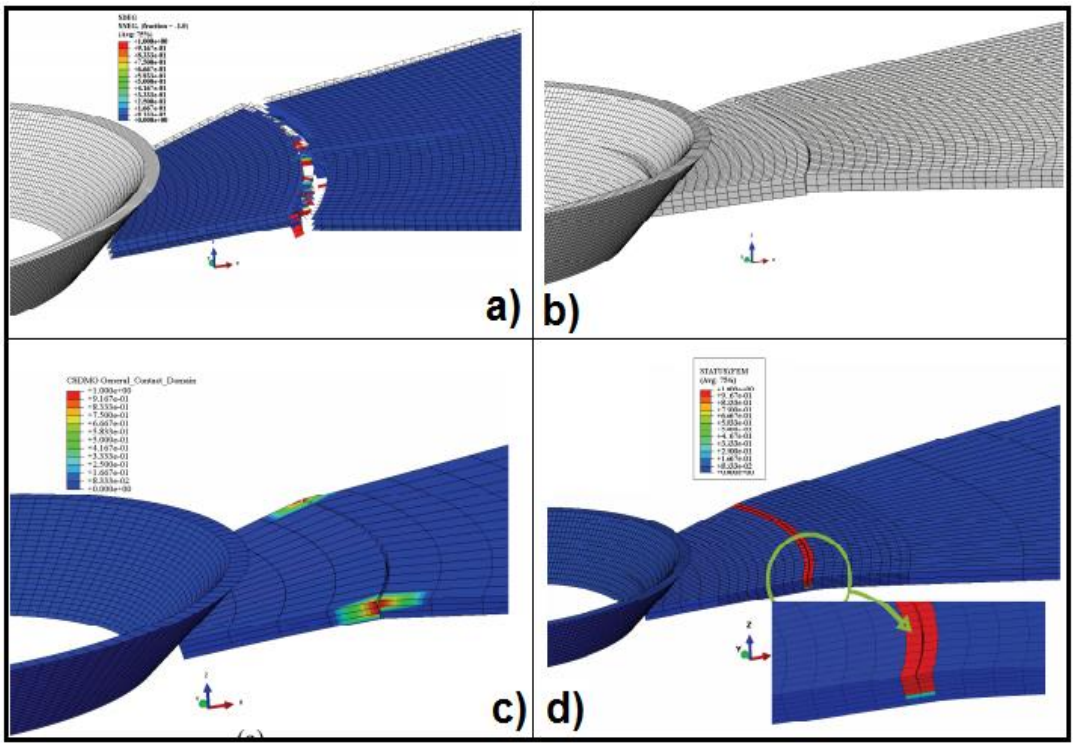

Figure 2.21 Modeling of bending crack initiation and propagation using different numerical methods [33] a) EEM; b) CEM; c) DEM and d) XFEM

Lau [39] introduced a discrete element method for modeling ship-ice interaction. The model was developed using the DECICE software to simulate interaction between the CCGS Terry Fox and level ice during advancing and turning operations. The model consisted of three components; the ship, floating level ice and a water foundation. The ship was considered as a rigid body with 6 DOF. In Lau's model, the ice was assumed as an isotropic elastic brittle material, and discretized with the 3D plate bending elements. Ice failure was based on the Mohr-Coulomb failure criteria with a tension cut-off that allowed the elements to fracture along the inter-element mesh line. Lau's model results for a straight run and a turning operation in level ice are given in Figure 2.22. One of the drawbacks with the model is that it does not allow the elements to fail, and hence the bending failure cannot be simulated using this model.

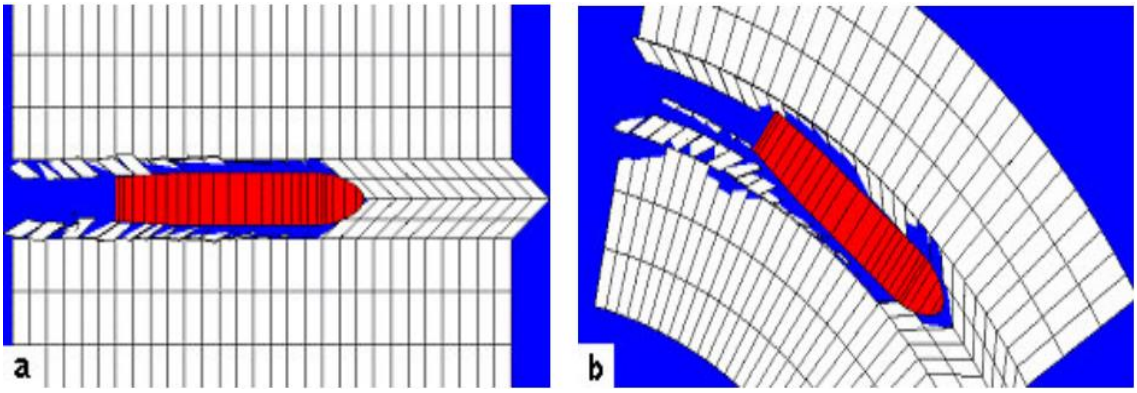

Figure 2.22 Simulation results for ship (CCGS Terry Fox) in level ice [39] a) advancing and b) turning at 10 m radius

Shunying et al. [61] provided another discrete element model to simulate the interaction between a ship hull and drifting ice floes in a broken ice field as shown in Figure 2.23.

The ice floes were modeled as 3D disk-like elements which considered buoyancy, drag and mass induced by the current. This type of model can be helpful to estimate the ice load when ship advances through ice, but may not be useful to model the fracture or failure in ice.

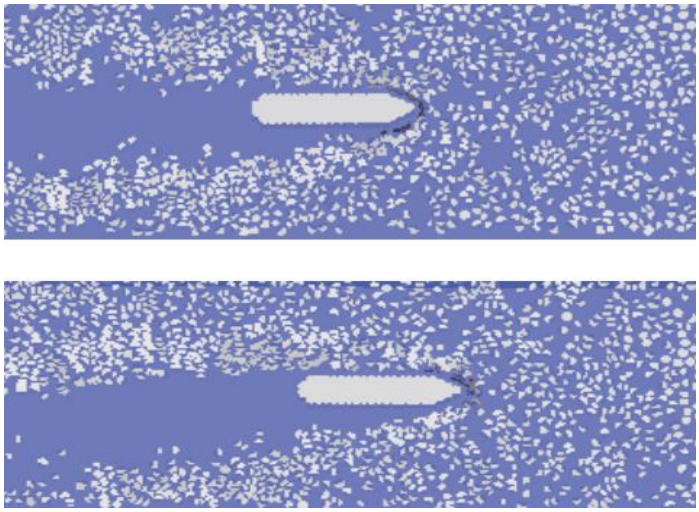

Figure 2.23 Discrete element model of ship advancing through broken ice fields [61]

Sawamura et al. [34, 35] implemented the finite element models of ship-ice wedge interaction in ABAQUS/Explicit to investigate dynamic bending failure. These models considered the ice as an elastic material, and the water foundation as an incompressible inviscid material. These models demonstrated the effect of dynamic loading, ice thickness, wedge angle, ship hull angle, water foundation etc. on the peak ice force and breaking length. These models ignored ice crushing at the contact point. From these models, it is not possible to directly relate ship velocity to the force applied at the interface. Moreover, the elastic ice model cannot produce the bending crack. The peak ice force and breaking length are obtained by observing the maximum stress from the FEM

results. Figure 2.24 indicates such type of FEM model for a 45^{o} ice wedge rested on the water foundation along with the boundary conditions and load scenarios.

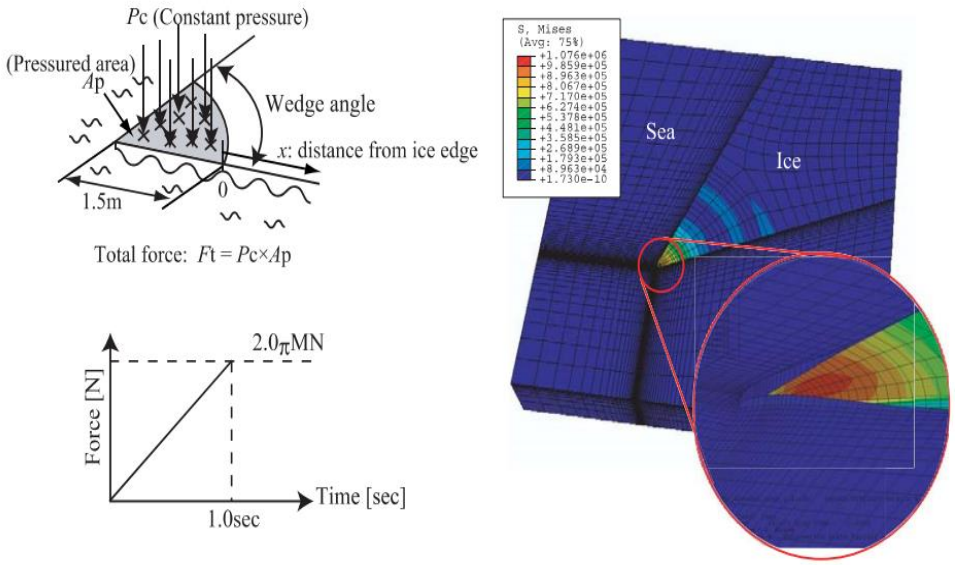

Figure 2.24 FEM model of ice wedge on water foundation along with edge boundary condition and loading scenario [35]

The selection of a proper ice material model is important for modeling the ship-icebreaking process. Ice is strain rate sensitive, and responds differently in tension and compression. Hence, numerically modeling ice is difficult. However, attempts have been made in the recent past to model the ice numerically for different applications [54-56, 58, 62]. For an example, Wang et al. [62] developed an ice model for a nonlinear dynamic FEM model of LNG ship-ice interaction using the commercial software DYTRAN. The ice was considered as a crushable body and discretized with solid elements. The ship was discretized with the shell elements and modeled as a deformable body with the elastic-

plastic material behavior. The interaction model and the simulated result are presented in Figure 2.25 which indicates that significant crushing occurs at the ice edge.

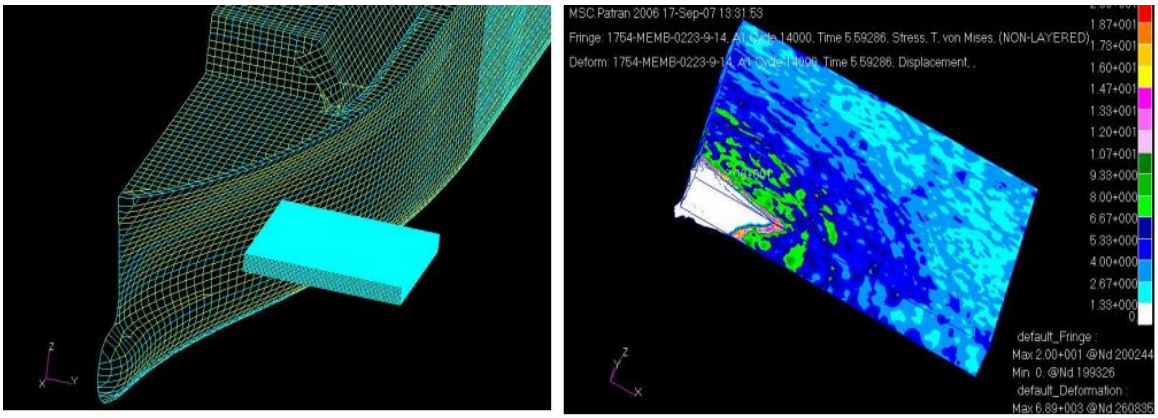

Figure 2.25 LNG ship-ice collision model (left) and ice edge crushing (right) [62]

Gagnon and Wang [63], Zong [56] and Kim [64] also developed several crushable foam models in LS DYNA to represent ice behavior. All of these models were formulated on a trial and error basis to meet some specific test conditions. Gagnon and Wang's [63] crushable foam model was used to simulate a collision between a tanker and a bergy bit. Kim's [64] ice model was tuned with the experimentally obtained compressive behavior of cone-shaped ice specimens. Zong [56] evaluated more than 30 ice crushable foam models in order to match different pressure-area relationships specified in the Polar Rules [9]. These models were used to simulate ice crushing behavior. However, suitability of these models for investigating generalized ice crushing is questionable because of the insensitivity to strain rate. Moreover, these models apply the same stress-strain relationship in tension and compression, which make them incapable of modeling bending behavior.

Carney et al. [58] and Pernas-Sanchez et al. [55] proposed plasticity based and strain rate sensitive ice material models. These models provided different behaviors in tension and compression which follow the Drucker-Prager yield criterion. These models also accounted for the strain rate sensitivity in compression, and assumed no sensitivity in tension. In these models, a pressure cut-off value was assigned for the element failure. However these models cannot produce a bending crack.

The commercial software LS DYNA [66] has several numerical solvers such as Lagrangian, Eulerian, Arbitrary Lagrangian Eulerian (ALE), and Smoothed Particles Hydrodynamic (SPH). Among these solvers, the Lagrangian finite element solver is computationally efficient and most common for modeling the continuum mechanics problem. In this solver, the mesh deforms with the material [56]. On the other hand, material flows through the fixed mesh and allows large deformation in an Eulerian solver. The ALE solver takes the advantage of both the Lagrangian and the Eulerian solvers and allows computationally efficient modeling for large deformation problem [55, 56]. For this reason, the ALE is widely used to model the fluid medium such as water and air in many fluid-structure interaction problems. Comparisons among three numerical solvers are illustrated in Figure 2.26.

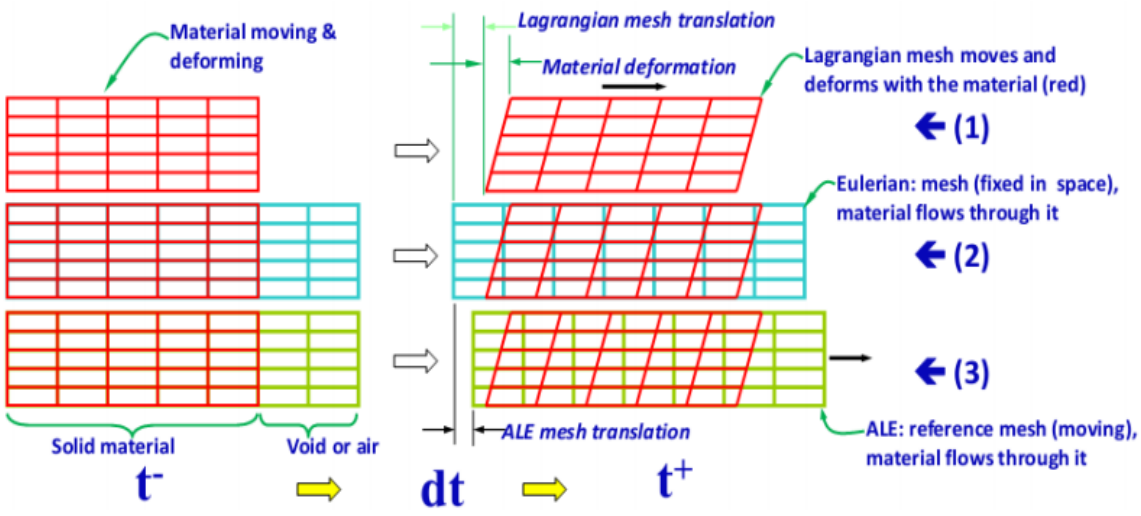

Figure 2.26 Comparisons among Lagrangian, Eulerian and ALE solvers [56]

The SPH is another innovative finite element solver in which the material is represented as a group of discretized particles [55]. In this mesh free method, particles are linked together with the material properties [55].

Pernas-Sanchez et al. [55] studied the performance of a plasticity based ice model using the Lagrangian, Arbitrary Lagrangian Eulerian (ALE) and Smoothed Particles Hydrodynamic (SPH) solvers. The study indicated that all these numerical solvers can be used for ice impact analysis. However, comparisons with experimental force time histories indicated that the Lagrangian solver with the element erosion technique is more accurate than other two.

The bending strength behavior of ice is crucial for modeling ship-ice interaction. A four point bending test is commonly used to determine the bending strength and to

characterize ice bending behavior. Ehlers and Kujala [54] developed an ice model using a traditional finite element method to simulate the bending behavior of ice using the MAT_PLASTICITY_COMPRESSION_TENSION material in LS DYNA. The model accounted for different responses in compression and tension. Based on bending beam theory and experimental results, the strain rate effect was assigned to both tension and compression. A pressure cut off value was defined for the beam failure to obtain a maximum bending load. The final model results were compared with force-deflection curves obtained from a four point bending test. The model results were found to be satisfactory, but did not produce a bending crack as expected to occur in the middle of the ice beam. Das et al. [65] further studied the ice bending model using a SPH numerical solver. Identical experimental results and modeling setup were used in this study with the exception of the failure criteria. The study utilized an equivalent plastic strain value instead of a pressure cut-off value as the failure criteria. This enabled the model to generate a bending crack as shown in Figure 2.27.

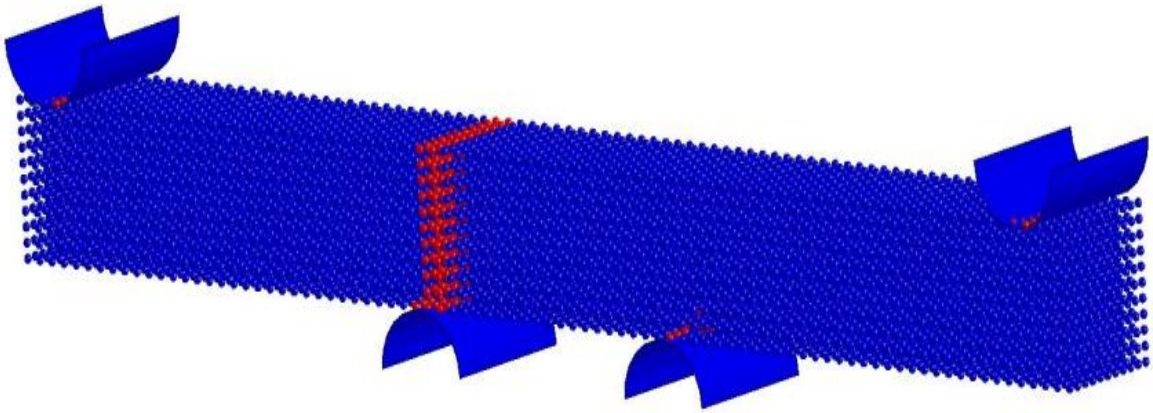

Figure 2.27 Four point bending model in SPH method indicating bending crack [65]

Das's [65] ice model results indicated that the SPH method with equivalent plastic strain failure criteria has the potential to simulate the bending failure. However, the SPH method is known to be computationally expensive and is still in the early stage of development.

Daiyan and Sand [57] introduced the Cohesive Element Method (CEM) to develop an ice model in LS DYNA for an ice-structure interaction problem. The model consisted of bulk ice, cohesive elements, air and a water foundation. The bulk ice was assumed as an isotropic linear plastic material, and modeled with the material MAT_PIECEWISE_LINIEAR_PLASTICITY. Two different material properties were used for cohesive elements in the horizontal and vertical directions to account for the anisotropic failure behavior. The MAT_COHESIVE_GENERAL material was used for the cohesive elements which were inserted at the inter-element interfaces of the bulk ice. These zero thickness cohesive elements enabled the ice model to simulate ice damage and fracture. In general, the cohesive elements follow a traction-separation curve for crack initiation and growth. This traction-separation curve was derived based on the ice fracture mechanics which is directly related to the fracture modes of ice. The air and the water foundation behavior were simulated using the MAT_NULL to model the fluid-structure and fluid-ice interactions. The final ice-structure interaction model was applied to the low velocity interaction problems. The model over predicted the horizontal force component when compared with the analytical result.

2.4 Polar Ship Design Practice

The development of a safe speed methodology for Polar ships is directly related to ship design practice. A brief discussion of Polar ship design practice follows.

Polar ship design and operation require ice strengthening of the ship structures. Strengthening ensures structural resistance to ice impact forces. In general, ship classification societies develop ice strengthening requirements based on ice conditions, ship structural particulars and ship operating conditions [7, 8, 67]. In addition, each classification society provides various ice classes in order to guide the ship design and operation in different ice conditions. Each ice class has its own ice strengthening requirements [56]. Table 2.1 lists the major classification societies and Rule systems along with the number of ice classes.

Table 2.1 Major ship classification societies/ rule systems and their ice classes [9, 56]

Ship Classification Societies/Rule Systems	**Ice Classes**
Canadian ASPPR/CAC	9 Classes
Russian MRS/NSR	9 Classes, 4 Icebreaker
Finnish Swedish Ice Class Rules (FSICR)	5 Baltic Classes
American Bureau of Shipping (ABS)	5 Polar Classes , 5 Baltic Classes
Det Norske Veritas (DNV)	3 Icebreaker, 3 Polar, 5 Baltic Classes
Lloyds Register (LR)	5 Polar, 5 Baltic Classes

In the recent past, industry pressed for a simple and common system of ice classes for ship design [9, 56]. In 1993-2006, the IACS and the IMO developed a harmonized set of ice classes for ships intended to operate in polar waters [9]. The IACS under the guidance of the IMO developed seven Polar ice classes to replace the member societies' current rule sets [7, 9, 67]. The Polar Rules are also known as Unified Requirements for Polar Ships or the Polar UR. The Polar UR represents the latest industry standards for Polar ship design and operation [7, 9]. The following sub-sections describe different ice classes, ice load design methodology and ship structural requirements specified in the Polar Rules.

2.4.1 Polar Ice Classes

The Polar ice rules and Baltic ice rules are the most widely adopted rules for designing ice class ships. The Finnish-Swedish Maritime Administration (FMA) developed six ice classes to guide ship operation in winter ice in the Baltic Sea, and the first year ice of sub-polar regions [6]. The IACS Polar Rules provide seven ice classes to deal with the multi-year ice along with light first year ice [6]. The descriptions and notations of these Polar ice classes are given in Table 2.2. In the Polar ice classes, the PC 1 is the upper end and allows the year-round operation in all polar water without limitations [8, 10]. The PC 7 is the lower end for the summer/autumn operation [8, 9]. Comparison with the Baltic ice classes indicates that the lowest Polar ice classes PC 6 and PC 7 are equivalent to the Finnish Swedish Ice Class Rules (FSICR) ice classes IA super and IA, respectively, as shown in Figure 2.28. The selection of proper ice class is based on the ice conditions, operational requirements and cost [9].

Table 2.2 Description of IACS Polar ice classes [9]

Polar Class	Ice Description (based on WMO Sea Ice Nomenclature)
PC 1	Year-round operation in all Polar waters
PC 2	Year-round operation in moderate multi-year ice conditions
PC 3	Year-round operation in second-year ice which may include multi-year ice inclusions
PC 4	Year-round operation in thick first-year ice which may include old ice inclusions
PC 5	Year-round operation in medium first-year ice which may include old ice inclusions
PC 6	Summer/autumn operation in medium first-year ice which may include old ice inclusions
PC 7	Summer/autumn operation in thin first-year ice which may include old ice inclusions

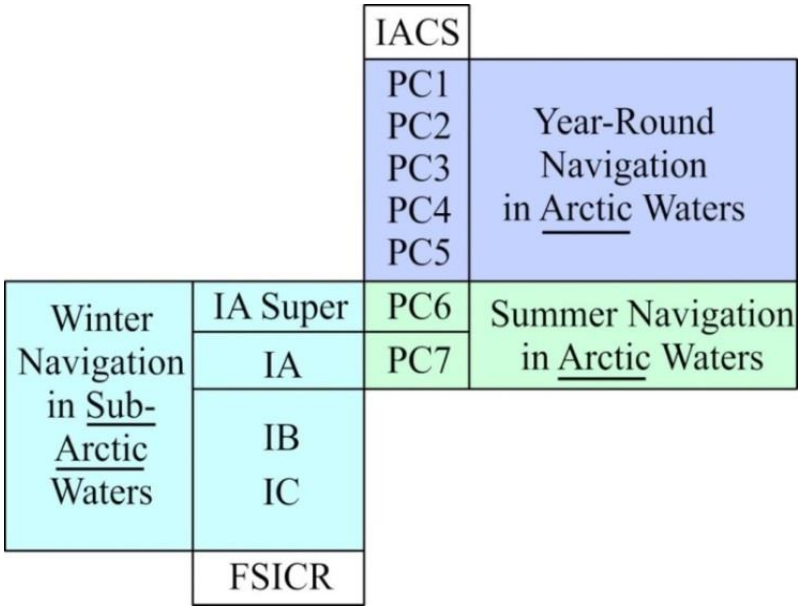

Figure 2.28 Approximate comparisons between Baltic and Polar ice classes [9, 10]

Both the Baltic and the Polar Rules require the ice strengthening of ship hull regions. These strengthening requirements are ice class dependent. In general, the hull regions are strengthened with the ice belt as indicated in Figures 2.29 and 2.30. Both the rules specify the ice strengthening requirements for each hull region and ice class. In the Polar Rules, the entire exterior hull must be strengthened as ice may interact with any part of the hull.

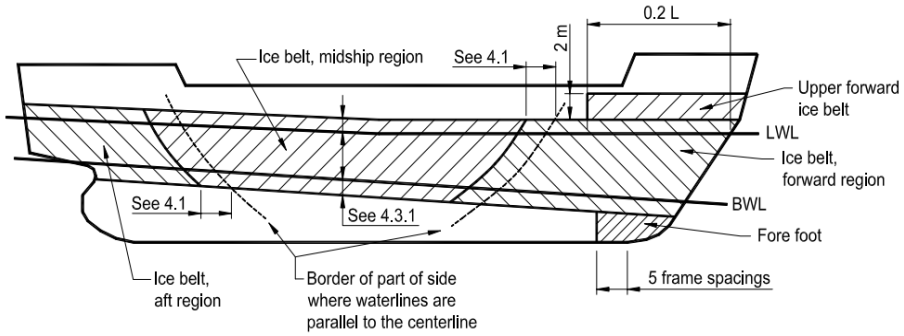

Figure 2.29 Ice strengthening requirements in Baltic ice rules [11]

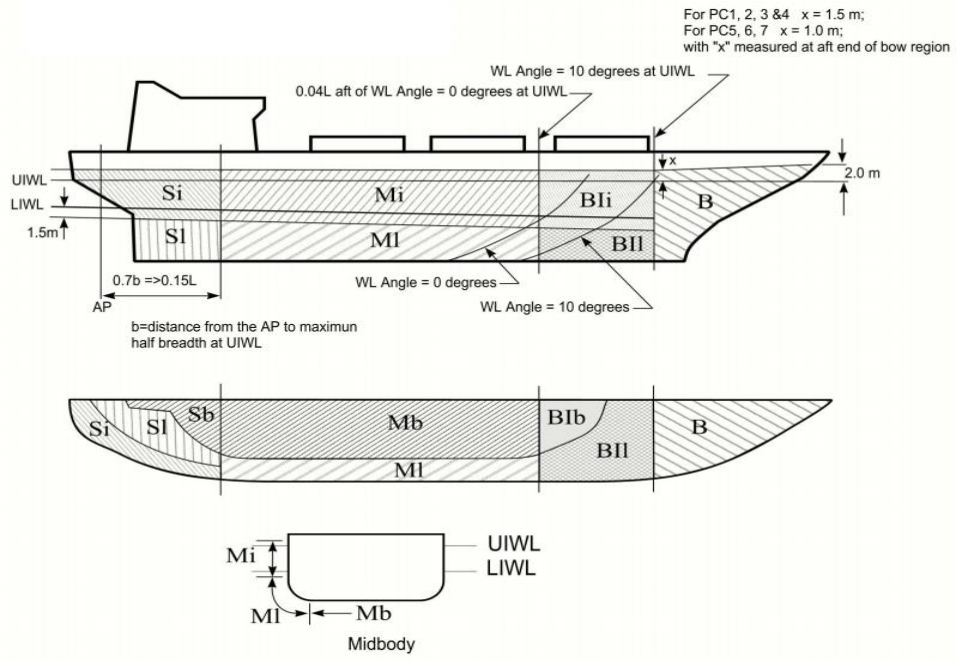

Figure 2.30 Ice strengthening requirements in Polar ice rules [11]

2.4.2 Polar Design Ice Load Scenario

In the Polar Rules, the ice load parameters are rationally linked with design scenarios of ship-ice interaction [8, 9]. The design scenario considers a glancing collision on the shoulders of the bow with an ice edge. During this glancing collision, the impact force is limited by the ice edge crushing or flexural failure [9]. Hence, two ice failure load models for the ice crushing and ice flexure are required to estimate the design ice load parameters. The Polar Rules design scenario indicating ice edge crushing and ice flexure is shown in Figure 2.31.

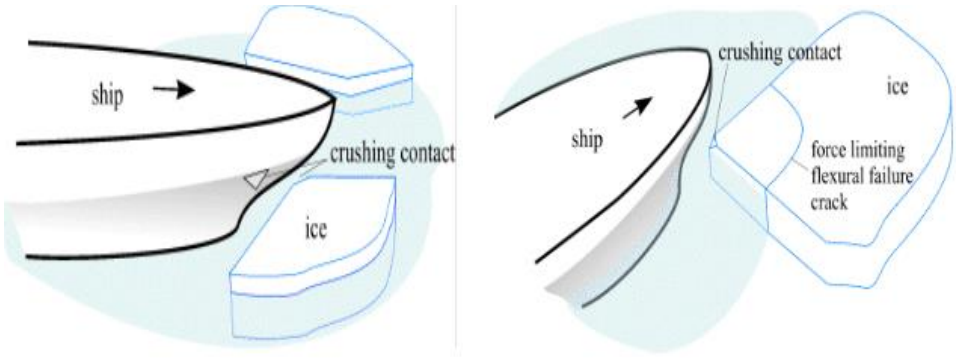

Figure 2.31 Polar Rules design scenario indicating ice edge crushing and ice flexure [8]

In the ice crushing failure model, the impact force is determined by equating the effective kinetic energy and energy required to crush the ice [7, 8, 12]. The model incorporates Popov [74] collision mechanics to simplify the six-degree of freedom (DOF) collision scenario to a single DOF collision scenario [7, 9]. In addition, the collision model includes a wedge shape ice edge and a pressure-area relationship. The pressure-area

relationship is used to define the ice crushing pressure. The pressure-area relationship adopted in the Polar Rules can be expressed as [7, 56]:

$$P = P_o A_n^{ex} \tag{2.5}$$

The pressure-area relationship in Eq. (2.5) requires the values of nominal strength (P_o) and exponent (ex) for different ice classes. Table 2.3 lists the values of P_o and ex for different ice classes. The nominal contact area (A_n) is calculated based on the indentation geometry. Further discussion on the Popov model, pressure-area relationship and ice crushing limit load model are given in Chapter 3.

Table 2.3 Parameters for pressure-area relationship in Polar Rules [56]

Polar Class	**P_o , MPa**	**ex**
PC 1	6	
PC 2	4.2	
PC 3	3.2	
PC 4	2.45	-0.1
PC 5	2.0	
PC 6	1.4	
PC 7	1.25	

The IACS Polar Rules provide a flexural failure model considering a 150^0 ice wedge. The model does not allow the ice crushing force to exceed the ice flexural force [8]. The IACS proposed flexural limit load model can be expressed as [7, 12]:

$$F_{flex\_Polar} = \frac{1.2\sigma_f h_{ice}^2}{\sin\beta'} \tag{2.6}$$

According to this model, flexural failure occurs when the vertical component of the impact force exceeds the flexural strength of ice. The model does not account for the effect of horizontal impact force components or the friction force between the ship and ice. Daley and Kendrick [12] modified this model to account for the ship hull-ice friction and the horizontal impact force component. The ice cusp geometry and contact forces considered in this modified model are indicated in Figure 2.32. The ice cusp length was taken to be equal to 10 times of the ice thickness.

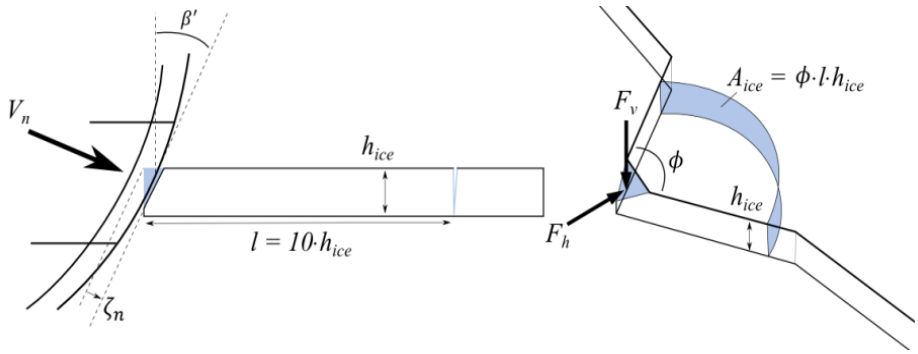

Figure 2.32 Ice cusp geometry and contact condition in Daley and Kendrick's flexural failure model [7]

Daley and Kendrick's proposed flexural limit load model is given in Eq. (2.7).

$$F_{flex\_Daley} = \frac{C\sigma_f h_{ice}^2 \theta}{\sin\beta' + \mu\cos\beta' - \frac{C}{10}(\cos\beta' + \mu\sin\beta')} \tag{2.7}$$

where, C is an empirical co-efficient and μ is a frictional coefficient between ship and ice. Equations (2.6) and (2.7) do not include a velocity effect, and are intended for the very thick ice. Daley and Kendrick [12] further extended this flexural failure model to

thinner ice and higher speed interactions. A Froude scaling method was introduced to consider the dynamic effect in the flexural failure model [7, 12]. The method scaled the flexural force with the ratio of dynamic Froude number (FN) and static Froude number (FN_s) as shown in Eqs. (2.8) and (2.9).

$$F_{flex\_Daley\_dynamic} = F_{flex\_Daley}\left(\frac{FN}{FN_s}\right)^n \tag{2.8}$$

$$FN = \frac{V_n}{\sqrt{g h_{ice}}} \tag{2.9}$$

The power (n) and the static Froude number in Eq. (2.8) were chosen as 0.33 and 0.1, respectively [7]. The model can provide a safe speed calculation. However, the model needs further improvement.

The minimum impact force from the ice crushing model and the ice flexural model provides the bow impact load. The bow impact load (F_i) is limited to a rule specified force value (F_l). The Polar Rules based bow impact load formula can be expressed as [8, 11]:

$$F_i = min\begin{Bmatrix} F_c = f_a C F_c D^{0.64} \\ F_f = \dfrac{1.2\sigma_f h^2}{sin\,\beta'} \\ F_l = 0.6 C F_c D^{0.64} \end{Bmatrix} \tag{2.10}$$

The shape coefficient (f_a) in Eq. (2.10) is defined as:

$$f_a = (0.097 - 0.68\left(\frac{x}{L} - 0.15\right)^2)\frac{\alpha}{\sqrt{\beta'}} \tag{2.11}$$

Equation (2.10) indicates that the bow impact load is a function of ice flexural strength (σ_f), ice thickness (h), crushing class factor (CF_c), ship displacement (D), impact location (x) with respect to ship length (L) and different hull angles such as water line angles (α) and normal ship frame angles (β'). The hull angles at impact locations can be calculated using Figure 2.33.

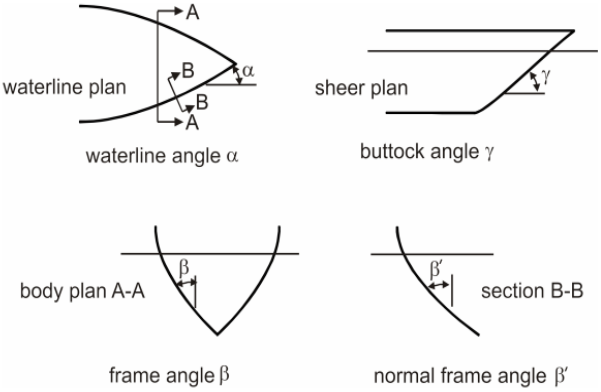

Note: β' = *normal frame angle at upper ice waterline [°]*
α = *upper ice waterline angle [°]*
γ = *buttock angle at upper ice waterline (angle of buttock line measured from horizontal) [°]*
$\tan(\beta) = \tan(\alpha) / \tan(\gamma)$
$\tan(\beta') = \tan(\beta)\cos(\alpha)$

Figure 2.33 Hull angle definition in Polar Rules [11]

In the Polar Rules, the bow impact load is calculated at four different bow locations. The impact load with the maximum magnitude is applied in the form of load patch to evaluate the structural strength [7-9, 11]. This load patch is acted over a triangular contact surface and cannot be applied to the ship structure directly [17]. Therefore, the triangular load patch is idealized to a rectangular load patch using specified formulas. The Polar Rules based load patch idealization and different load patch parameter calculation procedures are given in Chapter 6.

The hull area factors (AF) are introduced in the Polar Rules to reflect the relative magnitude of impact load in different hull regions [11]. The AFs for different Polar classes at various hull regions are given in Table 2.4.

Table 2.4 Hull area factors in Polar Rules [8-11]

Hull Area		Area	Polar Class						
			PC1	PC2	PC3	PC4	PC5	PC6	PC7
Bow (B)	All	B	1,00	1,00	1,00	1,00	1,00	1,00	1,00
Bow intermediate (BI)	Ice belt	BI_i	0,90	0,85	0,85	0,80	0,80	1,00 [1]	1,00 [1]
	Lower	BI_l	0,70	0,65	0,65	0,60	0,55	0,55	0,50
	Bottom	BI_b	0,55	0,50	0,45	0,40	0,35	0,30	0,25
Midbody (M)	Ice belt	M_i	0,70	0,65	0,55	0,55	0,50	0,45	0,45
	Lower	M_l	0,50	0,45	0,40	0,35	0,30	0,25	0,25
	Bottom	M_b	0,30	0,30	0,25	[2]	[2]	[2]	[2]
Stern (S)	Ice belt	S_i	0,75	0,70	0,65	0,60	0,50	0,40	0,35
	Lower	S_l	0,45	0,40	0,35	0,30	0,25	0,25	0,25
	Bottom	S_b	0,35	0,30	0,30	0,25	0,15	[2]	[2]

[1] See C.1.3
[2] Indicates that strengthening for ice loads is not necessary

Rahman [8] mentioned that measured ice loads can be quite peaky within a rectangular load patch. The effects of these peak loads are accounted with a peak pressure factor (PPF). The PPF values for different structural members are given in Table 2.5. The peak pressure factor magnifies the total patch load, and represents a pressure concentration on the localized structural members as shown in Figure 2.34.

Table 2.5 Peak pressure factor (PPF) in the Polar Rules [8-11]

Structural Member		Peak pressure factor (PPF_i)
Plating	Transversely-framed	$PPF_p = (1{,}8 - s) \geq 1{,}2$
	Longitudinally-framed	$PPF_p = (2{,}2 - 1{,}2 \cdot s) \geq 1.5$
Frames in transverse framing systems	With load distributing stringers	$PPF_t = (1{,}6 - s) \geq 1{,}0$
	With no load distributing stringers	$PPF_t = (1{,}8 - s) \geq 1{,}2$
Load carrying stringers Side and bottom longitudinals Webframes		$PPF_s = 1$, if $S_w \geq 0{,}5 \cdot w$ $PPF_s = 2{,}0 - 2{,}0 \cdot S_w / w$, if $S_w < (0{,}5 \cdot w)$
where: s = frame or longitudinal spacing [m] S_w = web frame spacing [m] w = ice load patch width [m]		

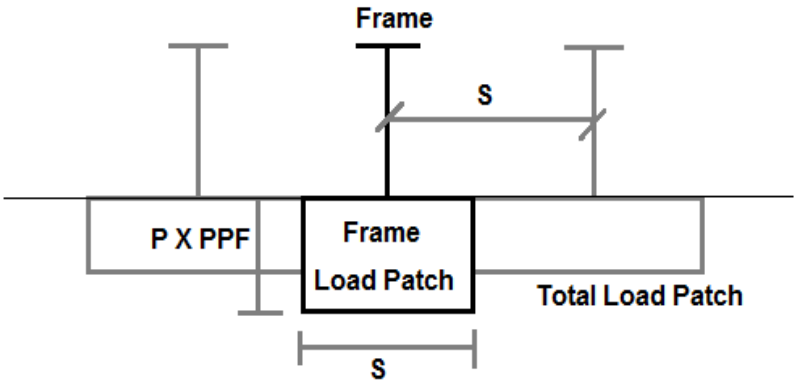

Figure 2.34 Peak pressure factor on structural member [8, 9]

2.4.3 Structural Limit State Analysis

Structural limit state analysis is important for the Polar ship design as limit states define the load bearing capacity of the structural members. The limit states determine whether a structural member will fail or not under the action of a particular design load patch. In general, the design load patch is applied to a structural member in the horizontal orientation as shown in Figure 2.35.

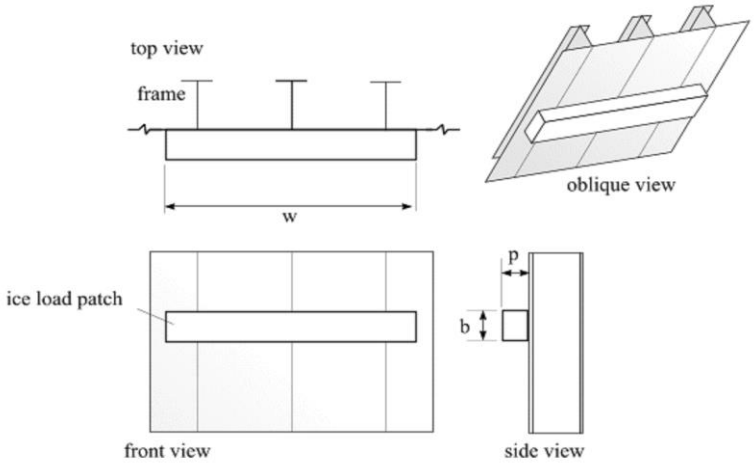

Figure 2.35 Application of design load patch to structural member [8]

Plates and frames are the primary structural members of Polar ships. The limit states of the plates and frames are determined based on plastic collapse mechanisms [7-9]. The IACS Polar Rules contain several analytical expressions for plastic capacity and limit state conditions for plates and frames [12]. These analytical expressions are derived based on the energy methods and validated with non-linear finite element analysis [68, 69].

The plastic collapse mechanism in Figure 2.36 is considered by Daley et al. [68] to determine the plate limit state equations. The figure indicates the possible hinge locations with different ratio of load height (b) to frame spacing (s) and frame span (l).

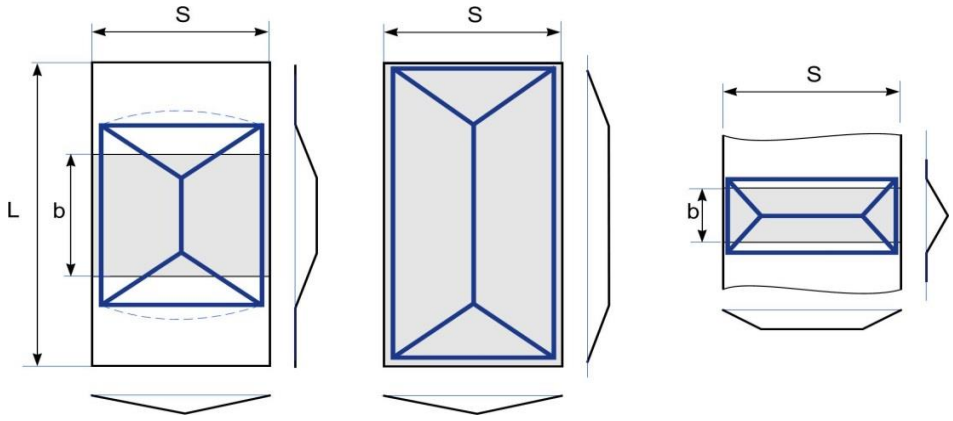

Figure 2.36 Plastic collapse mechanisms for plate limit state conditions [9]

For framing, three primary limit state conditions are considered in the Polar Rules. The collapse mechanisms corresponding to these limit state conditions are shown in Figures 2.37a to 2.37c. Further discussion on the plate and frame design and their limit state equations is carried out in Chapter 6.

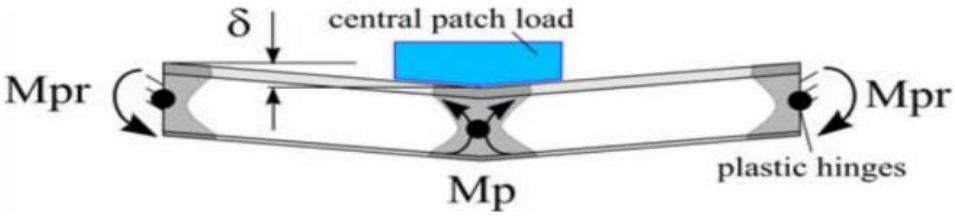

Figure 2.37a 1st limit state - 3 hinge formation in plastic frame [68]

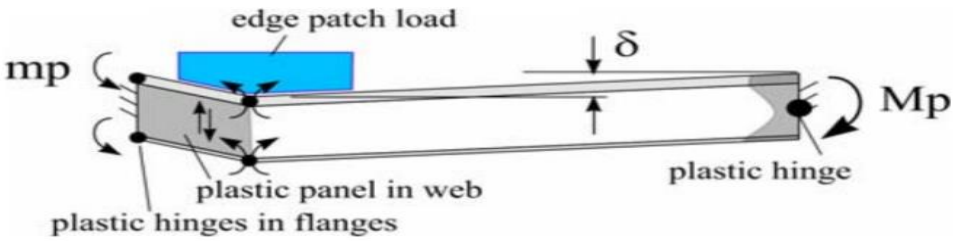

Figure 2.37b 2nd limit state - shear panel formation in plastic frame [68]

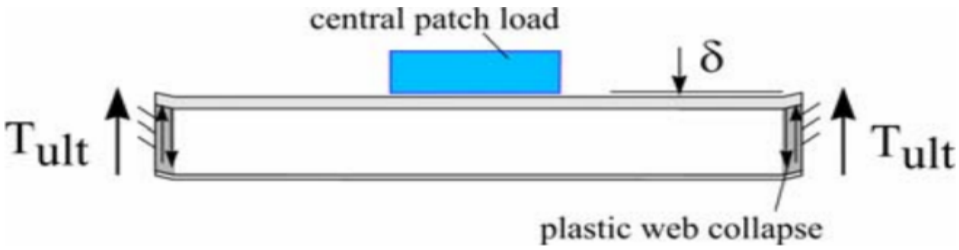

Figure 2.37c 3rd limit state - end shear in plastic frame [68]

2.5 Current Status of Safe Speed Methodology

Safe speed operation is of current interest to the IMO, classification societies and ship industries. The concept of Safe Speed is intended to provide operational guidance to Polar ships in different ice conditions [7, 12]. The concept is not new, yet few studies of

the idea are found in the literature. Dolney et al. [7] mentioned that the ice passport or ice certificate concept was first introduced in the mid 1970s by Russian scientists to ensure safety of the hull during ice operation, by regulating the ship speeds.

The design ice load model and structural limit state conditions are the primary elements of the ice passport and safe speed methodology. Several approaches are followed in the early forms of the Russian ice passport, and in the more recent safe speed methodology, to obtain the design ice load parameters and structural limit state conditions. The Russian ice passport considers Kurdyumov and Kheisin's velocity dependent hydrodynamic model for the local contact pressure which is combined with Popov collision mechanics [7]. The structural limit state conditions are obtained from yield and ultimate failure criteria. This provides two critical curves: a safe speed curve corresponding to yield criteria and a dangerous speed curve corresponding to ultimate failure criteria. A third curve of attainable speed in ice is also specified in the Russian passport concept which is established from the propeller thrust and ice resistance [3, 7]. The Russian ice passport concept is illustrated in Figure 2.38. Based on this concept Likhomanov et al. [3] developed an ice passport for the Canadian Coast Guard icebreaker "Pierre Radisson" in 1997. Recently, CNIIMF [70] established an ice certificate identical to the Russian ice passport for an Arctic Shuttle Tanker (LU 6). CNIIMF's ice certificate contains a different curve named as admissible speed curve which is obtained from the minimum of safe speed and attainable speed curves. CNIIMF's ice certificate diagram is shown in Figure 2.39.

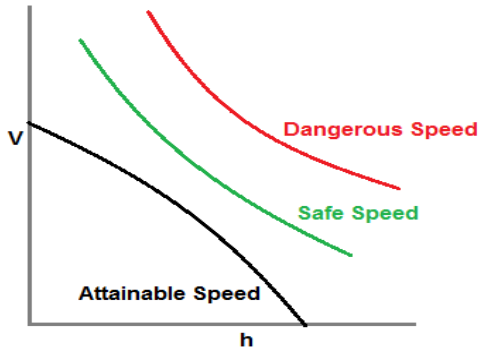

Figure 2.38 Concept of Russian ice passport [3]

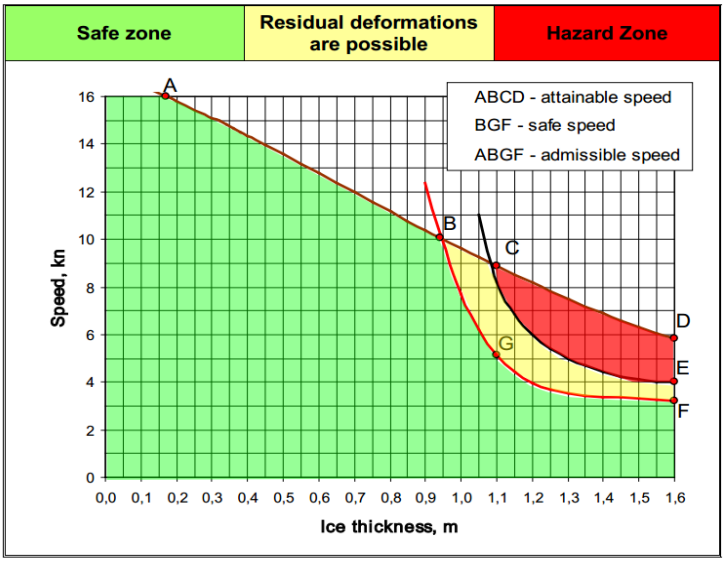

Figure 2.39 CNIIMF ice certificate for Arctic Shuttle Tanker [70]

The recent approach in safe speed methodology utilizes the Polar Rules structural limit state equations and design ice load model [7]. The plasticity based limit state analysis avoids over design of shell plating and framing [68, 69].

It is mentioned earlier that the Polar Rules based design ice load model requires an ice crushing model and an ice flexure failure model. Most of the recent approaches use these

two failure models to estimate the design ice load parameters for the safe speed methodology. The major limitation of these approaches is the flexural failure model which does not account for the velocity effects. Hence, these approaches are not suitable for thinner ice or higher ship speed applications.

Daley and Kendrick [12] extended the Polar flexural failure model to account for the velocity effect. This extended model further utilized to develop the safe speed methodology for different Polar class ships. The authors developed an excel spreadsheet named as SAFE.speed.check to allow a simple calculation of safe speed in different ice conditions. The SAFE.speed.check spreadsheet provides a tool for the safe speed guidance of Polar class ships. Dolney et al. [7] also utilized the extended model to develop a safe speed methodology which was illustrated with a PC 5 Ice class ship.

2.6 Literature Summary and Problem Statement

The literature review indicates a requirement to incorporate the velocity dependent ice flexural failure model into a more comprehensive safe speed methodology. At present there is no universally accepted dynamic flexural failure model found in the literature. However, the literature provides information which can be used as the theoretical basis and technical background for developing a velocity dependent flexural failure model leading to an improved safe speed methodology. The key information from this literature is extracted and summarized below to explain the motivation and methodology of the present work.

- Increasing shipping activities increase the possibility of accidental events in the Arctic. Ice class ship design does not always ensure the protection of the Arctic ship from these accidental events due to the ice actions. The concept of safe ship speed operation extends the responsibility for safety from the design to the operation. Therefore, the present work is focused on the development of safe speed methodology for the Polar ships.

- A velocity dependent flexural failure model is an important ingredient of a safe speed methodology. Current practice in the IACS Polar Rules and most of the existing models do not consider the velocity effect. Therefore, it is necessary to develop a velocity dependent flexural failure model.

- Development of velocity dependent flexural failure model requires a clear understanding of the ship-ice interaction process. In general, a ship-ice interaction process is idealized based on the observation of model scale and full scale tests. An idealized ship-ice interaction process consists of breaking phase, rotating phase and sliding phase. Investigation of the entire interaction process, considering all the phases is important for understanding the global ice force and the ice resistance. The local peak force is responsible for ship structural damage. Analysis of the breaking phase of a ship-ice interaction process is sufficient to extract this local peak force. Hence, the present study considers only the breaking phase of ship-ice interaction.

- There is no universally accepted description of the icebreaking pattern. However, different idealized icebreaking patterns by Kashteljan [29], Enkvist [30], Kortas [31] and Riska [20] indicate the formation of ice wedges or ice cusps. Many researchers suggested modeling simple ice wedge breaking instead of the full ice sheet, especially for the local contact force. The present study also considers the modeling of ship ice wedge breaking process.

- Existing models using the analytical and semi-empirical approaches (Kashteljan et al. [29], Kheisin [46], Lindqvist [36], Liu [21, 49], Lubbad and Loset [18], Sawamura et al. [5, 53], Su et al. [14], Zhou et al. [52], Tan et al. [24, 27, 28], Aksnes [18] etc.) focus mainly on the prediction of the global ice force and ice resistance for continuous icebreaking and maneuvering operations. Most of these models are simplified and ignore one or more influencing parameters. Nevertheless, these models are helpful to understand the individual mechanism involved in the ship-ice interaction.

- Advanced numerical techniques can be employed to develop new ice material models and ship icebreaking models. These models are valuable in investigating the dynamic bending behavior. Numerical methods such as FEM, CEM, DEM and XFEM [33, 35, 39, 54-59, 61-64], and different numerical solvers such as Lagrangian, ALE and SPH are employed for these modeling purposes. Many of these methods and solvers have the capability to generate the bending crack initiation and propagation. However, the finite element method with the element

erosion technique and the Lagrangian solver is indicated to be the most efficient method and hence is adopted in this study.

- Model validation is crucial for the acceptance of a developed model. Most of the ship-ice interaction models, which are intended to predict global ice forces and resistance forces, are validated against model scale and full scale tests. However, model scale and full scale tests are of limited value in characterizing the local contact mechanism. Many researchers (Daiyan and Sand [57], Sawamura et al. [34, 35] etc.) use analytical or semi-empirical approachs to validate their local contact force models. The present study validates the developed flexural failure model by comparing with existing analytical and semi-empirical models.

- Design ice load patch and structural limit state equations are the final element needed to develop the safe speed methodology. The IACS Polar Rules have well established procedures and guidelines to idealize the load patch parameters from calculated bow impact loads, and to determine the structural limit state equations from the plastic collapse mechanism. These procedures and guidelines are adopted in the present study.

Chapter 3

Material Models for Ice and Water (in LS DYNA)

3.1 Introduction

Material models are important to characterize the ice failure processes and to understand the water foundation effect in the icebreaking process. In general, the icebreaking process involves ice crushing and flexural failures which are influenced by the water foundation under ice. Three numerical tests are conducted in the commercial software package LS DYNA to develop material models of ice crushing failure, ice flexural failure and water foundation. This chapter provides a brief discussion of the icebreaking process explaining the ice failure processes and the water foundation effect, followed by a detailed procedure and methodology to develop these material models. A short discussion of the LS DYNA modeling approach is also presented in this chapter.

3.2 Ice Failure in Ship Icebreaking

Previous studies on ship-ice interaction process have shown that the icebreaking process is responsible for the local peak force. Therefore, only the icebreaking process is considered in this study. In general, an icebreaking process consists of edge crushing, flexural bending, and water foundation effect. A schematic diagram of the ship icebreaking process is shown in Figure 3.1.

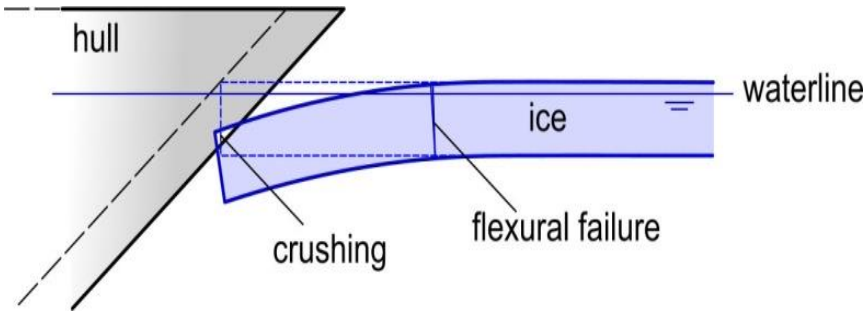

Figure 3.1 Fundamental ship icebreaking process

The ship icebreaking process is complex. The dynamic nature from ice inertia and water foundation makes the process even more complicated. When a ship interacts with ice at different velocities, the ice is subjected to dynamic loading. The ice behavior under this dynamic loading condition is drastically different from its behavior to a static loading condition. Therefore, it is very important to clearly understand the ice behavior and physics involved in ice failure when the ice is subjected to different dynamic loading conditions. This may facilitate the development of a simulation tool to better characterize the ship icebreaking process. The following sub-sections describe the ice crushing failure, flexural failure mechanisms and water foundation effect on the breaking process.

3.2.1 Ice Crushing Failure

When a ship interacts with the level ice, crushing takes place at the ice edge before flexural failure initiates and propagates. The crushing area at the contact interface increases as the ship advances. The normal impact force (F_n) also increases with the contact area until the flexural failure occurs. This normal impact force (F_n) can be determined from the nominal contact area (A_n) and average contact pressure using Eq. (3.1).

$$P_{avg} = \frac{F_n}{A_n} \tag{3.1}$$

The LS DYNA provides direct measurement of normal impact force. However, the contact area cannot be found easily. Daley [50] derived a number of useful contact area equations for different indentation geometry cases. These contact area equations are applicable to both ship-ice interaction and ice-structure interaction problems. Figure 3.2 is the indentation geometry of a wedge-shaped ice edge which is used to calculate the contact area. Daley's calculated contact area for an ice wedge is a function of hull geometry, hull position and ice wedge geometry. The contact area of an ice wedge is related to the ice wedge angle (θ), ship normal frame angle (β') and normal indentation (ζ_n). The equation for the contact area of an ice wedge edge is:

$$A_n = \frac{\zeta_n^2 . tan(\theta/2)}{sin\,\beta' . cos^2(\beta')} \tag{3.2}$$

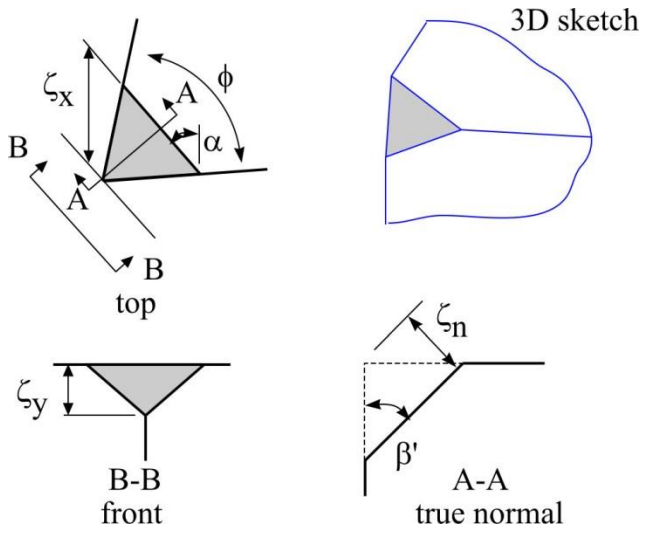

Figure 3.2 Indentation geometry of wedge-shaped ice for contact area calculation [50]

Direct measurement of normal impact force and the calculated contact area from Eq. (3.2) can be used to obtain the average contact pressure at the wedge-shaped ice edge from Eq. (3.1). In many studies this average contact pressure is assumed as constant over the whole contact area to determine the normal impact force [5, 21, 24, 53]. In reality, this contact pressure is not constant and changes with the contact area [4, 28]. It is mentioned earlier that the IACS Polar Rules adopted the pressure-area relationship to account for pressure variation at the contact interface. In the pressure-area relationship, the average contact pressure follows a decreasing pattern with the contact area as shown in Eq. (3.3).

$$P_{avg} = P_o A_n^{ex} \tag{3.3}$$

In Eq. (3.3), the nominal ice strength (P_o) is the pressure to crush 1 m^2 ice. This pressure-area relationship is also incorporated into the present study. To establish a pressure-area

relationship at the contact interface, the average pressure from the developed numerical model is calculated using Eq. (3.1) and tuned with a Polar class 1 (PC 1) pressure-area relationship given in Eq. (3.3). For PC 1 ships, the P_o is 6 MPa and the exponent (ex) is -0.1 [56]. The P_o value changes for other Polar class ships as shown previously in Table 2.3.

3.2.2 Ice Flexural Failure

A ship or sloping structure breaks the level ice in flexure. In flexure, when the vertical component of impact force exceeds the flexural limit, a flexural crack initiates and propagates. In general, the ice has much lower flexural strength (approximately 10 times less) than the crushing strength [54]. This can result in lower ice loads in flexural failure than for cases where the ice fails in crushing especially in thinner ice. Several analytical and semi-empirical models exist for the ice flexural failure. Most of these models express the failure load (F_f) as a function of ice flexural strength (σ_f), wedge angle (θ) and ice thickness (h). Kashteljan's bending failure model, given in Eq. (2.2), is widely used to predict the bending failure load. This semi-empirical model is based on the bearing capacity of a floating ice wedge. The model is rewritten here as this will be used for different comparative analysis in the present study:

$$F_f = C_f \left(\frac{\theta}{\pi}\right)^2 \sigma_f h^2 \tag{3.4}$$

The empirical coefficient (C_f) in Eq. (3.4) is approximately 1 for Kashteljan's model [14]. Daley and Kendrick [12] proposed a model similar to the Polar Rules flexural failure model as shown below:

$$F_f = C_f \sigma_f h^2 \theta \tag{3.5}$$

Daley and Kendrick [12] mentioned that the value of the coefficient C_f is 0.46 in the Polar Rules for a 150° wedge. Further, the C_f value is corrected to 0.39 by Daley and Kendrick. Equations (3.4) and (3.5) are applicable to the static or quasi-static conditions.

The ice flexural failure under a dynamic loading condition is significantly different from the static or quasi-static loading conditions. The ship with higher velocity is expected to experience a higher impact force from the ice. Unfortunately, there is no suitable dynamic flexural failure model available to explore this ship velocity effect. Therefore, a methodology is presented in Chapter 4 to estimate the dynamic flexural failure load based on different existing static load models and dynamic factor models.

3.2.3 Water Foundation Effect

Water under a floating ice sheet acts as an ideal elastic foundation for the ice. The foundation creates a hydrostatic pressure on the ice and influences the breaking process. In the presence of a foundation, the hull requires higher force to break the ice. Moreover, higher ship velocity modifies the hydrodynamic pressure of the water foundation and results in a significant increase in the ice load. The water foundation can be considered as a soft linear elastic material having a low modulus of elasticity (E_w) and standard water

density (ρ_w). The hydrostatic pressure (P_{hs}) can be expressed as a function of vertical deflection of the ice wedge (ϑ) in the following equation:

$$P_{hs} = \rho_w g \vartheta \tag{3.6}$$

3.3 Material Models for Ice and water

For a good ship icebreaking model, the selection of proper material models and input parameters are important. Three individual numerical tests are conducted to select the material models and parameters for the ice crushing behavior, ice flexural behavior and water foundation effect. The models and parameters are used in the final ship icebreaking model which will be described in Chapter 4. For the ice crushing material model, an ice crushing test is performed. A four point bending test provides the material model of ice flexure, and a simple foundation test is conducted to select the material properties of water foundation.

There are several commercial finite element software packages available. In this analysis, the LS DYNA is used to develop the material models for ice and water. The LS DYNA is widely used as a numerical tool for analyzing the impact and non-linear dynamic problems. It has a large collection of material models, and capable of modeling different material failure modes, crack initiation-propagation, crushing etc. A general guideline of the finite element methodology and modeling approach of LS DYNA is shown in Figure 3.3. The LS DYNA methodology and modeling approach for material models and properties of ice crushing, ice flexure and water foundation are described in Sub-sections

3.3.1 to 3.3.3. The LS DYNA Keyword files of these material models are presented in Appendix A.

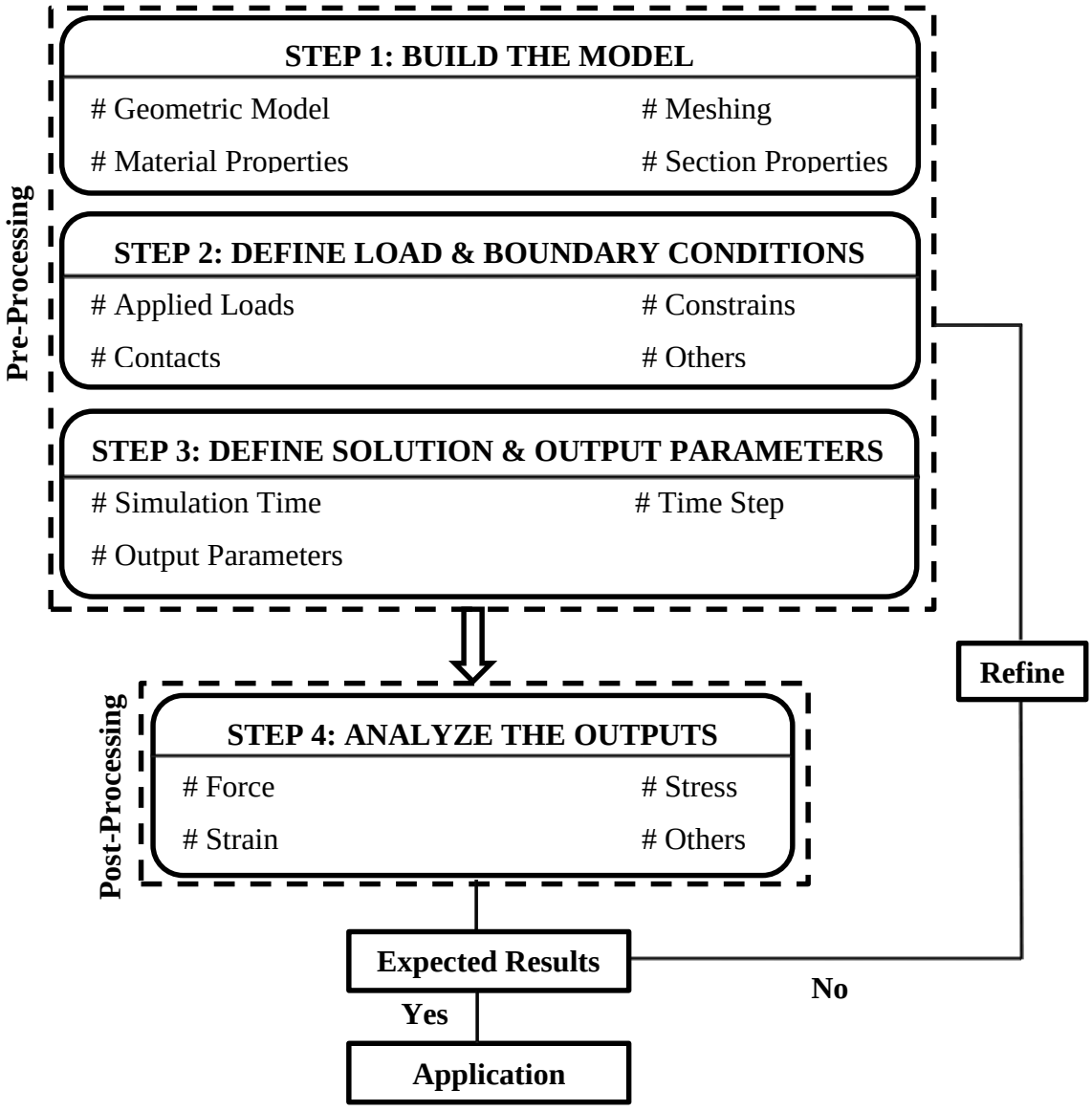

Figure 3.3 Methodology and modeling approach in LS DYNA

3.3.1 Material Model for Ice Crushing

An ice crushing test is performed to develop a material model for the ice crushing behavior. In this test, an inclined indenter impacts and crushes the edge of a short ice wedge. The geometric model of the crushing test is shown in Figure 3.4. The indenter is assumed as a rigid steel material and discretized with the shell elements. A simple elastic-perfectly plastic material model *MAT_PLASTIC_KINEMATIC is used for the ice wedge. The input parameters of the model are estimated from the physical and mechanical properties of ice. The compressive strength (σ_c) and Young's modulus (E) of ice are tuned to establish a similar pressure-area relationship suggested in the Polar Rules for PC 1. The details of the indenter and ice wedge are shown in Table 3.1 and 3.2, respectively.

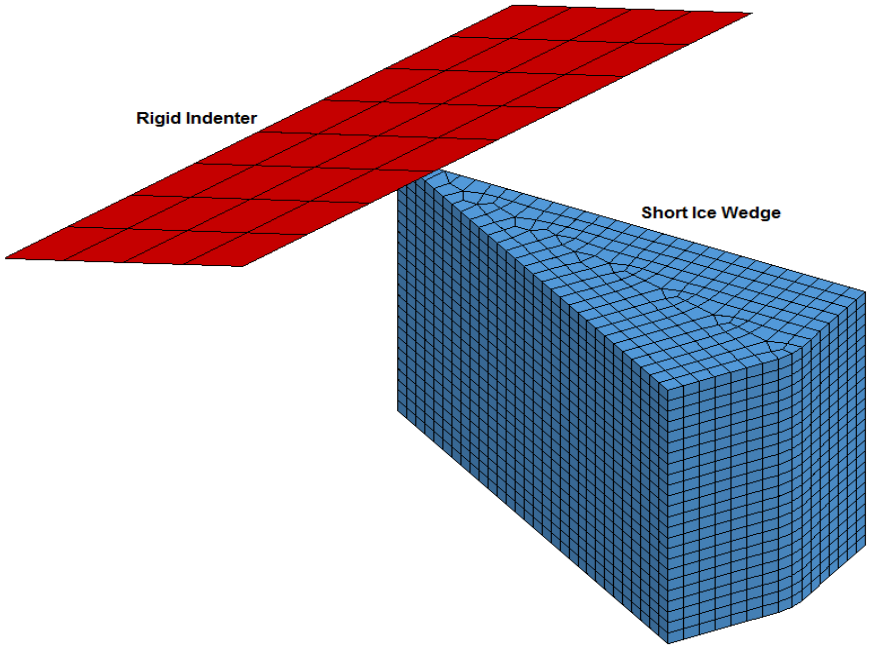

Figure 3.4 Geometric model of ice crushing test indicating indenter and short ice wedge

Table 3.1 Details of indenter in ice crushing test

Dimensions	2x4x0.37 m; 45^0 inclined
Element type	SHELL
Material card	*MAT_RIGID
Density, ρ	7850 kg/m^3
Young modulus, E	200 GPa
Poisson's ratio, υ	0.3

Table 3.2 Details of ice wedge in ice crushing test

Dimensions	30^0 wedge; 2 m thick; 3 m length
Element type	SOLID
Material card	*MAT_PLASTIC_KINEMATIC
Comp. strength, σ_c	4.5 MPa
Density, ρ	900 kg/m^3
Young modulus, E	5 GPa
Poisson's ratio, υ	0.3

In the test, the rigid indenter is moved horizontally towards the ice wedge with a velocity of 0.5 ms^{-1}. The bottom surface of the ice wedge is fixed in all DOFs. As the indenter advances, both the interface force and contact area are increased. Figure 3.5 indicates the change in Von-Mises stress distribution and crushing area at two different times.

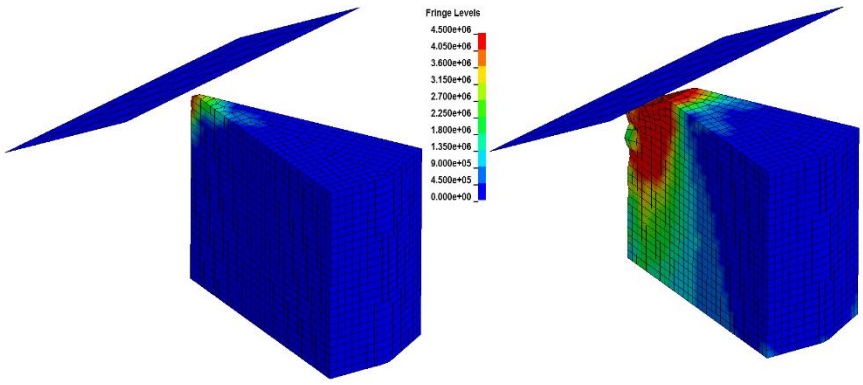

Figure 3.5 Von-Mises stress distribution and change in crushing area

The impact force time history is observed and recorded using the LS-PrePost software (also from lstc.com). For a 30^0 ice wedge and 45^0 indenter, the contact area in Eq. (3.2) can be written in terms of indenter velocity (V) and time interval (t):

$$A_n = 0.295\,(Vt)^2 \tag{3.7}$$

The normal impact force and contact area time histories from the crushing test are presented in Figure 3.6. The figure indicates that both the impact force and contact area increase with time.

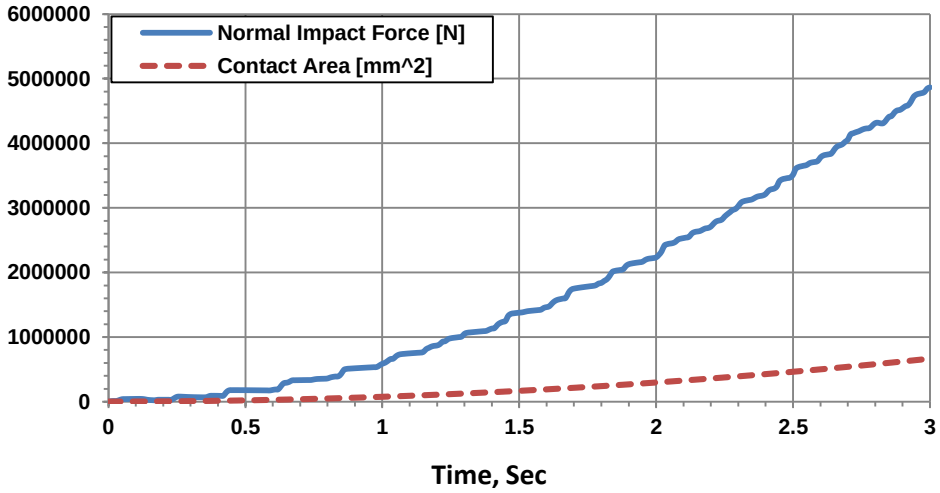

Figure 3.6 Normal impact force and contact area time histories in ice crushing test

A model pressure-area curve is established using the contact area and the normal impact force time histories given in Figure 3.6. This model pressure-area curve and the PC 1 pressure-area curve from Eq. (3.3) are plotted in Figure 3.7. The model results are in reasonable agreement with the PC 1 pressure-area relationship. Both the curves indicate the decreasing trends of average pressure with the contact area although there is some fluctuation about the mean trend in the model. The triangular shaped fluctuations in the model pressure–area curve are due to coarse element size in the crushing model. This coarseness of the element may influence the crushing failure pattern slightly but it will not affect the magnitude of bending failure load in the final numerical ship icebreaking model.

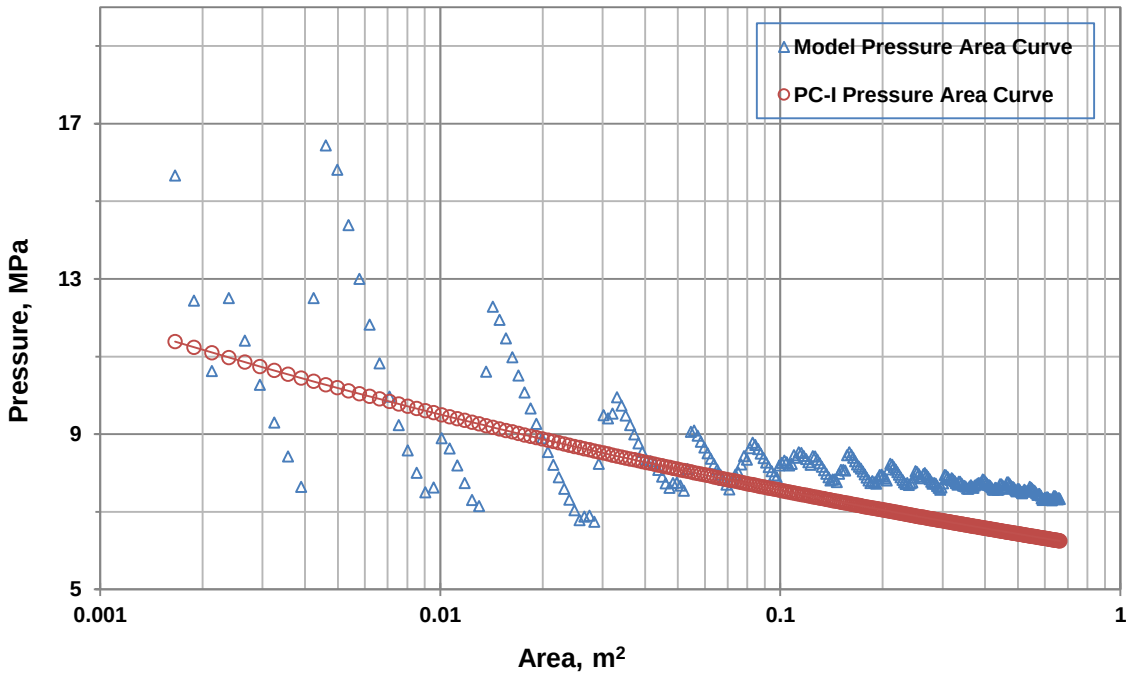

Figure 3.7 Comparison between model and PC 1 pressure-area curves

3.3.2 Material Model for Ice Flexure

Four point bending tests and in-situ cantilever beam tests are the most widely used and acceptable method to characterize the ice flexural failure behavior. Both the tests are capable of generating flexural cracks. The cantilever beam test with the element erosion modeling technique may exhibit some local crushing at the loading point. Therefore, the present study performs a numerical four point bending test in order to achieve pure ice flexure behavior. In this type of four point bending test, the whole beam between the two load points (loading supports) is subjected to be constant bending moment and is not affected by the direct compression below the load.

A similar geometric configuration of four point bending test used in Ehlers and Kujala [54] is considered in the present study. Ehlers and Kujala's four point bending test model and measurements do not provide all the required material parameters. Therefore, the present study utilizes different material input parameters and compares the test results with theoretical results.

From a four point bending test, it is possible to determine the maximum bending load and bending crack location. The theoretical failure load in bending (F_b) can be calculated from the following equation:

$$F_b = \frac{\sigma_f W H^2}{3D} \tag{3.8}$$

where, W, H and D are the beam width, height and distance between upper and lower supports, respectively. In a four point bending test, the maximum bending moment occurs

at the mid-section of the beam. Hence, the bending crack occurs in the mid-section. The material model of ice flexure is developed by comparing the model results with the theoretical bending loads calculated from Eq. (3.8), and by observing the crack locations.

In the test, the upper supports and lower supports are placed at a distance of 2 m and 0.5 m, respectively, from the center of the ice beam. The element type and material properties listed in Table 3.1 are used for all the supports. The geometric model of four point bending model is given in Figure 3.8.

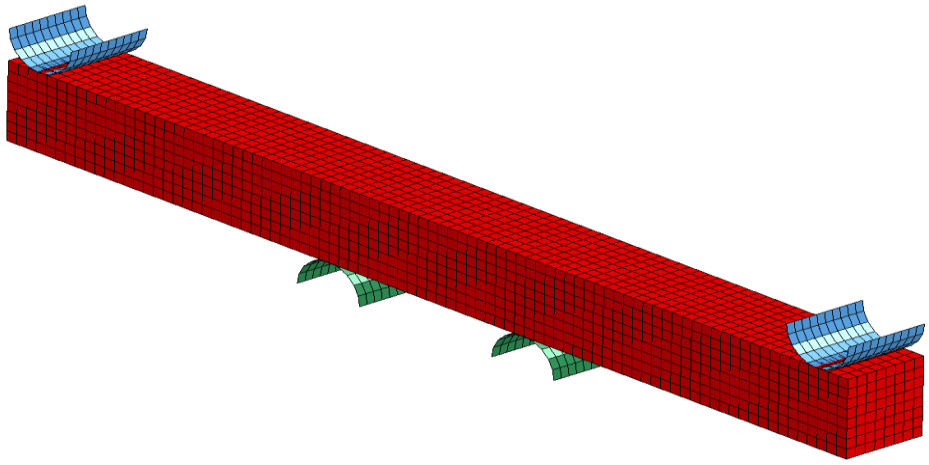

Figure 3.8 Geometric model of four point bending test

For the ice beam model, the input parameters are selected based on the physical and mechanical properties of sea ice [33, 54, 57, 63]. An isotropic elasto-plastic model, *MAT_PLASTICITY_COMPRESSION_TENSION is used to represent the ice flexural failure. The model requires several material parameters and curves. The main reason for selecting this material model is its ability to model different responses in compression and tension. Moreover, it can also account for the strain rate sensitivity. The details of geometric dimensions and material properties are given in Table 3.3.

Table 3.3 Details of ice beam in four point bending test

Dimensions	4.32x0.365x0.392 m; distance between upper and lower supports (D), 1.5 m
Element type	SOLID
Material card	*MAT_PLASTICITY_COMPRESSION_TENSION
Density, ρ	900 kg/m^3
Young modulus, E	5 GPa
Poisson's ratio, υ	0.3
Initial comp. strength, σ_c^o	5.8 MPa
Initial tensile strength, σ_t^o	$0.1\sigma_c^o$
Plastic hardening modulus, E_p	6 MPa
Effective plastic failure strain, ϵ_f	7.0e-4
Compressive mean stress, σ_{mc}	$\sigma_c^o/_3$
Tensile mean stress, σ_{mt}	$\sigma_t^o/_3$

Three different material curves are used in this analysis. Two different yield stress vs effective plastic strain curves are used, one for tension and one for compression. The third curve is a strain rate vs scaled compressive yield stress factor (CYSF) curve which is used to account for the strain rate effect on compressive strength. It is assumed that the flexural strength is independent of strain rate. Both the curves of yield stress (σ_y) vs effective plastic strain (ϵ_p) in tension and compression are developed from the following equation:

$$\sigma_y = \sigma_y^o + E_p\epsilon_p \tag{3.9}$$

where, the same plastic hardening modulus (E_p) is assumed for both the compression and tension. The initial compressive yield strength (σ_c^o) is calculated at 10^{-3} s^{-1} strain rate ($\dot{\epsilon}$) from the following equation given by Pernas-Sanchez et al. [9]:

$$\sigma_c^o = 10.976\dot{\varepsilon}^{0.093783} \tag{3.10}$$

The equation (3.10) indicates the relationship between the strain rate and compressive strength. This relationship was established based on several experimental results (Figure 3.9).

The initial yield strength in tension (σ_t^o) is assumed 10 times less than the initial compressive strength [54]. To formulate the strain rate vs compressive yield stress scale factor (CYSF) curve, the initial compressive strengths at different strain rates are determined from Eq. (3.10). These compressive strengths are further normalized with the compressive strength (5.8 MPa) at 10^{-3} s^{-1}. The Strain rates and the corresponding compressive yield stress scale factors (CYSF) are shown in Table 3.4.

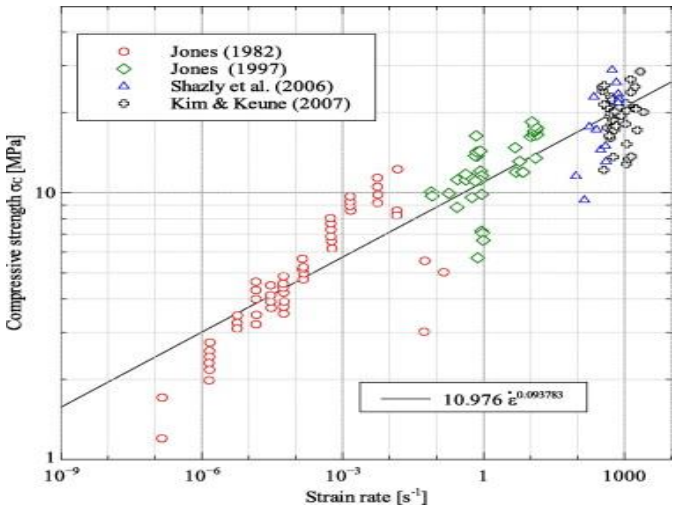

Figure 3.9 Relationship between compressive strength and strain rate [9]

Table 3.4 Strain rates and compressive yield stress scale factors

$\dot{\epsilon}$, s^{-1}	CYSF	$\dot{\epsilon}$, s^{-1}	CYSF
10e-9	0.27	10e-2	1.22
10e-8	0.336	10e-1	1.52
10e-7	0.417	1.0	1.89
10e-6	0.52	10.0	2.348
10e-5	0.643	100.0	2.91
10e-4	0.8	1000.0	3.62
10e-3	1.0		

An equivalent plastic strain failure criterion is used in this analysis. When the equivalent plastic strain of an element reaches the defined critical value (ϵ_f), the element is deleted. The ϵ_f value is adjusted to get the proper bending response.

To achieve bending failure at quasi-static condition, the lower supports are given an upward velocity of 0.001 ms^{-1}. The upper supports are constrained in all DOFs, while the lower supports are allowed only to move in the vertical direction. The reaction force, between the ice beam and supports, increases with time until it reaches the flexural limit of ice. The effective plastic failure strain value is tuned until the bending crack is observed at the mid section of the beam and the model bending load is close to the theoretical bending load. Figures 3.10 and 3.11 indicate the bending crack formation and force-time history obtained from the four point bending test. Figure 3.11 indicates that the ice beam fails at 7.74 kN which is close to the analytical failure load (7.78 kN) calculated from Eq. (3.8).

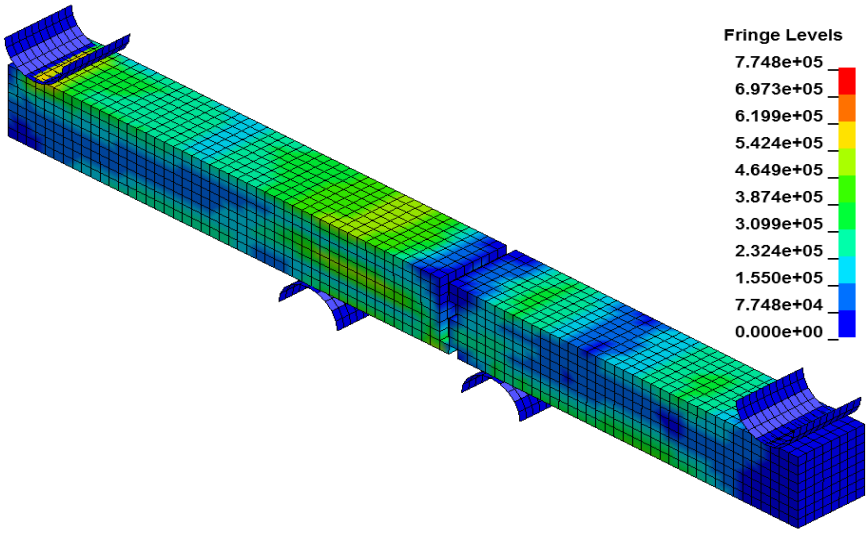

Figure 3.10 Bending failure of ice beam in four point bending test

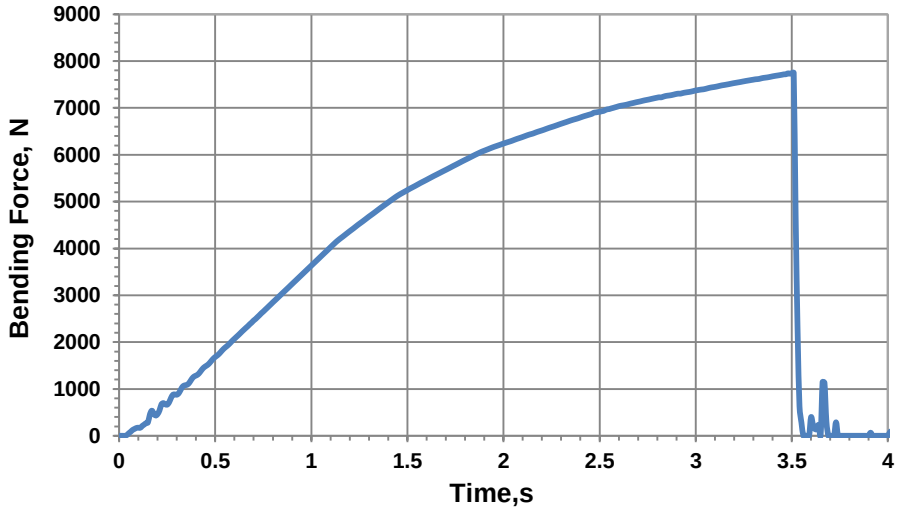

Figure 3.11 Force-time history in four point bending test

It should be noted that the material properties of this model are different from the Ehlers and Kujala's [54] four point bending test models and measurements. Therefore, the force time history obtained from this model cannot be compared with the Ehlers and Kujala's four point bending test results.

3.3.3 Material Model for Water Foundation

Modeling of a fluid medium or water foundation is still a big challenge. The existing material models of water foundation are complicated and computationally expensive. Therefore, an alternative and simple methodology is introduced here to develop the material model of water foundation which provides an equivalent hydrostatic pressure on the bottom surface of the ice wedge.

Simple foundation tests are conducted to select the material properties of water foundation. The test is carried out for three different ice thicknesses (h) and four different wedge angles (θ). The foundation is assumed as a linear elastic material, and modeled with the material card *MAT_ELASTIC. The dimensions and elastic modulus are adjusted to match as close as possible to the hydrostatic pressure of water on the lower ice surface. The details of water foundation are given in Table 3.5.

Table 3.5 Details of water foundation

h, θ	**Dimensions LxWxH**	**Density, ρ_w**	**Young modulus, E_w**
0.5, 30^0	8.5x4.6x1.7 m		13.63 kPa
1.0, 30^0	16x9x1.8 m		17.4 kPa
1.5, 30^0	24.7x15x3 m		29.3 kPa
0.5, 45^0	8.5x6.8x0.8 m		7.78 kPa
0.5, 60^0	8.5x8.6x0.8 m	1000 kg/m^3	8.0 kPa
1.0, 45^0	16x13.1x1.8 m		17.0 kPa
1.5, 60^0	24.7x26.7x3 m		28.4 kPa
0.5, 150^0	8.5x15.8x1.7 m		15.32 kPa

In these tests, the ice wedge is assumed as a rigid solid body so that the reasonable Young modulus values of water foundation can be obtained within efficient computational time. The rigid material properties listed in Table 3.1 are used for the ice wedge. Figure 3.12 indicates the geometric model of water foundation test for a 0.5 m thick and 30^0 ice wedge on the elastic foundation.

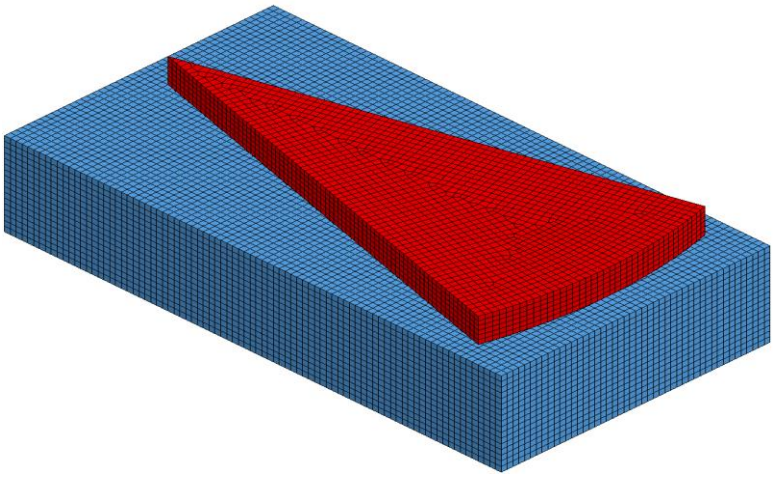

Figure 3.12 Geometric model of water foundation test for 0.5 m thick and 30^0 ice wedge

In these tests, the ice wedges are allowed to move vertically downward with a velocity of 0.001 ms^{-1}. The bottom and side faces of the water foundation are fixed in all DOFs. The contact card CONSTRAINT_NODES_TO_SURFACE is assigned to define the contact between the ice wedges and water foundations. The interface pressure between the ice wedges and foundations is measured by a numerical force sensor (FORCE_TRANSDUCER_CONSTRAINT). The interface pressure distribution for the 0.5 m thick ice wedges with 30^0 and 60^0 opening angles are shown in Figure 3.13 and 3.14, respectively. These figures indicate that a higher surface area on the water

foundation is required to capture the complete interface pressure distribution of an ice wedge with a higher opening angle. Therefore, the dimensions of the water foundations are varied for different ice wedge angles as shown in Table 3.5. The dimension of water foundation for the higher ice wedge angle (150^0 wedge) would be used for other cases. However, this is not recommended for the lower ice wedge angles because of computational efficiency.

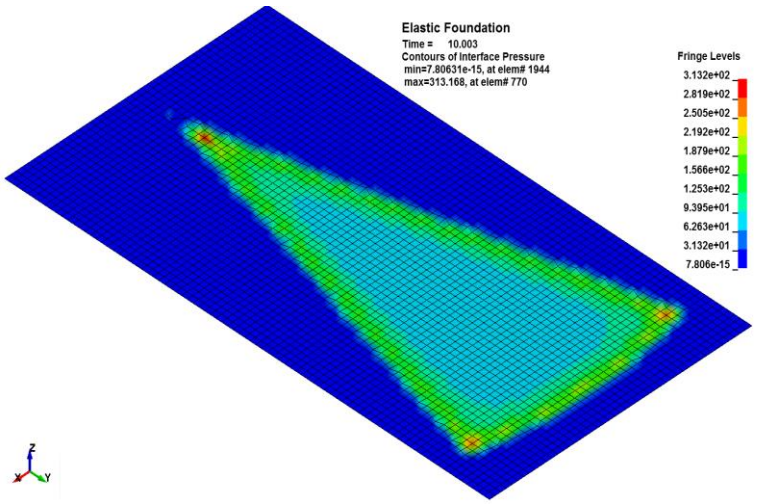

Figure 3.13 Interface pressure distribution for 0.5 m thick and 30^0 ice wedge

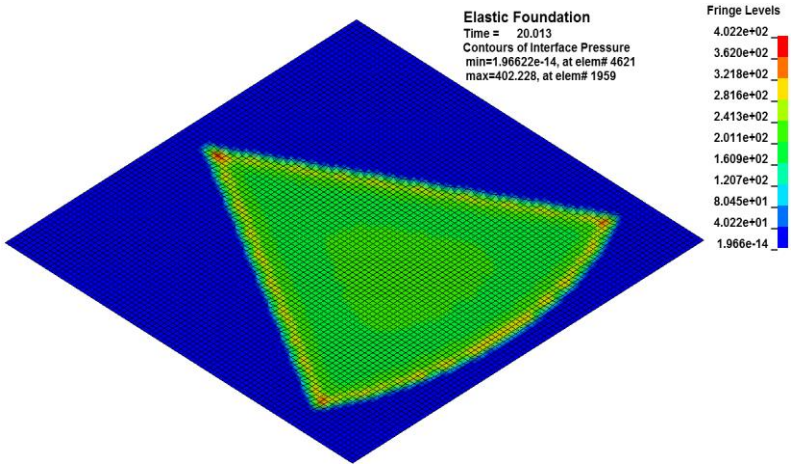

Figure 3.14 Interface pressure distribution for 0.5 m thick and 60^0 ice wedge

The interface pressure time history is recorded and used to establish a relationship between the average hydrostatic pressure and vertical deflection of the ice wedge. The pressure deflection curve in Figure 3.15 provides a slope of 9778.9 Pa/m which is equivalent to the theoretical value calculated from Eq. (3.6). Similar results are obtained for other test conditions.

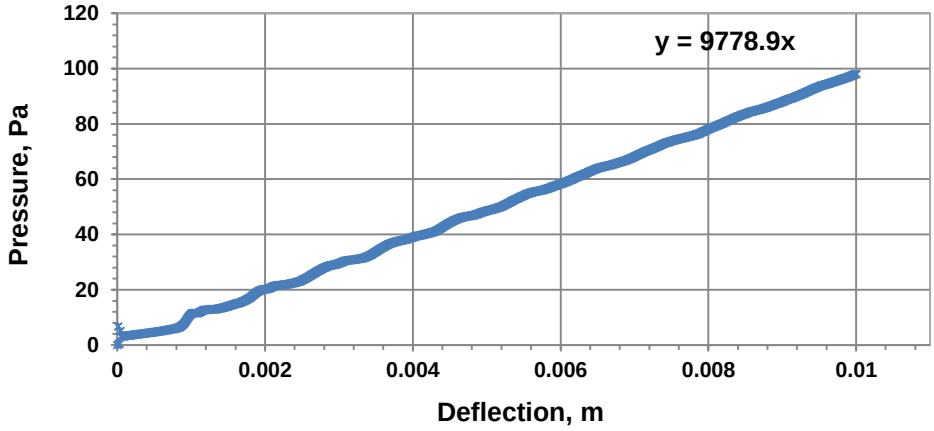

Figure 3.15 Pressure deflection curve for 0.5 m thick and 30^0 ice wedge

It should be noted that the primary objective of developing simplified material models is to capture the overall ship icebreaking scenario especially the ice flexural behavior. For faster and more stable solution, some compromises are done with the overall quality of the ice crushing model and water foundation model. The element size in the crushing model is relatively coarse which causes the triangular shaped fluctuations in the pressure-area curve. The water foundation is modeled as a "soft" solid rather than a fluid which would require use of ALE or other expensive fluid modeling techniques.

For the four point bending test, the sensitivity study focusing on the beam element size and input parameters is not extensively carried out into the present study. In the test, the effective plastic failure strain is tuned to obtain proper bending responses instead of refining the beam element size in several steps. The effective plastic failure strain is strongly dependent on the element size. Therefore, the tuning process with the effective plastic failure strain value can also be called as mesh convergence study.

Due to the lack of specific physical test data and model scale data under different loading conditions, all the material models are developed at static or quasi-static loading conditions. However, the material models are expected to exhibit some velocity effect under dynamic loading conditions due to the body dynamics and inertia. The numerical ship icebreaking models in Chapter 4 exhibit this velocity effect when they utilize these material models.

Nevertheless, the developed material models are useful to simulate the ice crushing behavior, ice flexural behavior and water foundation effect. The models can also be used to investigate the ship-ice interaction problems.

Chapter 4

Numerical Model of Ship Icebreaking

4.1 Introduction

This chapter presents numerical models of the ship icebreaking process to explore the velocity effect on ice flexural failure. These numerical models account for the ice edge crushing, ice flexural failure and water foundation effect. The material models developed in Chapter 3 are incorporated into these ship icebreaking models. Two breaking conditions; an ice wedge breaking condition and a level icebreaking condition are considered for the head-on collision and shoulder collision scenarios. For the ice wedge breaking, the effect of ship velocity on the breaking process is investigated for different ship angles, ice wedge angles and ice thicknesses. The level icebreaking is investigated with and without existing radial cracks for three different breaking conditions.

In the absence of a standard dynamic ice load model, a simple methodology is presented to formulate four dynamic ice load models based on existing static load models and

dynamic factor models. Two existing analytical/semi-empirical formulas are also presented to predict the ice wedge breaking length. To validate the numerical models, the results are compared with the formulated dynamic ice load models and presented breaking length formulas. The developed numerical models of ship icebreaking as well as the formulated dynamic ice load models can be useful in estimating the ice load on the ship or offshore structure.

4.2 Numerical Model of Ship Icebreaking

The numerical models of ship icebreaking consider two collision scenarios. One is the head-on collision with a flat inclined face of ship, and another is the shoulder collision with an R-Class ship. For the head-on collision, two breaking conditions are considered; the ice wedge breaking and level icebreaking. The shoulder collision is only investigated for the level icebreaking. Both the collision scenarios with all the ship icebreaking conditions are numerically modeled using the commercial FEM software package LS DYNA. Sub-sections 4.2.1 and 4.2.2 describe the LS DYNA modeling approach for these two collision scenarios. Appendix B consists of the LS DYNA keyword files for the ship icebreaking models.

4.2.1 Head-on Collision with Flat Inclined Face of Ship

For the head-on collision, two icebreaking scenarios are considered; a simple ice wedge breaking and a level icebreaking. A rigid ship with a flat inclined face is considered to study this head-on collision. The front inclined face of the ship results in a waterline

angle (α) of 90^0. This simple ship shape allows the investigation of the striking angle effect on the icebreaking process. In a real ship type, the striking angle is equivalent to the normal ship frame angle (β').

4.2.1.1 Simple Ice Wedge Breaking

The numerical model of ship and simple ice wedge consists of three main components; a rigid ship, a cantilever ice wedge and a water foundation. In the model, a flat inclined face of the rigid ship impacts the edge of a cantilever ice wedge. The ice wedge rests on the water foundation. Figure 4.1 shows the geometric model of the rigid ship. The material properties for the rigid indenter mentioned in Table 3.1 are also used for this ship.

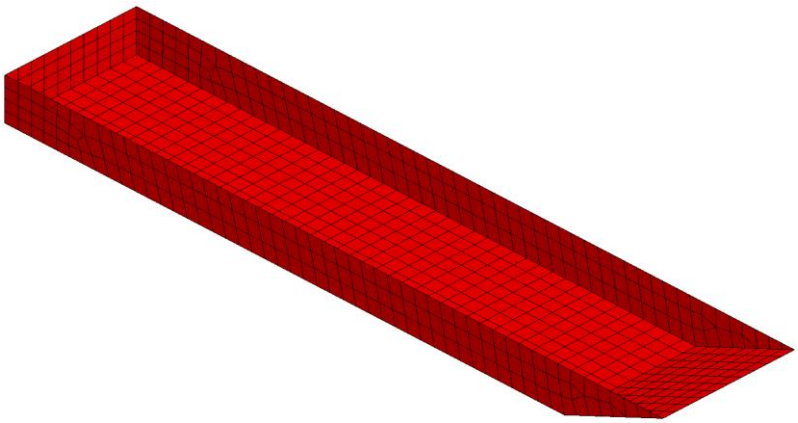

Figure 4.1 A rigid ship for ship icebreaking model

The ship is discretized with the shell elements, and constrained in all DOFs except the horizontal direction. Three different normal ship frame angles are considered. The principal dimensions of the ship are shown in Table 4.1.

Table 4.1 Principal dimensions of ship

Parameters	Value
Length, L	100 m
Beam, B	20 m
Depth, D	7 m
Normal ship frame angle, β'	45^0, 55^0, 65^0

For the ice wedge models, three different ice thicknesses (0.5 m, 1.0 m and 1.5 m) and three different ice wedge opening angles (30^0, $45^0$and 60^0) are considered. These ice wedges have two distinct zones; the ice crushing zone and the ice bending zone as shown in Figure 4.2. Both zones share common nodes and no duplicate node exists between these two zones. The length of these wedges is 15h having crushing zone length of 1.85h. It is assumed that no bending failure occurs within this crushing zone. The ice crushing material model developed earlier is used for this zone. The remaining portion of the ice wedges is the bending zone. The material properties mentioned in sub-section 3.3.2 are used for this zone.

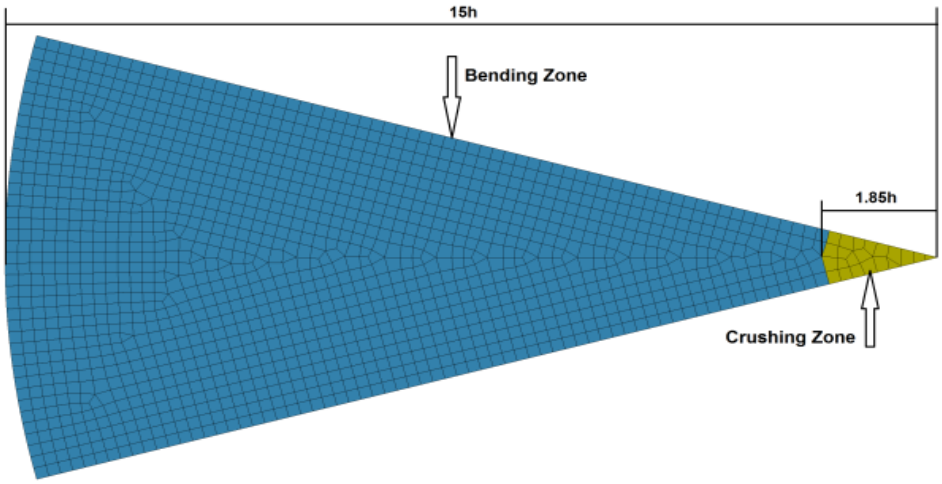

Figure 4.2 Top view of ice wedge indicating ice crushing and bending zones

The Element Erosion Method (EEM) is used in this model to obtain ice bending failure. In this method, when the equivalent plastic strain of an element reaches the defined critical value (ϵ_f), the element is deleted. The critical value (ϵ_f) is highly dependent on the element size. The ice wedge is meshed such that the same element-length ratio, used in the four point bending test, is maintained in the analysis.

The dimensions and material properties in Table 3.5 are used for water foundation modeling. The bottom and side faces of the water foundation are fixed in all DOFs. The final ship icebreaking model is shown in Figure 4.3.

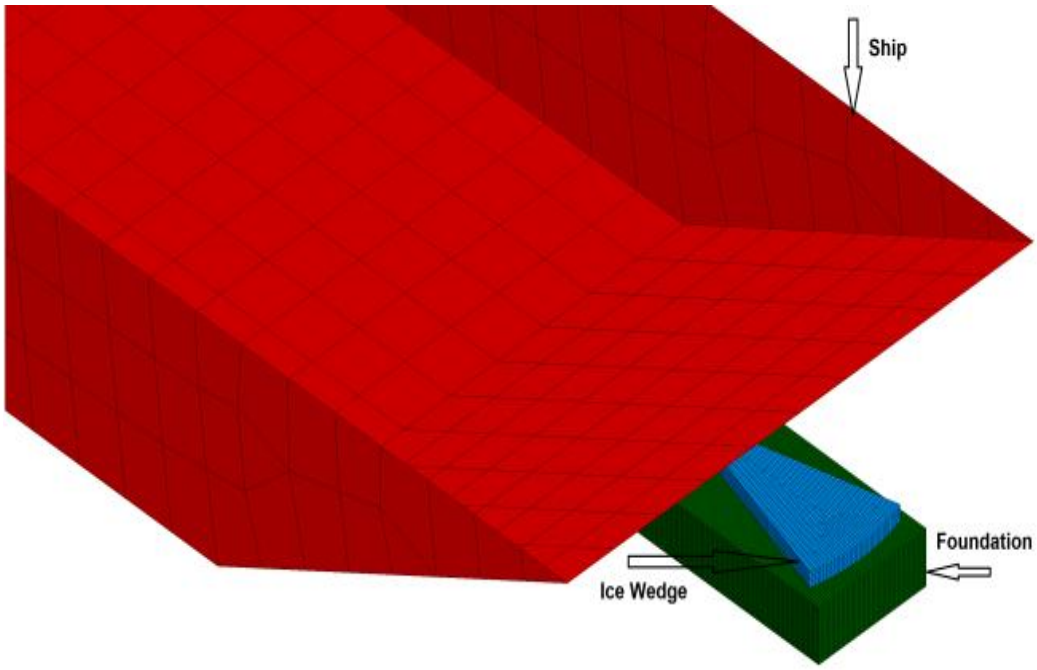

Figure 4.3 Final model of ship ice wedge breaking process in head-on collision

The model requires proper contact definition between the components. The AUTOMATIC_NODES_TO_SURFACE contact model is used to define the interaction between the ship and ice crushing zone. The water foundation is constrained to the ice wedge with the CONSTRAINT_NODES_TO_SURFACE model. It is assumed that no interaction takes place between the ship and water foundation. The time step factor in the model is set to 0.6 for stable solution. The final model code is compiled using the LS DYNA Program Manager, and runs until the ice beam fails in flexure.

4.2.1.2 Level Icebreaking (150^0 Ice Wedge)

For the level icebreaking conditions, a similar numerical approach of simple ice wedge breaking is used. The ice wedge with 150^0 opening angle is assumed as equivalent to the level ice sheet. Three breaking conditions are considered to study the effect of radial cracks. The first condition is the breaking of single 150^0 ice wedge without any radial crack. The second condition is the breaking of ice wedge with two radial cracks. The ice wedge with two radial cracks consists of three 50^0 ice wedges. The third condition is the breaking of five 30^0 wedges which contain four radial cracks. The radial cracks separate the ice wedges with duplicated nodes. These duplicated nodes create area of weakness between two adjacent wedges which represent the existing radial crack in the level ice. This analysis is performed for a normal ship frame angle of 65^0 and ice thickness of 0.5 m. Figure 4.4 is the geometric model of ship level icebreaking for five 30^0 wedges rested on the water foundation.

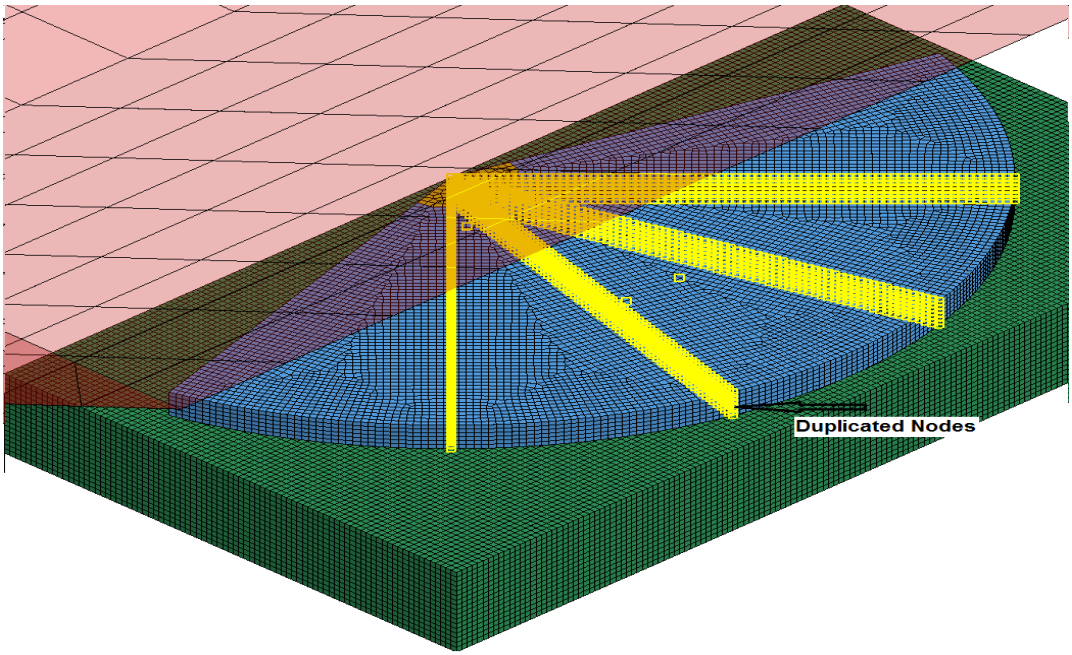

Figure 4.4 Ship level icebreaking in head-on collision indicating wedges separated with duplicated nodes

4.2.2 Shoulder Collision with R-Class Ship

This sub-section demonstrates the modeling of shoulder collision scenario with a real ship type similar to the IACS Polar design scenario. In this model, the level ice or 150^0 ice wedge interacts with the shoulder region of an R-Class ship. The R-Class ship is constructed from the ship parameters, bodylines and body planes diagram given in Makinen et al. [71]. Only the front half portion of the ship is considered here. At the contact point, the waterline angle and normal ship frame angle are 32.5^0 and 55^0, respectively. The level icebreakings with four radial cracks and without a radial crack are investigated. Figure 4.5 is the collision model for the R- Class ship with the level ice.

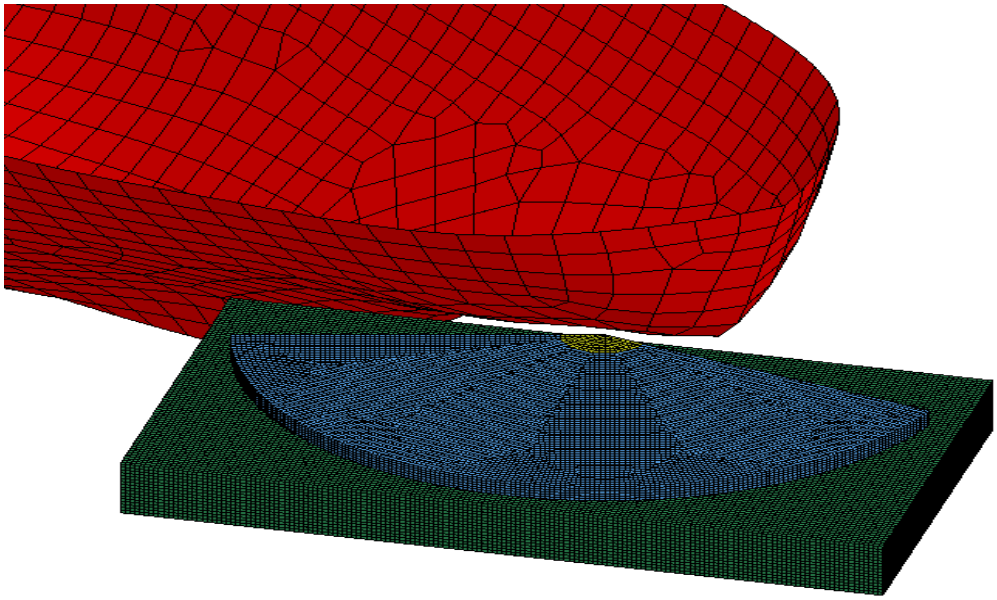

Figure 4.5 Shoulder collision with R-Class ship

4.3 Model Results and Analysis

The numerical results of icebreaking process for both the collision scenarios are presented here. The effect of ship velocity on the impact force and ice failure pattern is investigated for all the icebreaking processes.

4.3.1 Simple Ice Wedge breaking in Head-on Collision

Velocity Effect on Breaking Pattern

The Von Mises stress distribution and failure pattern of the simple ice wedge breaking for different breaking conditions are shown in Figures 4.6a to 4.6g. These figures indicate that the crushing is observed at the edge for all the breaking conditions. The circumferential bending crack initiates and propagates in the bending zone. For a

particular ship frame angle, ice thickness and ice wedge; the bending crack location shifts towards the ice crushing zone at higher ship velocity (Figures 4.6a to 4.6d). These figures also indicate that the bending crack location and breaking pattern are influenced by the wedge angle (Figure 4.6a and 4.6e), ice thickness (Figure 4.6c and 4.6f) and normal ship frame angle (Figure 4.6b and Figure 4.6g).

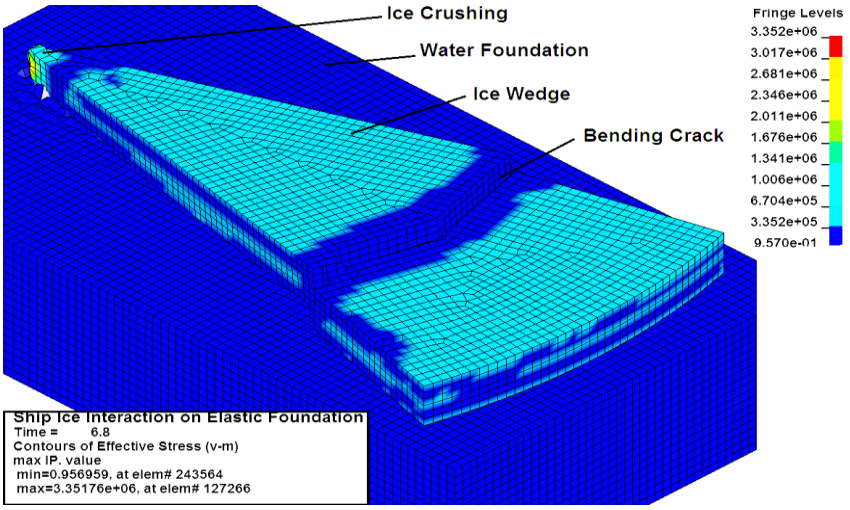

Figure 4.6a Simple ice wedge breaking pattern (h=0.5 m, $\beta'=65^0$, $\theta= 30^0$, V=0.1 ms^{-1})

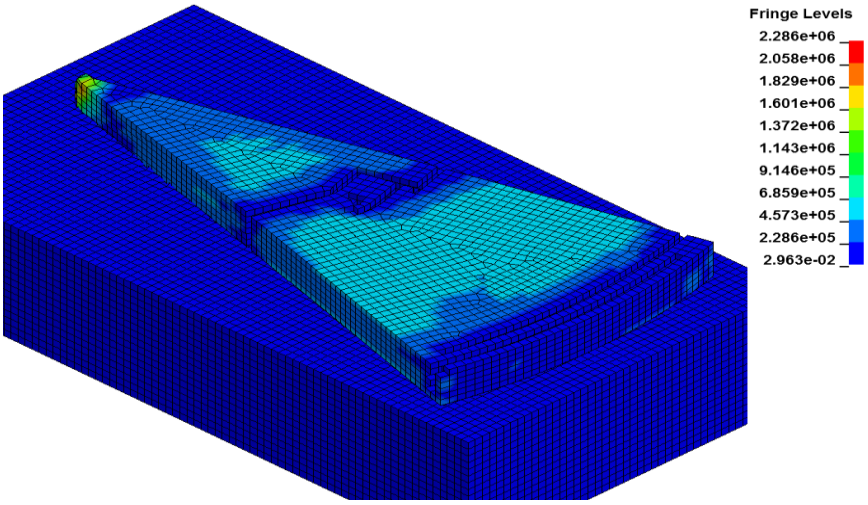

Figure 4.6b Simple ice wedge breaking pattern (h=0.5 m, $\beta'=65^0$, $\theta= 30^0$, V=0.5 ms^{-1})

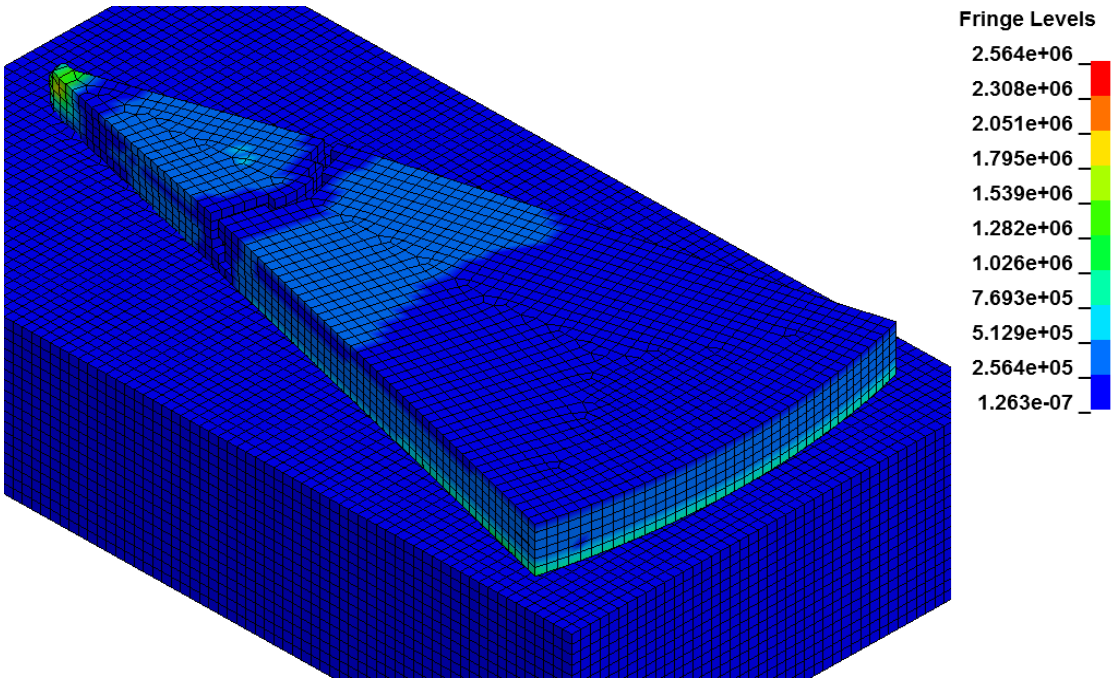

Figure 4.6c Simple ice wedge breaking pattern (h=0.5 m, $\beta'=65^0$, $\theta= 30^0$, V=1.0 ms^{-1})

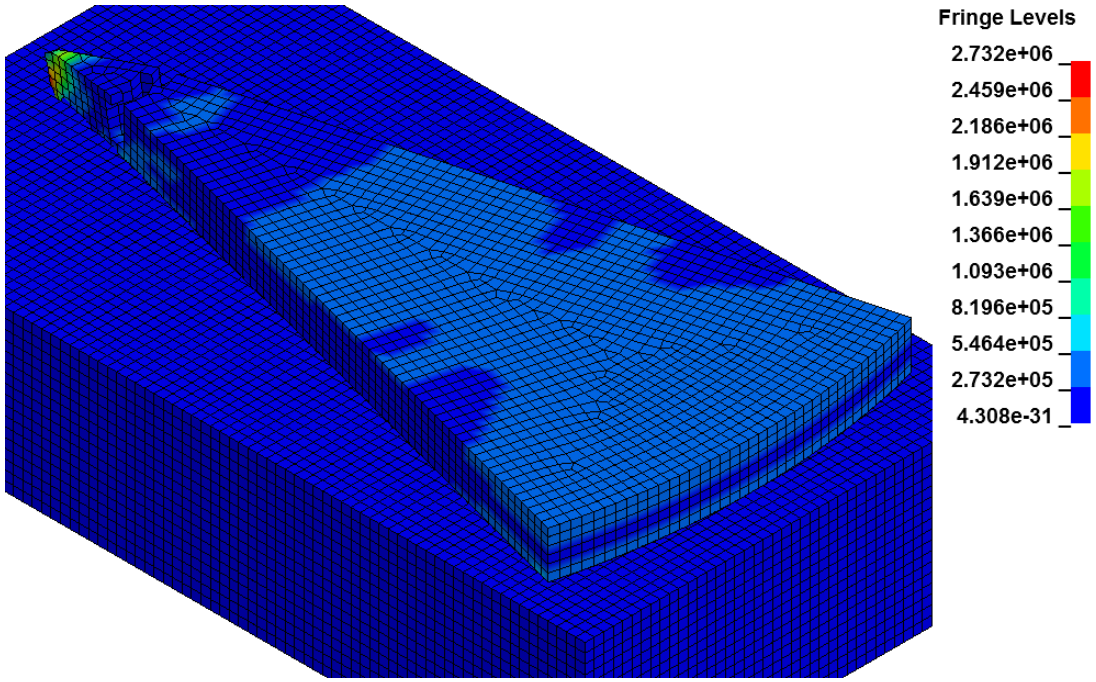

Figure 4.6d Simple ice wedge breaking pattern (h=0.5 m, $\beta'=65^0$, $\theta= 30^0$, V=5.0 ms^{-1})

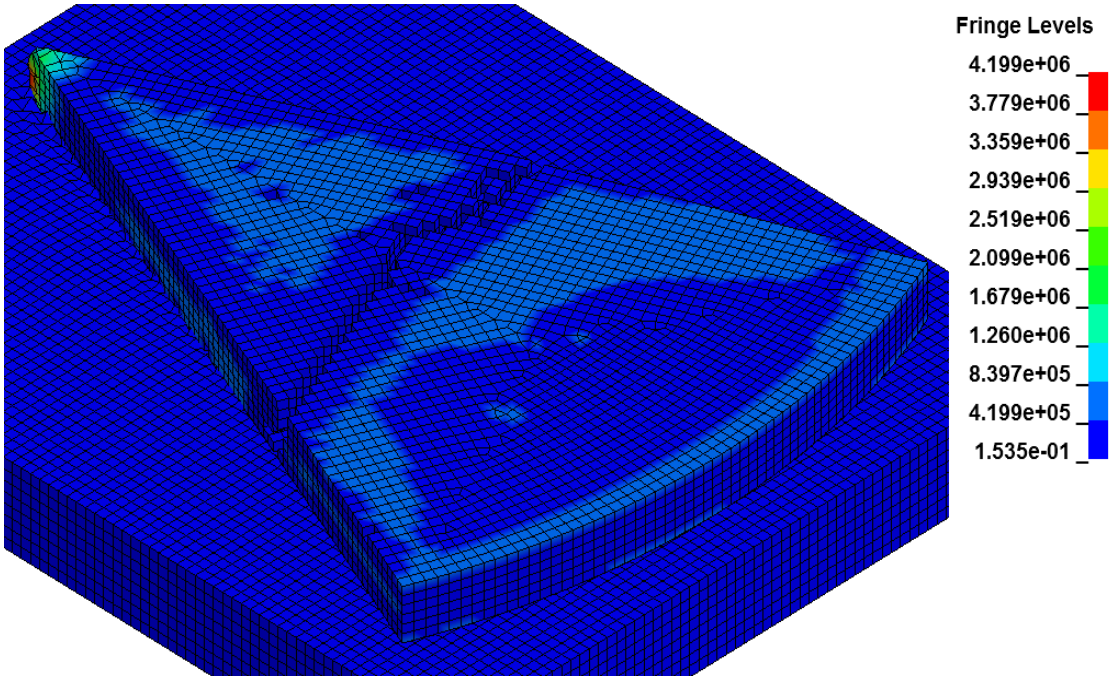

Figure 4.6e Simple ice wedge breaking pattern (h=0.5 m, $\beta'=65^0$, $\theta= 45^0$, V=0.1 ms^{-1})

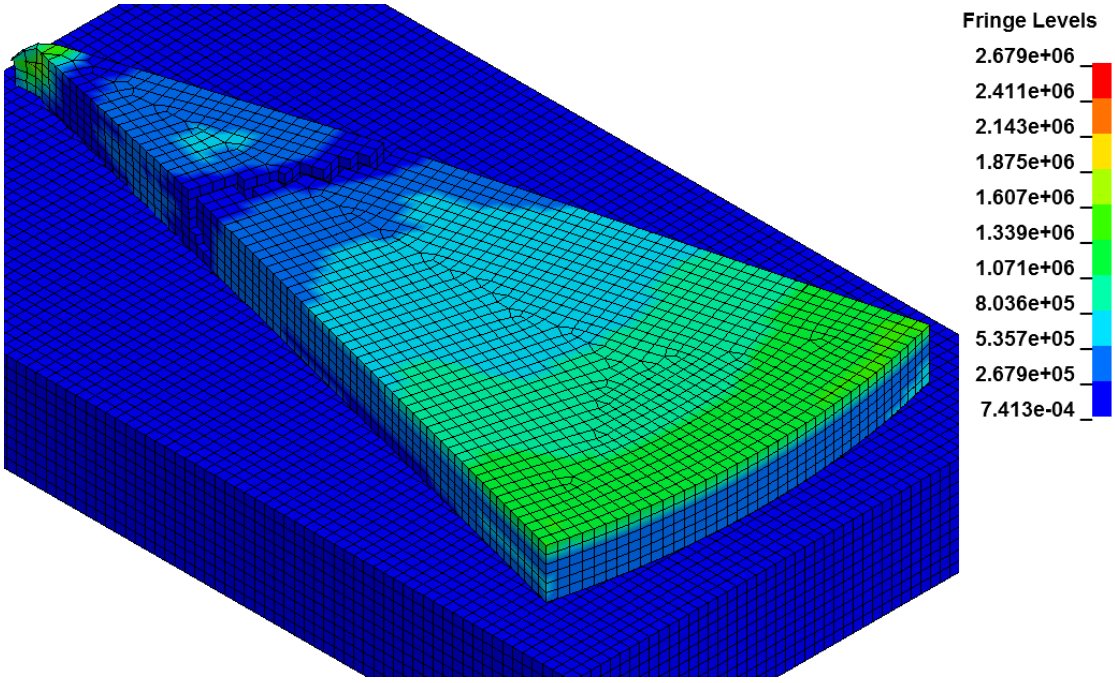

Figure 4.6f Simple ice wedge breaking pattern (h=1.5 m, $\beta'=65^0$, $\theta= 30^0$, V=1.0 ms^{-1})

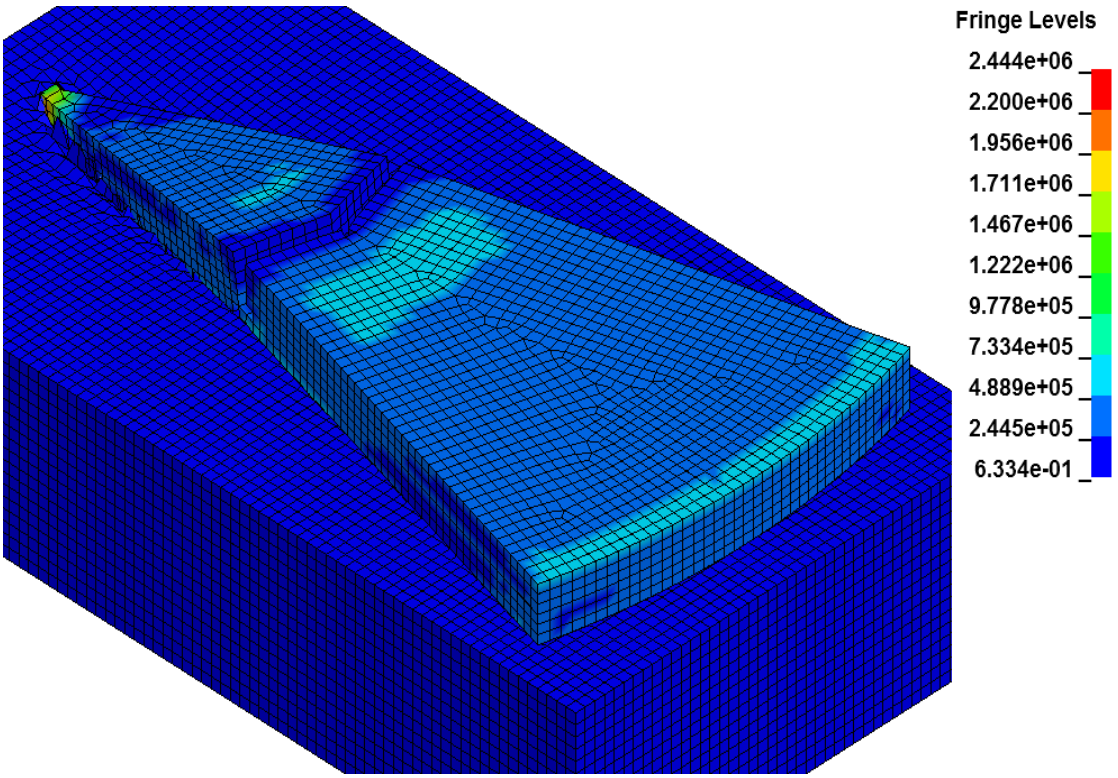

Figure 4.6g Simple ice wedge breaking pattern (h=0.5 m, $\beta'=45^0$, $\theta= 30^0$, V=0.5 ms^{-1})

Velocity Effect on Impact Force

The normal impact force time histories at different ship velocities are given in Figures 4.7a to 4.7c. These figures indicate that the impact force increases with time and reaches a maximum value where the flexural failure occurs. These figures also indicate that the ship with a higher velocity takes less time to fail and experiences a higher impact force from the ice wedge; for a constant ship frame angle, ice thickness and ice wedge. The maximum impact force and failure time for different ice conditions and ship velocities are recorded and plotted in Figures 4.8a, 4.8b.

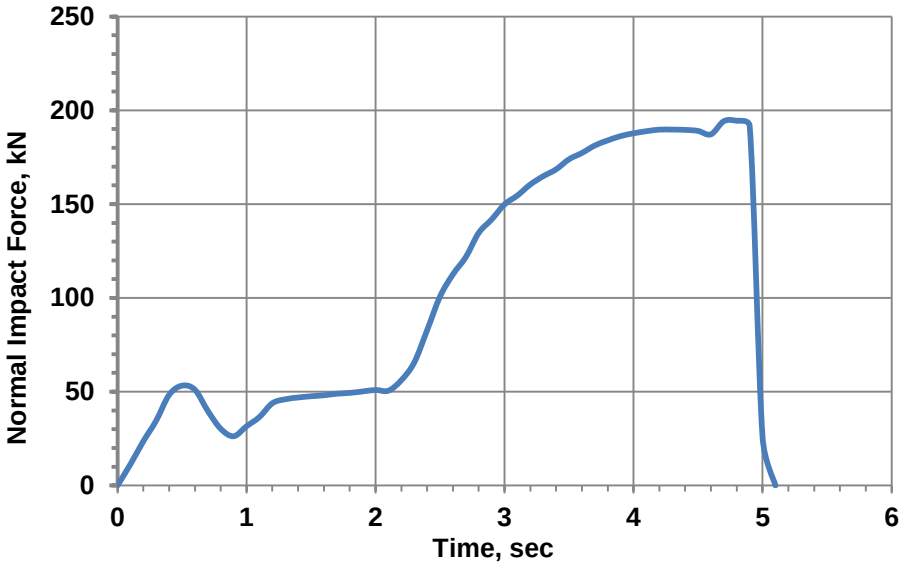

Figure 4.7a Impact force vs time in simple ice wedge breaking (h=1.0 m, $\beta'=65^0$, $\theta= 45^0$, $V=0.1\ ms^{-1}$)

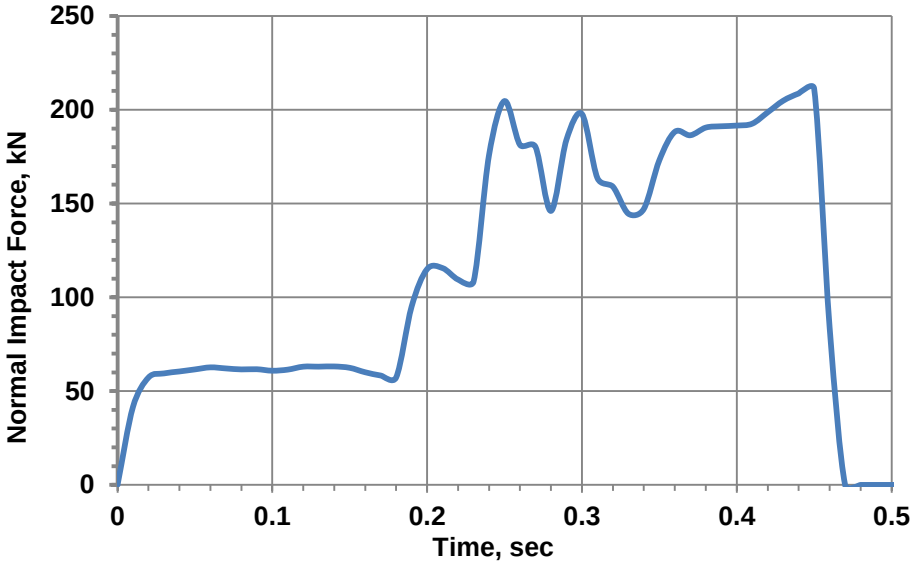

Figure 4.7b Impact force vs time in simple ice wedge breaking (h=1.0 m, $\beta'=65^0$, $\theta= 45^0$, $V=1.0\ ms^{-1}$)

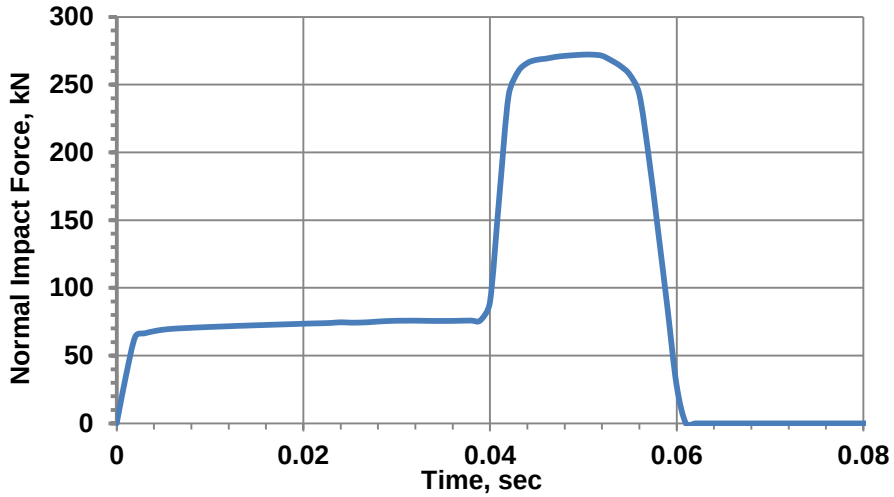

Figure 4.7c Impact force vs time in simple ice wedge breaking (h=1.0 m, $\beta'=65^0$, $\theta= 45^0$, V=5.0 ms^{-1})

Figures 4.8a and 4.8b indicate that the impact force increases and the failure time decreases with the ship velocity. These figures also indicate that the thicker ice requires higher impact force and longer time to fail for a given ship velocity.

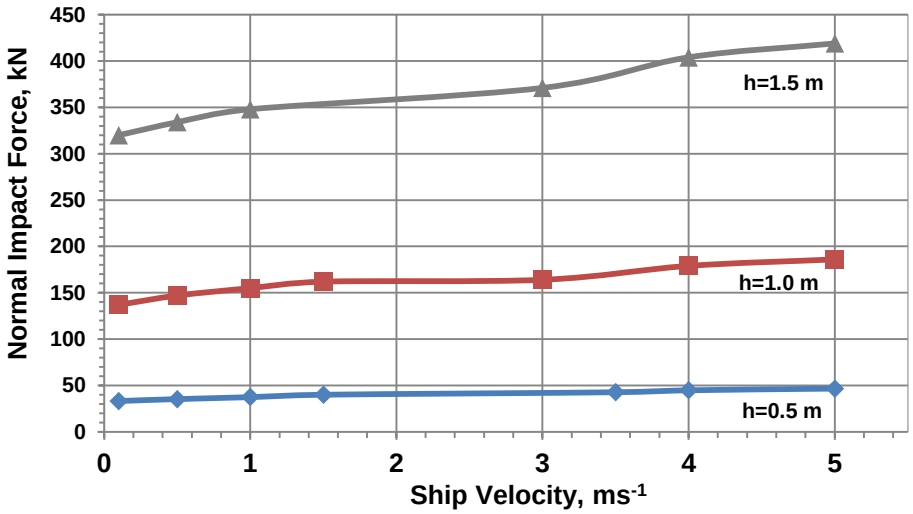

Figure 4.8a Impact force vs velocity in simple ice wedge breaking for different ice thicknesses ($\beta'=65^0$, $\theta= 30^0$)

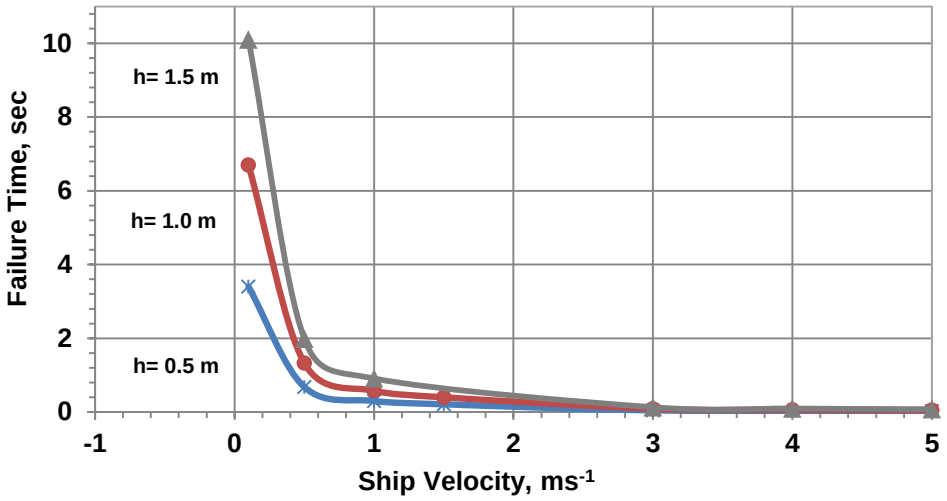

Figure 4.8b Failure time vs velocity in simple ice wedge breaking for different ice thicknesses ($\beta'=65^0$, $\theta= 30^0$)

Figure 4.9 illustrates the ship velocity effect on the impact force for different ice wedge angles. The figure indicates that the ice wedge with higher opening angle produces higher impact force for a given ship shape and ice thickness.

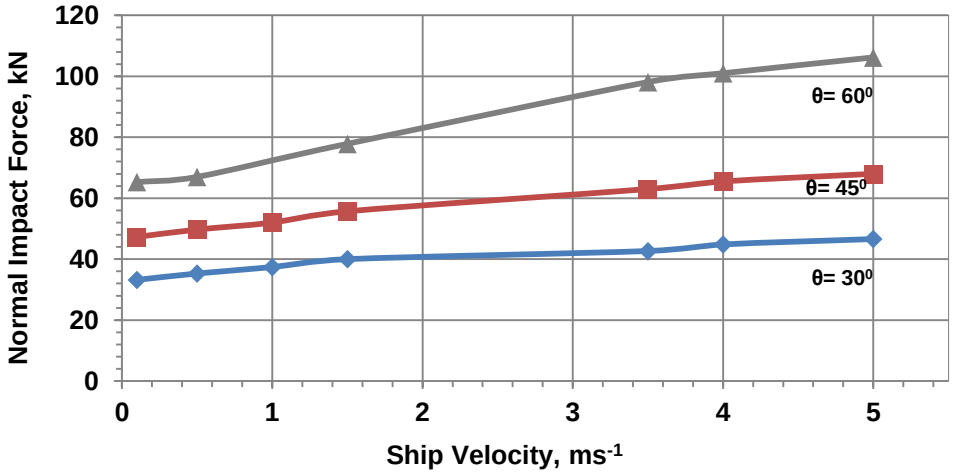

Figure 4.9 Impact force vs velocity in simple ice wedge breaking for different wedge angles (h=0.5 m, $\beta'=65^0$)

Figure 4.10 demonstrates the effect of ship velocity on the impact force for different normal ship frame angles. This figure indicates that the ship with lower frame angle provides higher impact force for a given ship velocity and ice condition.

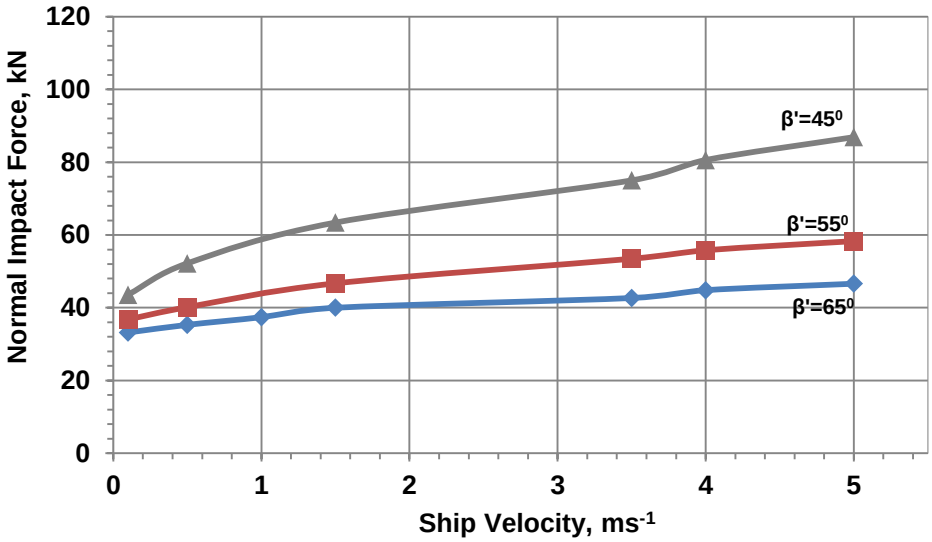

Figure 4.10 Impact force vs velocity in simple ice wedge breaking for different ship angles (h=0.5 m, $\theta = 30^0$)

Velocity Effect on Icebreaking Length

The icebreaking length is another important parameter for the ship icebreaking process. Figures 4.11a to 4.11c are the plot of icebreaking lengths for different ice wedge breaking conditions. For different ice thicknesses, the breaking length (L_b) is normalized with the corresponding ice thickness as shown in Figure 4.11a. The figure indicates that all the L_b/h ratio vs ship velocity curves follow a decreasing trend along the mean line. Similar decreasing trends are also observed for different wedge angles and ship angles as indicated in Figure 4.11b and 4.11c. These decreasing trends of breaking length with the ship velocity are consistent with the observation of Lubbad and Loset [13].

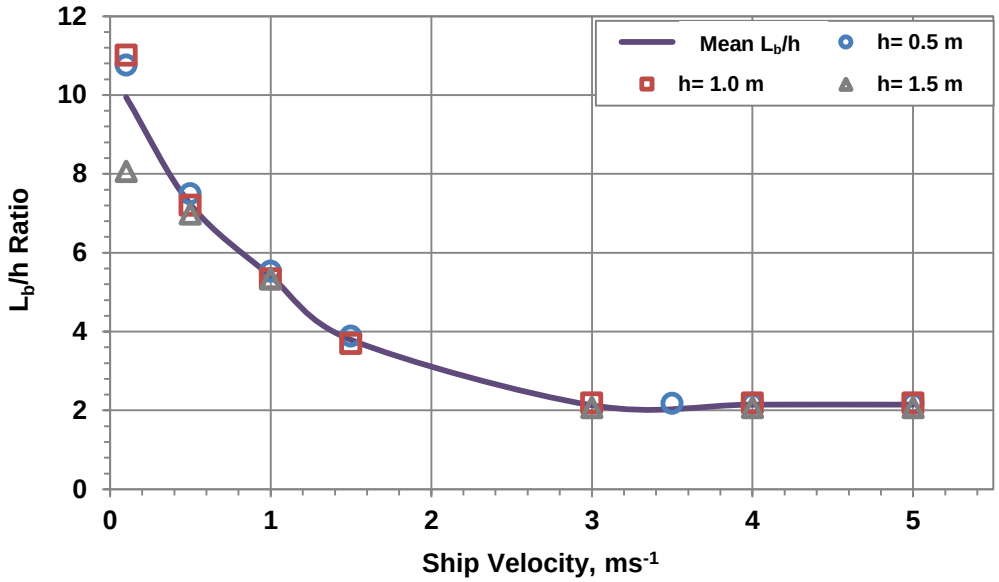

Figure 4.11a Breaking length/ice thickness ratio vs velocity for different ice thicknesses ($\beta'=65^0$, $\theta= 30^0$)

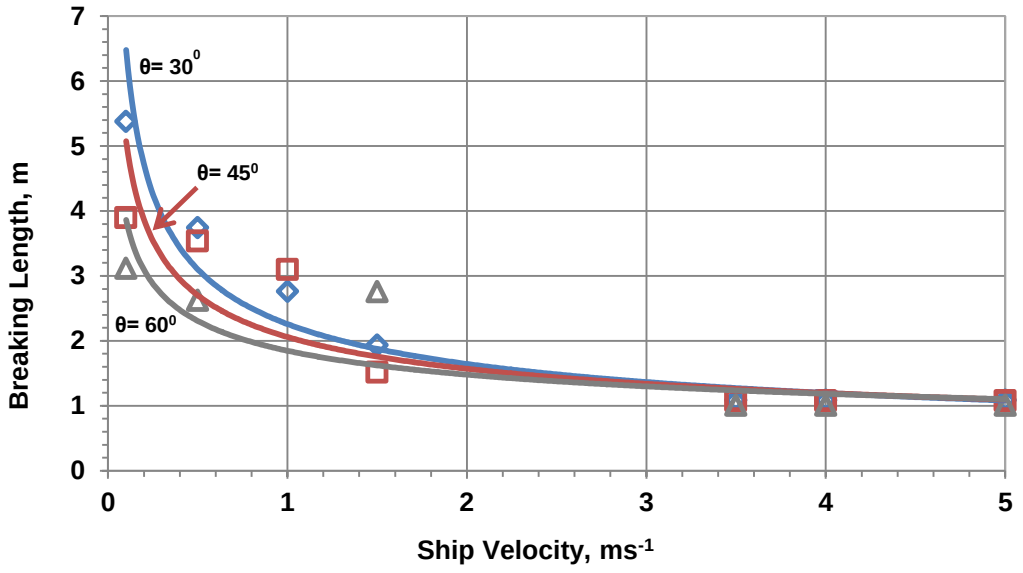

Figure 4.11b Breaking length vs velocity for different wedge angles (h=0.5 m, $\beta'=65^0$)

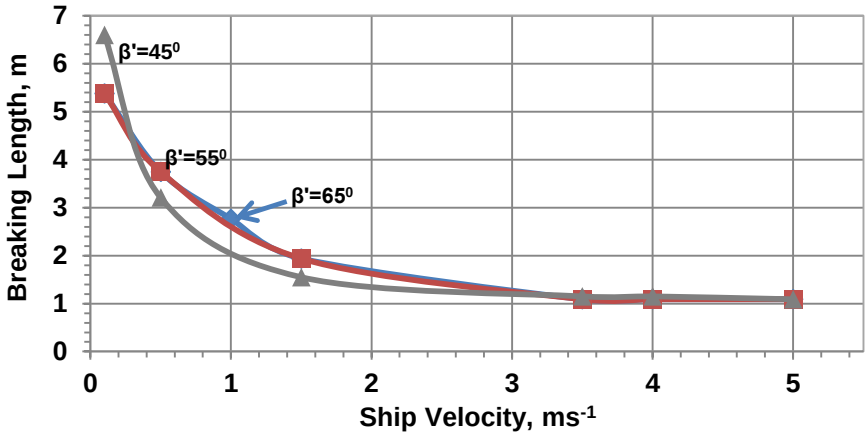

Figure 4.11c Breaking length vs velocity for different ship angles (h=0.5 m, θ= 30^0)

The above numerical ship icebreaking model results indicate that the ice impact force and the icebreaking length are strongly velocity dependent although the ship ice breaking models utilize the quasi-static material models. This velocity dependency is due to the body dynamics and inertia as discussed in Chapter 3.

4.3.2 Level Icebreaking in Head-on Collision

Effect of Ship Velocity and Radial Cracks on Breaking Pattern

For the level icebreaking in head-on collision, the breaking patterns and the von-Mises stress distribution of different conditions are presented in Figures 4.12a to 4.12f. These figures illustrate the effect of ship velocity and radial cracks on level icebreaking pattern.

Figures 4.12a to 4.12c are the level icebreaking patterns without existing radial cracks. In these breaking conditions, the bending failure occurs close to the ice crushing zone. The location of circumferential crack due to this bending failure does not significantly change

with the ship velocity. Similar breaking patterns are observed at low to high ship velocities for this breaking condition.

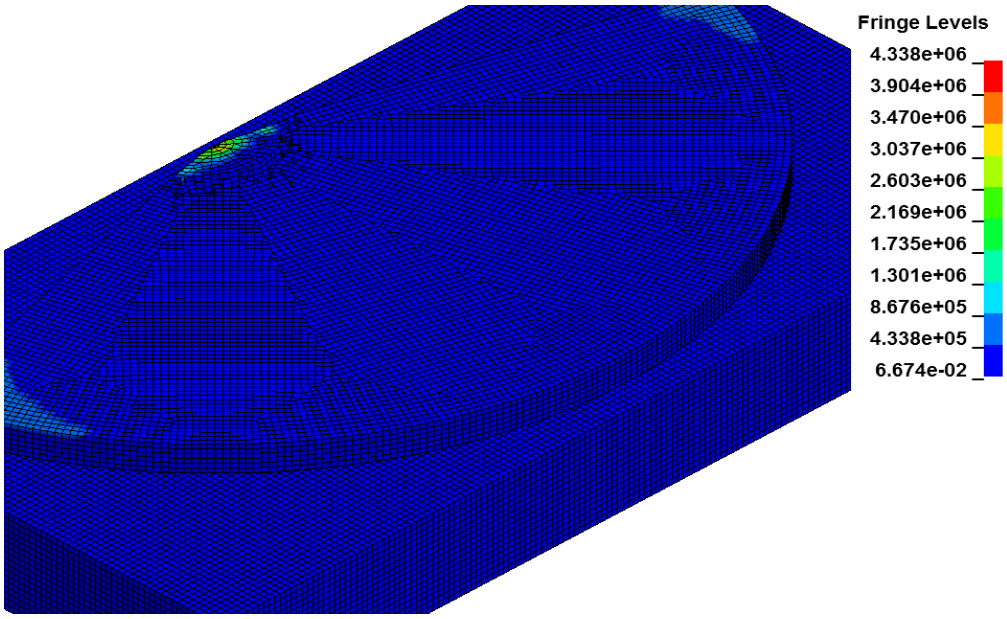

Figure 4.12a Level icebreaking in head-on collision without radial cracks at 0.1 ms^{-1}

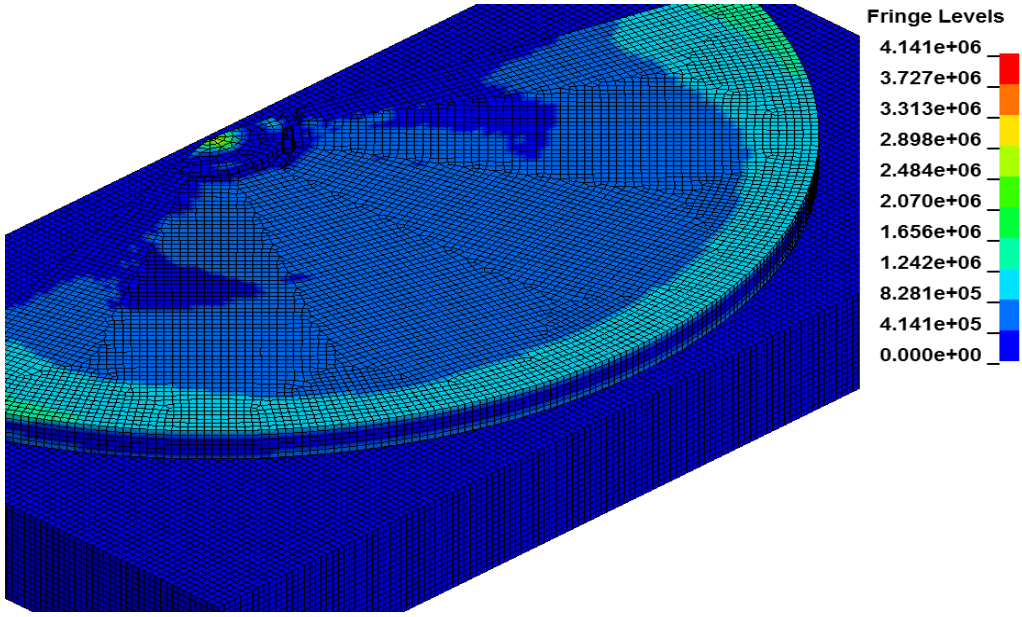

Figure 4.12b Level icebreaking in head-on collision without radial cracks at 1.0 ms^{-1}

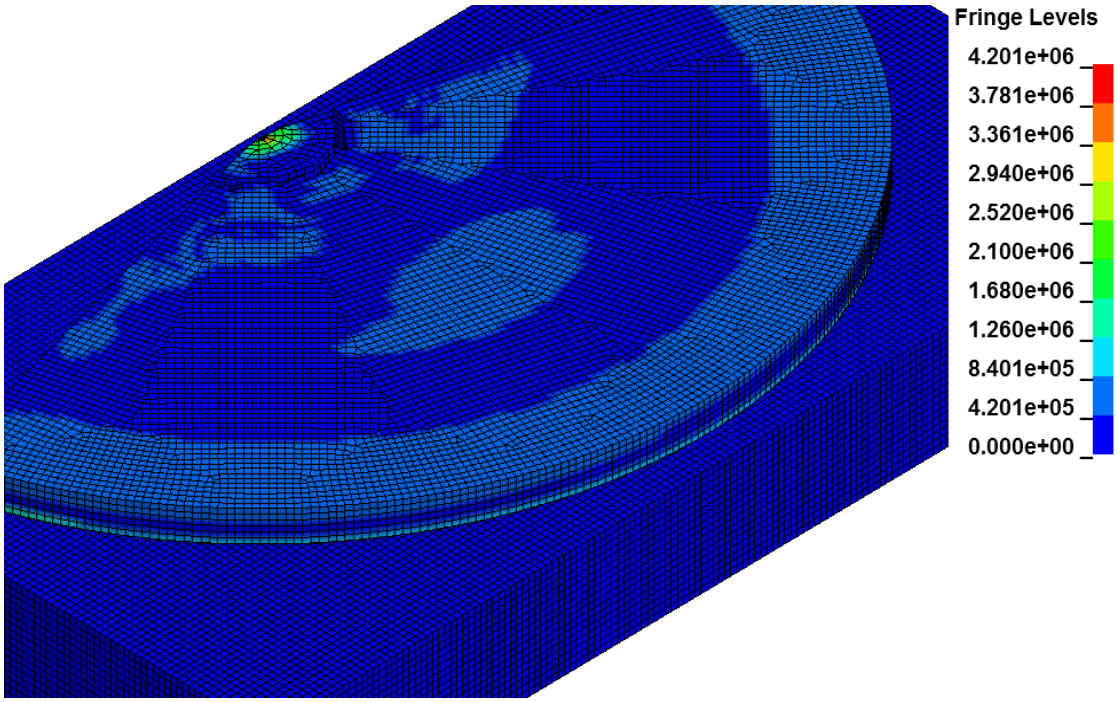

Figure 4.12c Level icebreaking in head-on collision without radial cracks at 5.0 ms^{-1}

In the presence of radial cracks in level ice, more realistic distributions of bending cracks are observed as shown in Figure 4.12d and 4.12e. The radial cracks create areas of weakness within the level ice. These areas of weakness result distributed breaking patterns. The breaking condition with four radial cracks contains more areas of weakness than the condition with two radial cracks and the condition without a radial crack. For this reason, the level icebreaking with four radial cracks produces more distributed breaking patterns than the other two conditions as indicated in Figure 4.12b to 4.12d. However, the distribution of breaking pattern is shifted towards the ice crushing zone at higher ship velocity as shown in Figure 4.12f.

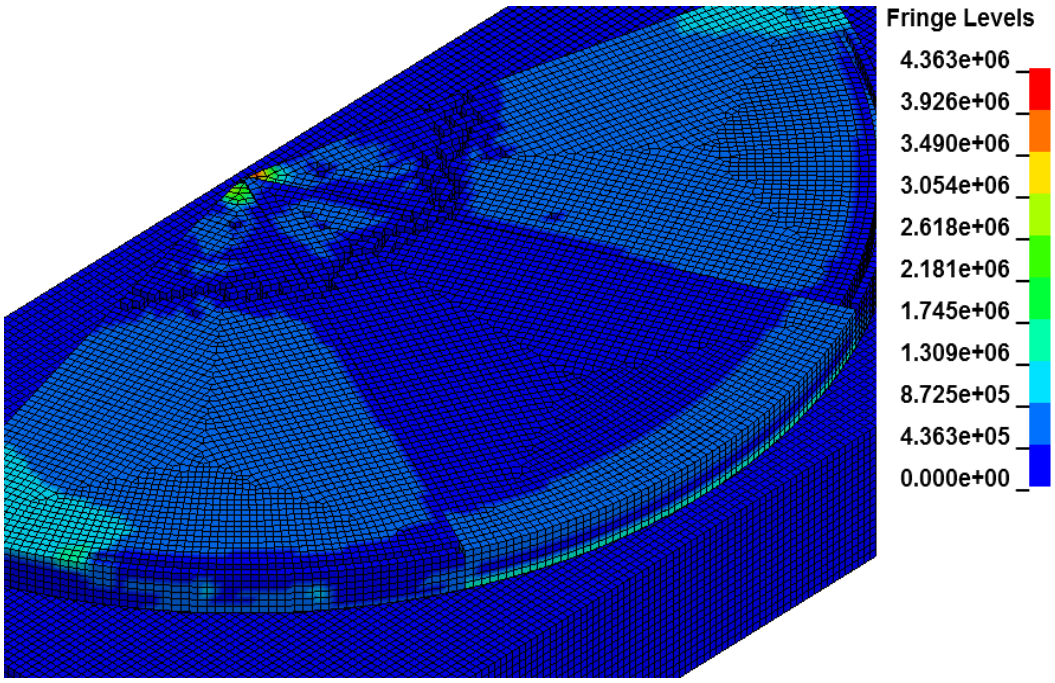

Figure 4.12d Level icebreaking in head-on collision with two radial cracks at 1.0 ms^{-1}

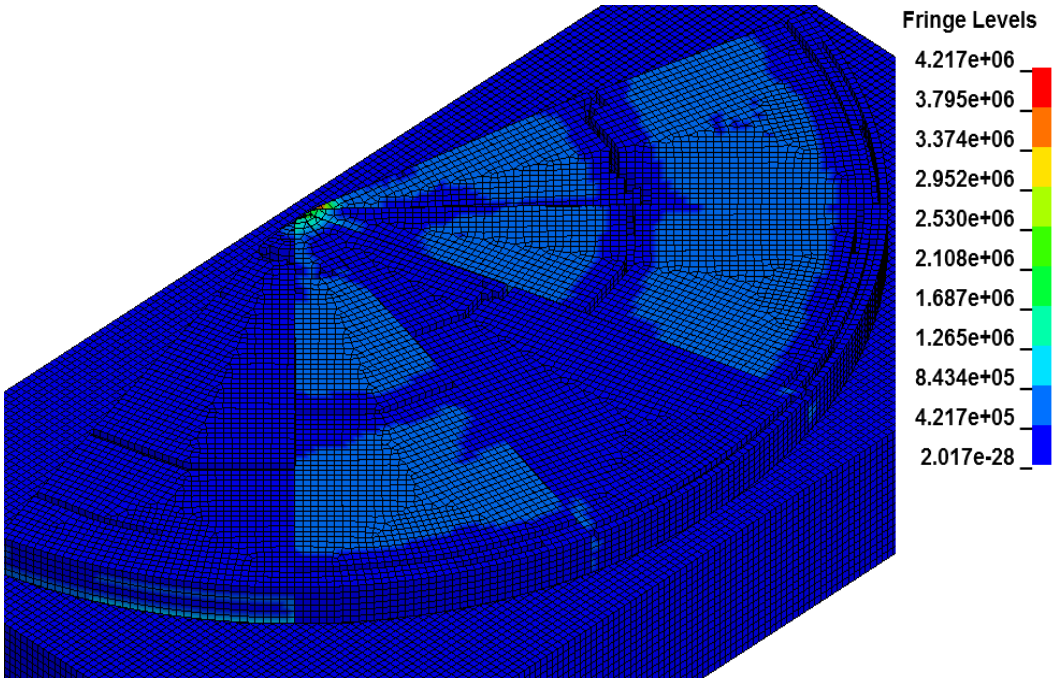

Figure 4.12e Level icebreaking in head-on collision with four radial cracks at 1.0 ms^{-1}

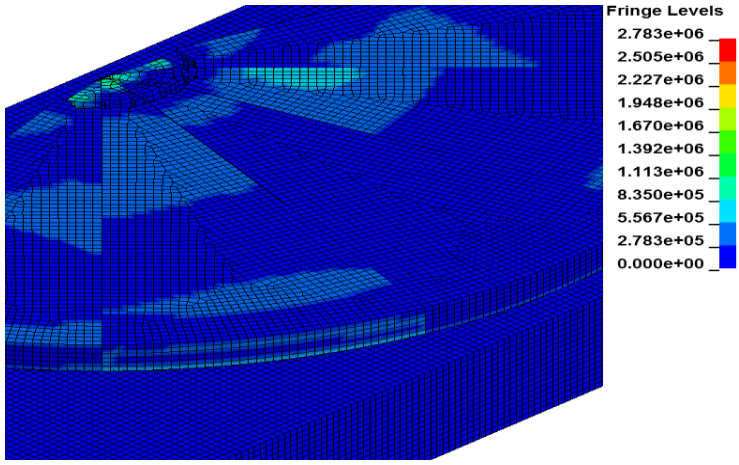

Figure 4.12f Level icebreaking in head-on collision with four radial cracks at 5.0 ms^{-1}

Effect of Ship Velocity and Radial Cracks on Impact Force

The effect of ship velocity and radial cracks on the maximum impact force is plotted in Figure 4.13 for three level icebreaking conditions. This figure indicates that the impact force increases with the velocity but decreases with the number of existing radial cracks. The level ice without a radial crack produces higher impact force for a given ship velocity.

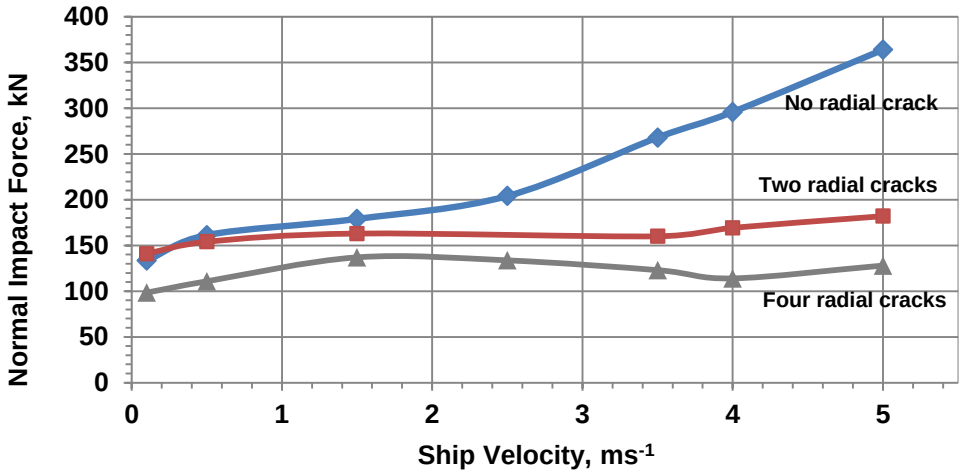

Figure 4.13 Impact force vs ship velocity for level icebreaking in head-on collision

4.3.3 Level Icebreaking in Shoulder Collision

For shoulder collisions, the failure patterns of level ice (150^0 wedge) at an intermediate ship velocity of 1 ms^{-1} are shown in Figures 4.14a and 4.14b. These figures indicate that the failure pattern changes in the presence of existing radial cracks. In addition, the ice wedge without a radial crack results higher impact force. The effect of ship velocity on the impact force and bending crack pattern is similar to previously mentioned level icebreaking condition of the head-on collision.

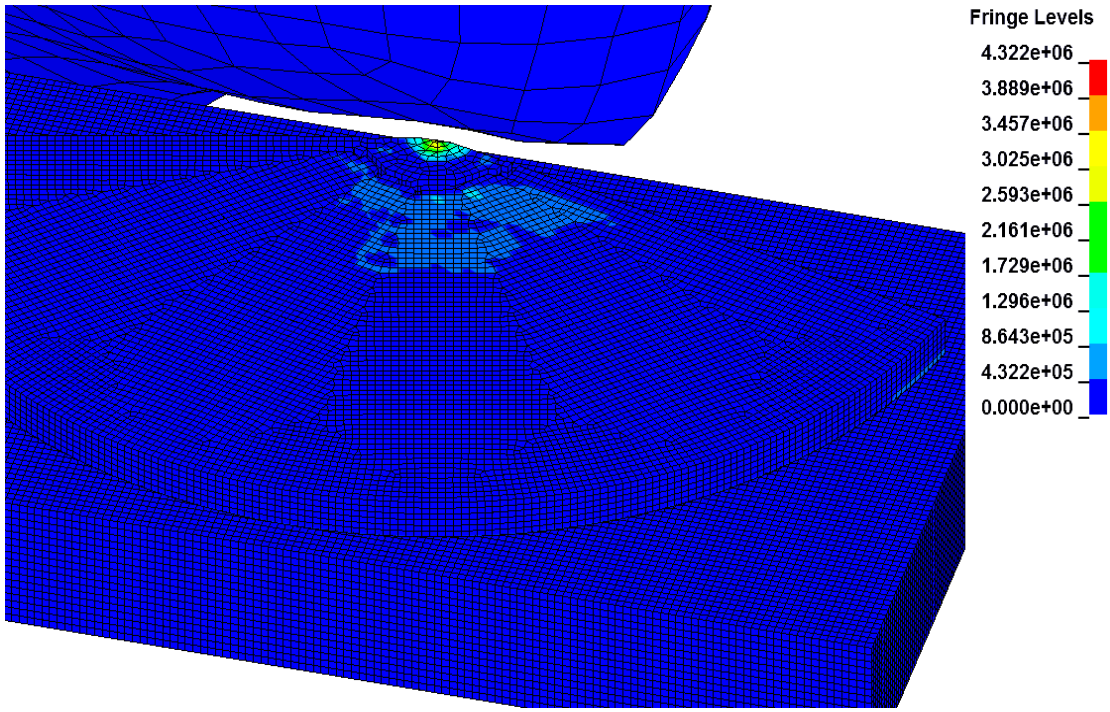

Figure 4.14a Level icebreaking in shoulder collision without radial cracks at 1.0 ms^{-1}

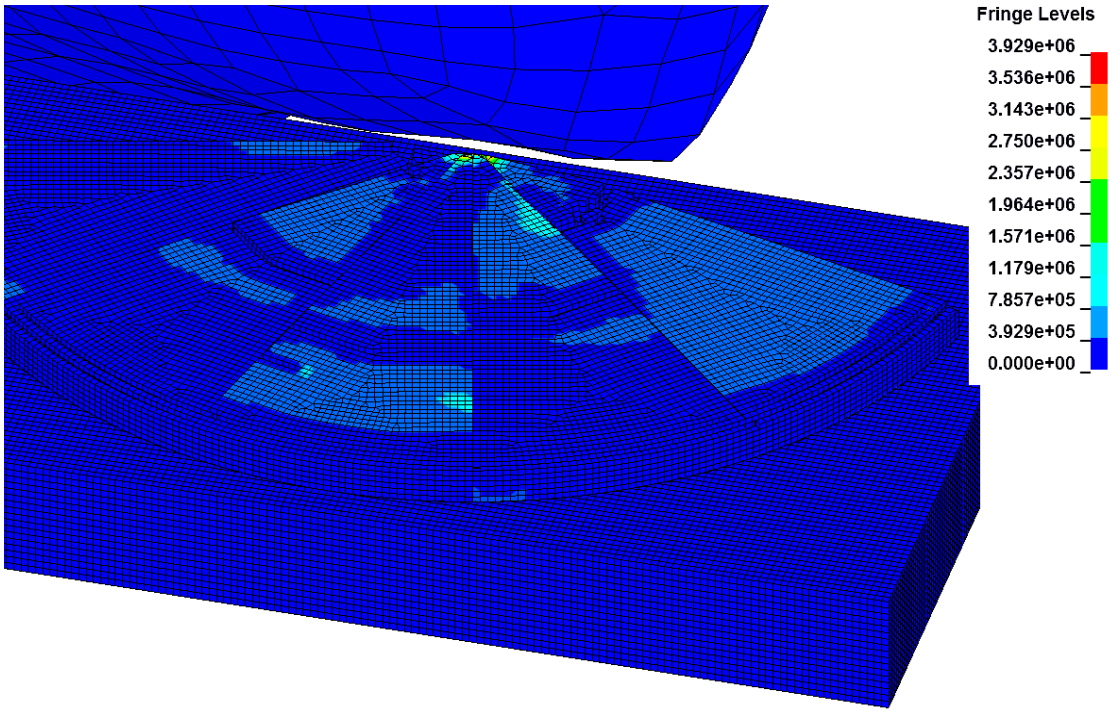

Figure 4.14b Level icebreaking in shoulder collision with four radial cracks at 1.0 ms^{-1}

4.4 Methodology to Formulate Dynamic Ice Load Models

There remains the need for better validation of the numerical results. Validation is not easy due to the lack of specific type of full scale test data, where both local loads and detailed ice observations are available. In addition, most of the existing analytical and semi-empirical models are applicable to the static or quasi-static loading conditions. Further testing is needed with a specific focus on local ice loads during operations in the level ice.

This section describes a methodology to formulate four different dynamic ice load models from the available analytical and semi-empirical models. In addition, two existing

breaking length models are presented to explore the velocity effect on the icebreaking length. The formulated dynamic ice load models and presented breaking length models will be used to validate the numerical model results.

Dynamic Ice Load Models

Two static ice load models and two dynamic factor models are selected from the existing analytical and semi-empirical models in order to formulate the dynamic ice load models. For the static ice load models, Kashteljan's model in Eq. (3.4) and Daley's proposed model in Eq. (3.5) are considered. Both the models provide identical results for a given ice wedge condition. Su et al. [14] mentioned that Kashteljan's model results in a quite small force value. Based on several experimental cases, a higher C_f value is suggested. The Nguyen et al.'s model [32] used 4.5 for C_f as mentioned in Su et al. [14]. Therefore, both Kashteljan's model and Daley's model are modified and multiplied with 4.5.

Daley and Kendrick [12] derived a dynamic factor (K_v) in terms of Froude Number (Fr) to account for the velocity effect for a particular ice condition. The equations of K_v and Fr are given as below:

$$K_v = max\begin{Bmatrix} 2.14\ Fr^{0.33} \\ 1 \end{Bmatrix} \tag{4.1}$$

$$Fr = \frac{V \sin\alpha\ cos\beta'}{\sqrt{gh}} \tag{4.2}$$

Lindqvist used a similar dynamic amplification factor for predicting the ice resistance [22]. The dynamic factor proposed by Lindqvist is given in the following equation:

$$K_v = 1 + 1.4\frac{V \sin\alpha \ cos\beta'}{\sqrt{gh}} \tag{4.3}$$

The dynamic factors in Eqs. (4.1) and (4.3), and the modified static or quasi-static models in Eqs. (3.4) and (3.5) are combined to produce four different dynamic ice load models. These four dynamic ice load (F_{df}) models are given in Eqs. (4.4) to (4.7).

Modified Kashteljan static load with Daley dynamic factor model (MK-D model):

$$F_{df} = 4.5\left(\frac{\theta}{\pi}\right)^2 \sigma_f h^2 . max\begin{Bmatrix} 2.14\ Fr^{0.33} \\ 1 \end{Bmatrix} \tag{4.4}$$

Modified Daley static load with Daley dynamic factor model (MD-D model):

$$F_{df} = C_f \sigma_f h^2 \theta . max\begin{Bmatrix} 2.14\ Fr^{0.33} \\ 1 \end{Bmatrix} \tag{4.5}$$

Modified Kashteljan static load with Lindqvist dynamic factor model (MK-L model):

$$F_{df} = 4.5\left(\frac{\theta}{\pi}\right)^2 \sigma_f h^2 . \left(1 + 1.4\frac{V \ \sin\alpha \ cos\beta'}{\sqrt{gh}}\right) \tag{4.6}$$

Modified Daley static load with Lindqvist dynamic factor model (MD-L model):

$$F_{df} = C_f \sigma_f h^2 \theta . \left(1 + 1.4\frac{V \sin\alpha \ cos\beta'}{\sqrt{gh}}\right) \tag{4.7}$$

The values of coefficient C_f in Eqs. (4.5) and (4.7) are 0.351, 0.438 and 0.585 for 30^0, 45^0 and 60^0 wedges, respectively.

Breaking Length Models

The location of the flexural crack or the beaking length is needed to achieve a realistic scenario of the icebreaking process. The following expression for the icebreaking length (L_b) is suggested by Daley:

$$L_b = \frac{8h}{K_v} \leq 8h \tag{4.8}$$

Liu [21] presented another formula for the breaking length as a function of characteristic length (l_c) of ice beam as given below:

$$L_b = \frac{0.2 l_c}{C_{vo} + C_v V \sin\alpha \, cos\beta'} \tag{4.9}$$

The empirical coefficient C_{vo} and C_v are 0.75 and 0.3, respectively. The characterictic length (l_c) of an ice beam can be calculated as:

$$l_c = \left(\frac{Eh^3}{12\rho_w g(1-\vartheta^2)}\right)^{1/4} \tag{4.10}$$

4.5 Validation of Numerical Models

Due to a lack of specific model test data and full scale data, the numerical results of simple ship ice wedge breaking are compared with the formulated dynamic ice load model results discussed in section 4.4. In general, the vertical component of impact force is primarily responsible for the bending failure. Therefore, these vertical impact forces or the bending failure loads from the numerical models along with the theoretical results

calculated from Eqs. (4.4) to (4.7) are plotted in Figures 4.15 to 4.17. These figures indicate that the numerical results are in general agreement with the comparative models.

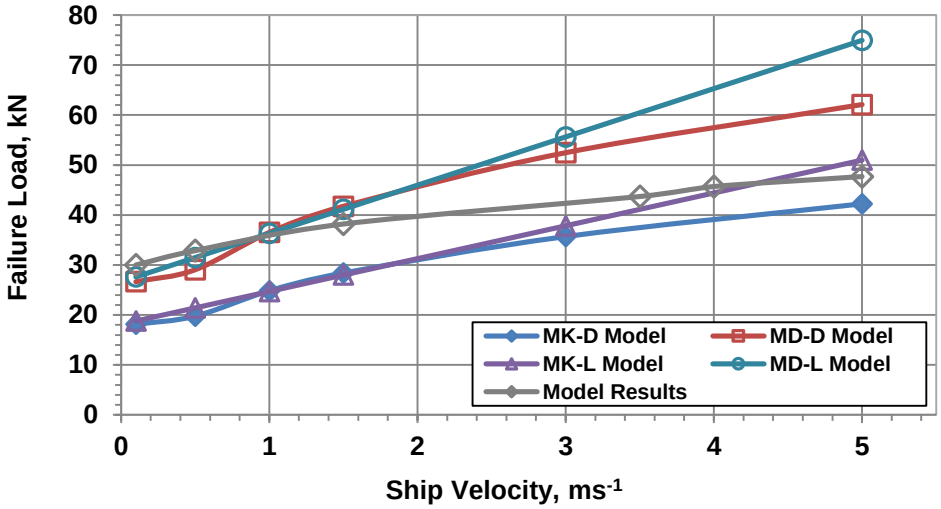

Figure 4.15 Comparison of bending failure loads in simple ship ice wedge breaking (h= 0.5 m, $\theta=30^0$, $\beta'=55^0$)

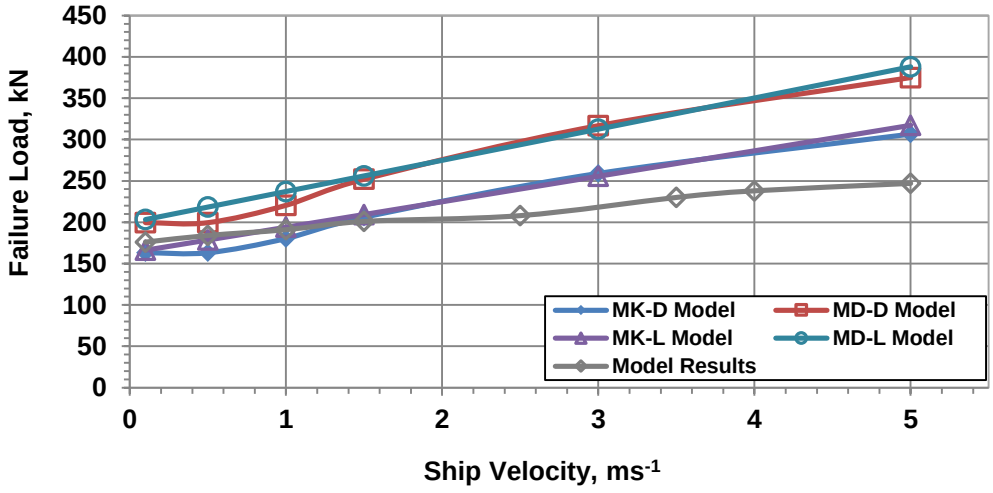

Figure 4.16 Comparison of bending failure loads in simple ship ice wedge breaking (h= 1.0 m, $\theta=45^0$, $\beta'=65^0$)

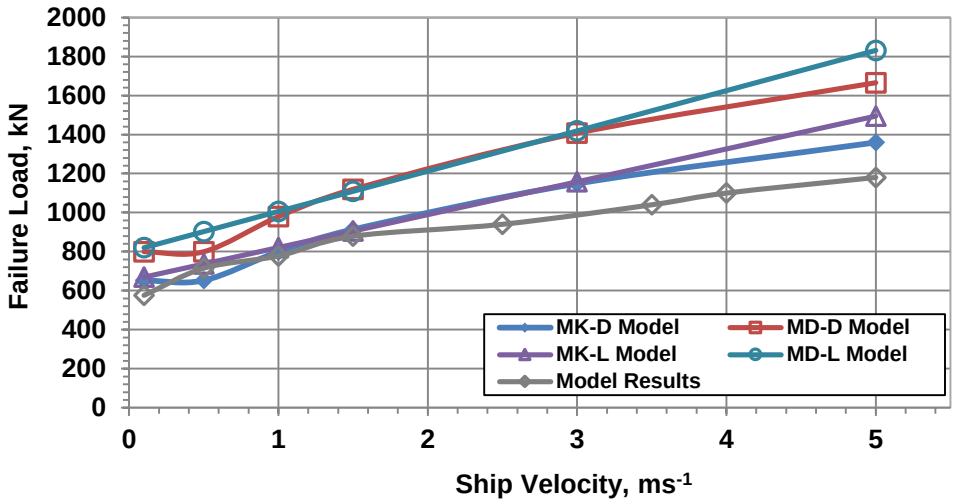

Figure 4.17 Comparison of bending failure loads in simple ship ice wedge breaking (h= 1.5 m, $\theta=60^0$, $\beta'=45^0$)

The model icebreaking lengths for different icebreaking conditions along with the theoretical breaking lengths are shown in Figures 4.18 and 4.19. These curves indicate that the model breaking length does not match with the theoretical results exactly. However, these curves follow a similar decreasing trend with the ship velocity.

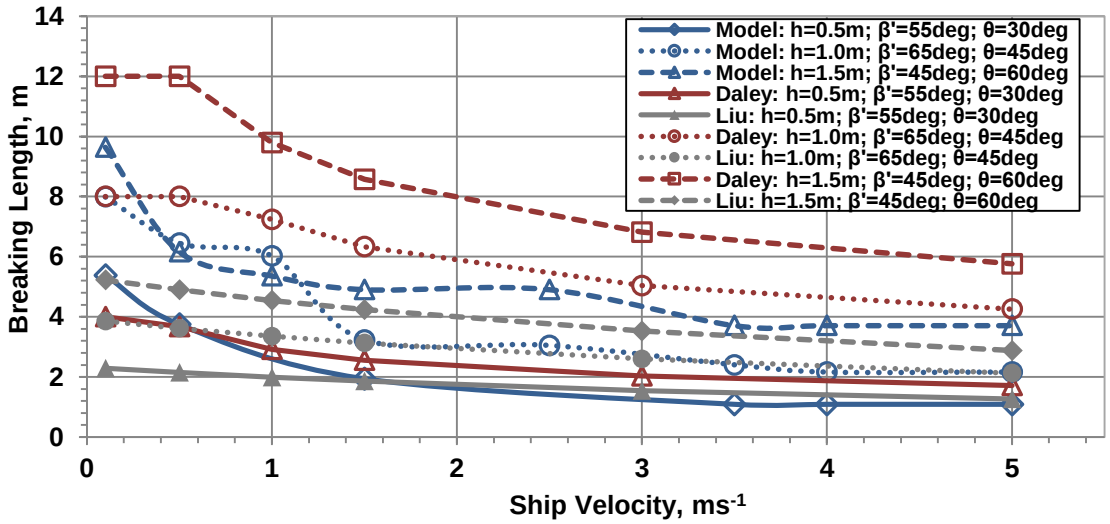

Figure 4.18 Comparison of ice wedge breaking lengths in different models

Chapter 5

Velocity Dependent Ice Flexural Failure Model

5.1 Introduction

This chapter presents an analytical closed form model of velocity dependent flexural failure to predict the dynamic ice load from ship icebreaking process. The model is based on numerical investigation of the ship icebreaking conducted in Chapter 4. The quality of the model is checked against the numerical results considering different icebreaking conditions and collision scenarios. The developed model is validated against full scale ice impact test data and a non-linear dynamic bending load model. Application of the velocity dependent flexural failure model to predict the bow impact load is demonstrated for an example ship type (PC 1 ship). These bow impact load results are compared with the IACS Polar Rules based results.

5.2 Velocity Dependent Flexural Failure Model

The comparison between the numerical and theoretical results in the previous chapter indicated that the developed numerical models are well suited to predict the dynamic impact force. These numerical models can be used for further ship icebreaking investigations. The results from the numerical models have been used as the basis of a new analytical closed form model for the velocity dependent force required to break an ice wedge. Four factors; ship velocity, normal ship frame angle, ice thickness and ice wedge angle are considered in this analysis. One factor at a time (OFAT) approach is used to establish this empirical relationship between the ship velocity and impact force for different icebreaking conditions. Equation (5.1) is the new flexural failure model of vertical impact force for dynamic ice wedge breaking.

$$F_{vd} = 0.29\, n^{0.7} k_v\, \sigma_f\, h^2 \theta \tag{5.1}$$

where n is the number of wedge. The dynamic factor is defined as:

$$K_v = 1 + 2.57 \sin\alpha \cos\beta'\, \theta^{0.2} Fr^{0.26} \tag{5.2}$$

where Froude Number (Fr) is defined in Eq. (4.2). The normal impact force can be expressed in the following form:

$$F_{nd} = \frac{F_{vd}}{\sin\beta'} \tag{5.3}$$

In the new model, the flexural strength (σ_f) is assumed as linearly related to the impact force similar to Eqs. (4.4) to (4.7). Hence, further investigation is needed to establish the actual relationship between the flexural strength and impact force.

5.3 Comparison with Numerical Model

This section examines the quality and accuracy of the developed flexural failure model against the numerical model results. The results from the developed model are compared with numerical model results for different breaking conditions considering both the head-on and shoulder collision scenarios. For simple ice wedge breaking in head-on collision, the vertical impact force vs ship velocity curves of the flexural failure model along with the numerical results are plotted in Figures 5.1 to 5.4. These curves illustrate the effect of ice thickness, ice wedge angle and normal ship frame angle on the velocity dependent ice failure load. The curves of the flexural failure model are well fitted with the numerical model results. Therefore, the developed velocity dependent flexural failure model can be used to explore the dynamic ship icebreaking process.

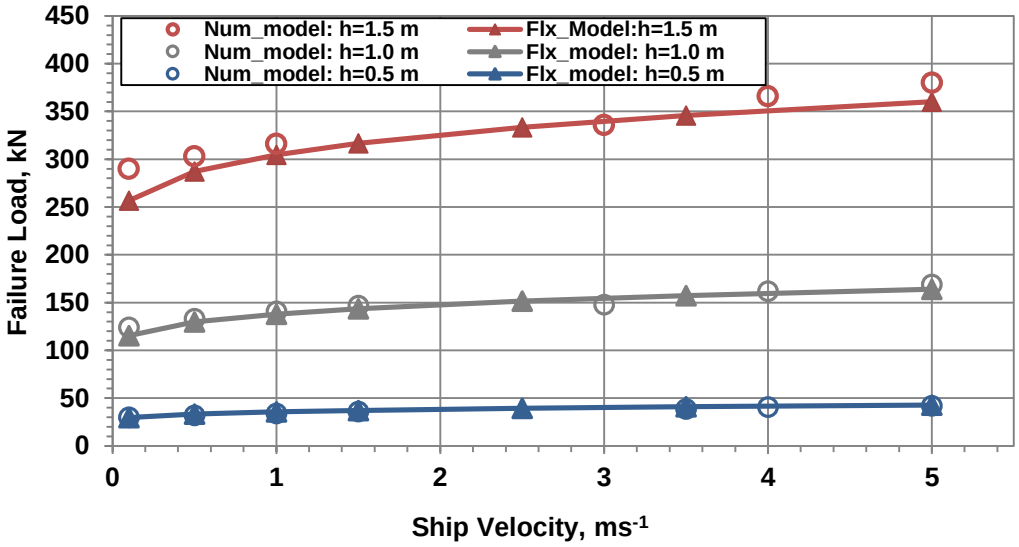

Figure 5.1 Comparison of velocity dependent flexural failure model with numerical model for ice wedge breaking in head-on collision at different ice thicknesses ($\beta'=65^0$, $\theta=30^0$)

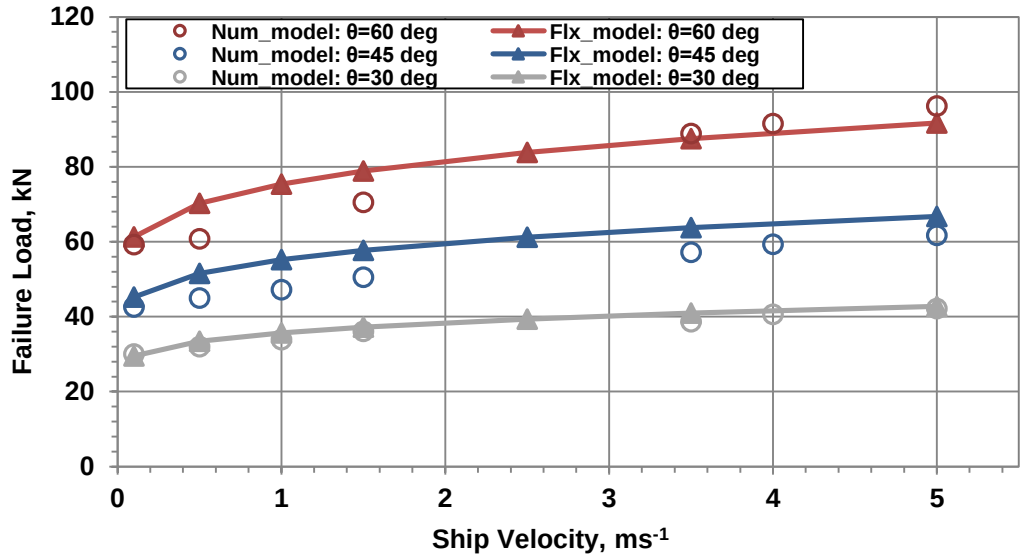

Figure 5.2 Comparison of velocity dependent flexural failure model with numerical model for ice wedge breaking in head-on collision at different ice wedge angles (h=0.5 m, $\beta'=65^0$)

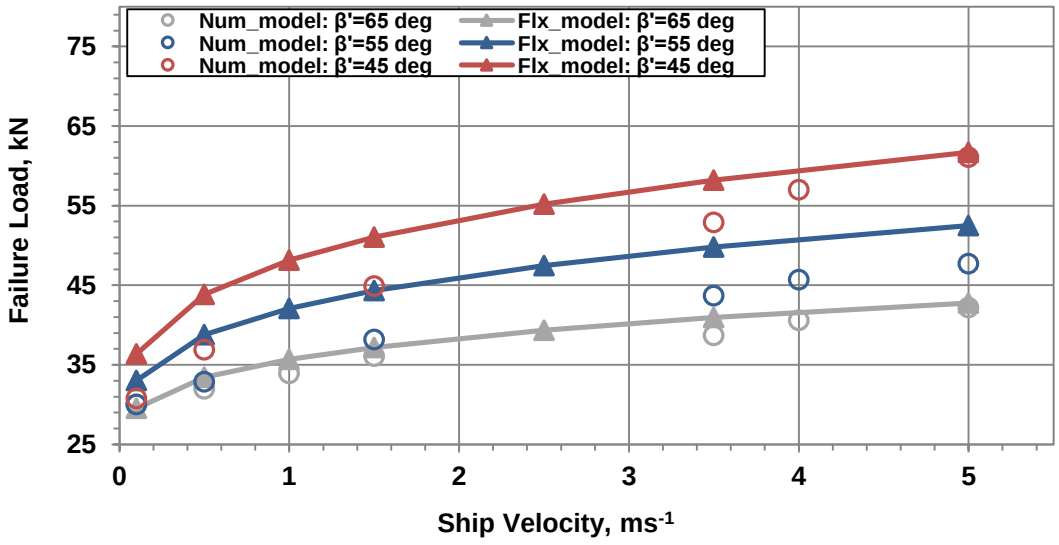

Figure 5.3 Comparison of velocity dependent flexural failure model with numerical model for ice wedge breaking in head-on collision at different normal ship angles (h=0.5 m, $\theta=30^0$)

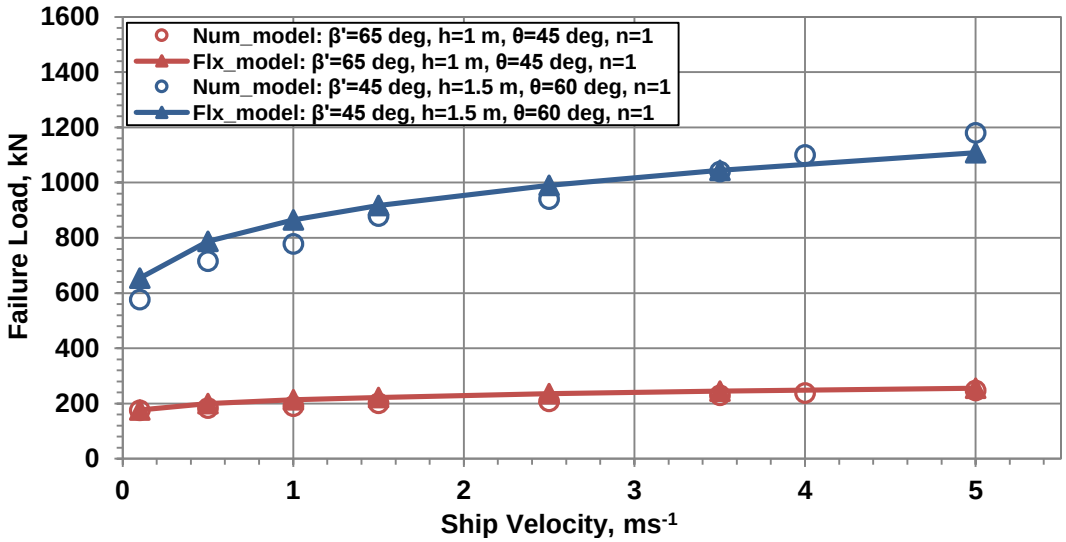

Figure 5.4 Comparison of velocity dependent flexural failure model with numerical model for ice wedge breaking in head-on collision with random breaking parameters

The developed flexural failure model can also be applied to the level icebreaking scenario. Results from the flexural failure model are plotted with the numerical results in Figures 5.5 to 5.7 for both collision scenarios. These figures indicate that the developed model is well suited to the level icebreaking condition with and without any radial crack.

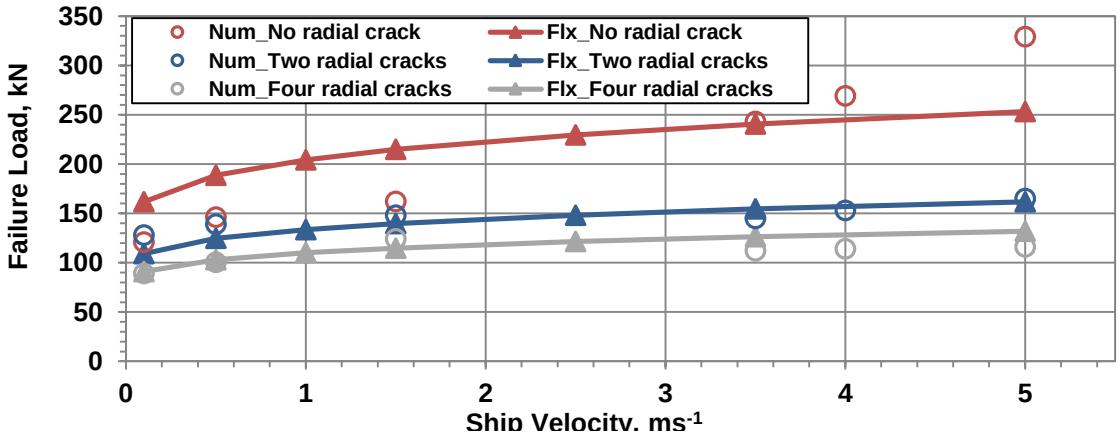

Figure 5.5 Comparison of velocity dependent flexural failure model with numerical model for level icebreaking in head-on collision with and without radial cracks

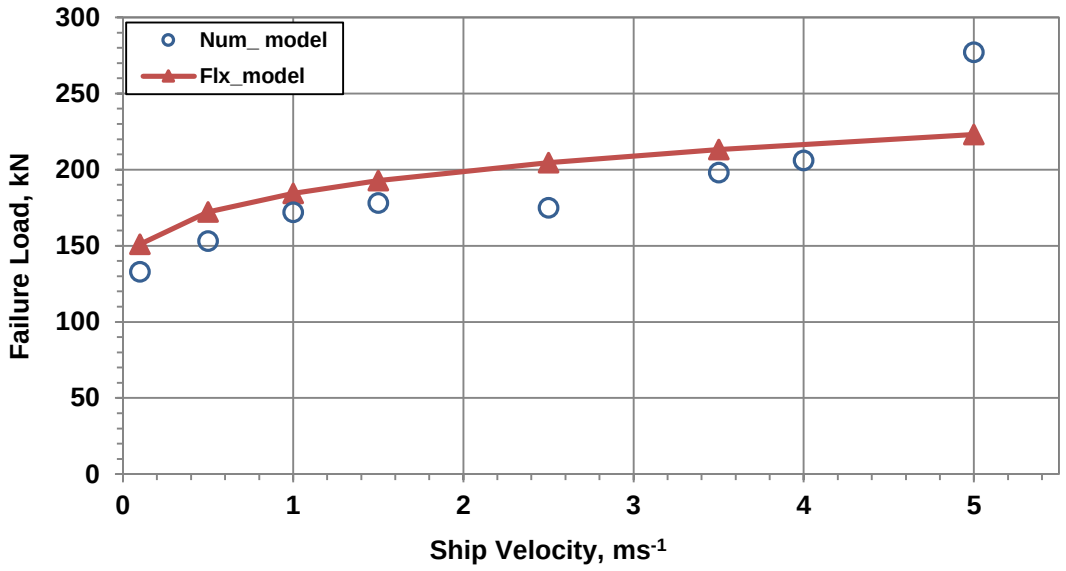

Figure 5.6 Comparison of velocity dependent flexural failure model with numerical model for level icebreaking in shoulder collision without radial cracks

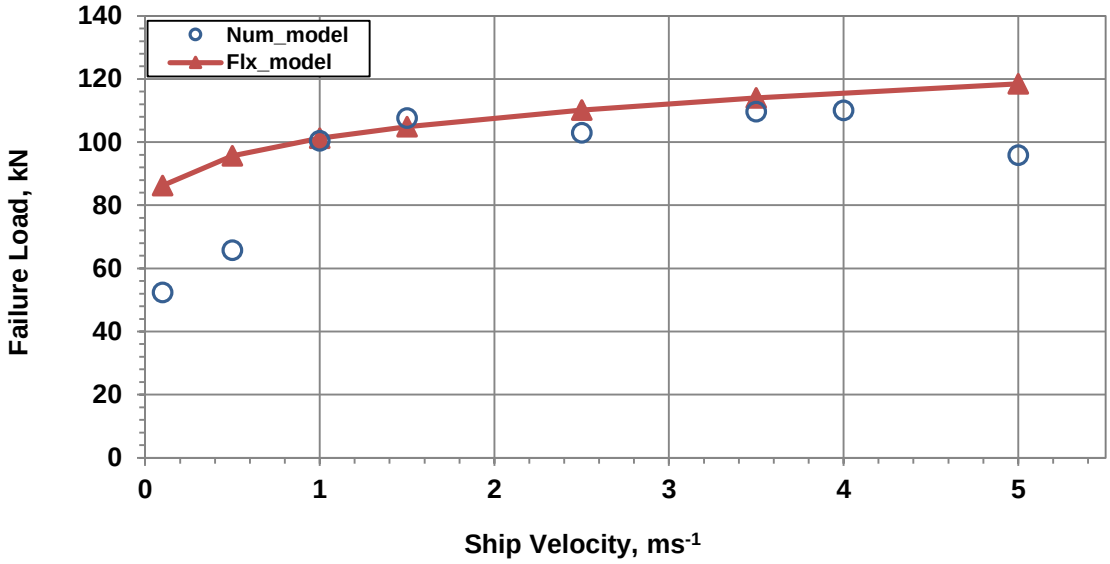

Figure 5.7 Comparison of velocity dependent flexural failure model with numerical model for level icebreaking in shoulder collision with four radial cracks

5.4 Validation with Full Scale Test Data

In this section, the velocity dependent ice flexural failure model is validated against full scale ice impact test data and against a finite element based non-linear dynamic bending load model provided in Varsta [47].

In 1983, Rauma Shipyard conducted a full scale test with an artificial land craft bow in order to investigate the effects of ship speed and frame angle on the ice load [47]. The landing craft bow was installed at the front of the tug Rauma I. This makes the waterline angle (α) equal to 90^0. A general arrangement of this ice impact test is shown in Figure 5.8.

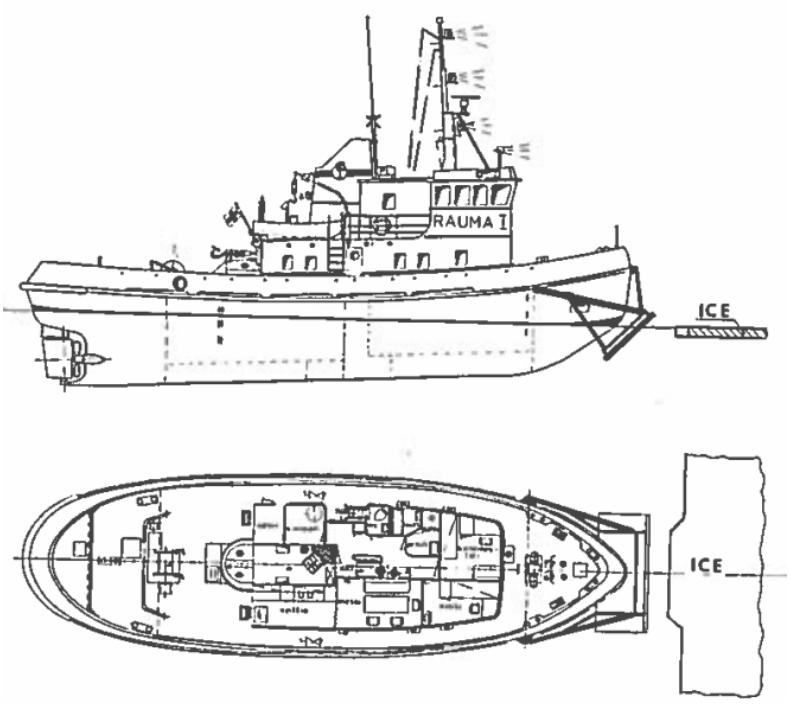

Figure 5.8 Ice impact test arrangement indicating landing bow craft and ice wedge shape [47]

In the test, the ice wedge was pre-sawned to achieve a controlled test condition. The geometric dimensions of the ice wedge and the landing craft bow particulars are given in Table 5.1. Further details of the test can be found in Varsta [47].

Table 5.1 Ice wedge geometry and landing craft bow particulars in full scale impact test

Parameters	**Values**
Wedge edge length (l_c)	3.5 m
Wedge depth (l_d)	0.5 m
Wedge opening angle (θ_w)	45^0
Ice temperature on top surface (T_i)	-2°C to -6.6°C
Waterline angle of landing bow (α)	90^0
Normal ship frame angle/striking angle (β')	30^0 (9 tests) and 50^0 (20 tests)

Varsta [47] developed a non-linear dynamic ice bending model based on the finite element method. The model was further refined by comparing the above discussed full scale test data. Varsta's model assumed an average ice thickness of 0.35 m and ice flexural strength of 1.2 MPa. The present study also considers these ice thickness and flexural strength values for the validation purpose. In addition, the present study assumes that the ice wedge forms an opening angle of 90^0 at the ship ice contact point instead of flat contact edge which is the case with the Varsta's model and full scale test. This assumption is reasonable especially for the thinner ice where the flexural failure dominates the ice failure process. Figure 5.9 indicates the assumed ice wedge geometry along with the original ice wedge geometry.

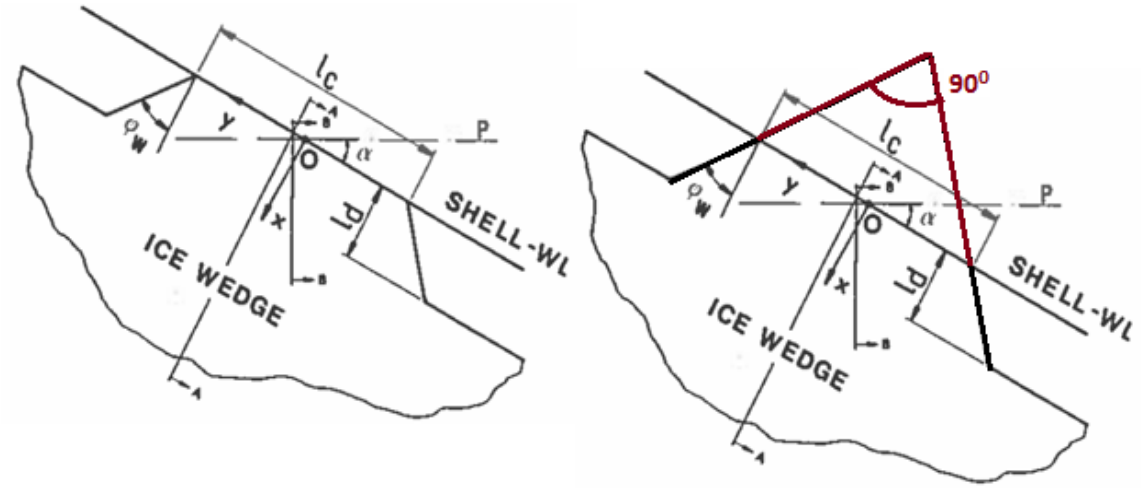

Figure 5.9 Ice wedge geometry in full scale test (left), Varsta's model (left) and present model (right)

The full scale test data, Varsta's model results and the velocity dependent ice flexural failure model results are plotted in Figure 5.10. The figure indicates that the developed velocity dependent ice flexural failure model provides almost identical results to Varsta's model for the normal ship frame angles of 30^0 and 50^0. These results are also in good agreement with the full scale test data. At lower normal ship frame angle (25^0) some differences are observed between the Varsta's model and present model. However, no full scale data is available at this ship frame angle to explain the differences.

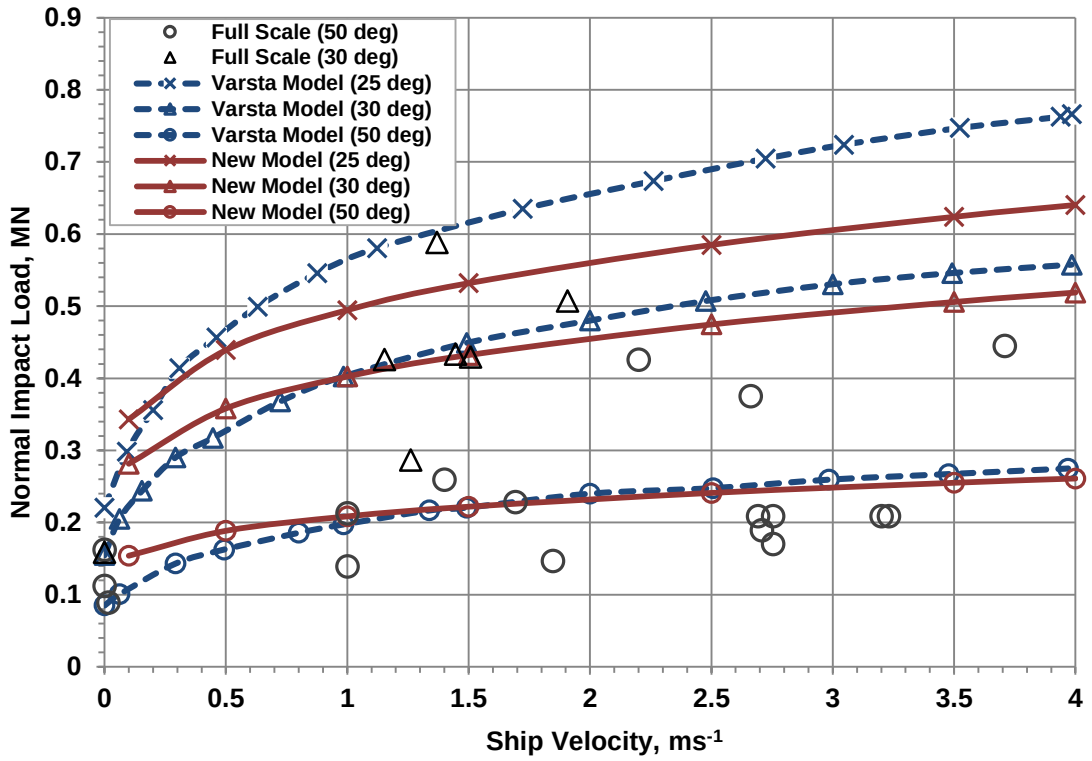

Figure 5.10 Validation of velocity dependent ice flexural failure model with full scale test data and Varsta's model

5.5 Application to Bow Impact Load Estimation

The bow impact load is an essential component for the design ice load model, and hence for the Polar ship design and safe speed methodology. The minimum ice failure load from the flexural failure model and crushing failure model is the effective bow impact load. Therefore, the bow impact load can be expressed as a function of the ice flexure failure load (F_f) and the ice crushing load (F_c):

$$F_{bow} = min\,(F_c, F_f) \tag{5.4}$$

The Polar Rules based formula given in Eq. (2.7) can also be used to calculate the bow impact load. However, the flexural failure load (F_f) in this Polar equation is insensitive to the ship velocity. Therefore, the developed velocity dependent flexural failure model is adopted here to investigate the ship velocity effect on the bow impact load.

For the ice crushing load, the Polar Rules based crushing failure model is used. The Polar ice crushing failure model is reasonably good for estimating the ice crushing load and to account for the ship velocity effect [12]. The model is derived based on the energy principle, and incorporated the Popov collision mechanics and pressure-area relationship. The final ice crushing failure load model in the Polar Rules is presented in Table 5.2. Details derivation of the model can be found in Daley [50] and Daley and Kendrick [12].

Table 5.2 Ice crushing failure load model in IACS Polar Rules [12, 50]

Ice Crushing Limit Load Model	
Ice crushing failure load: $$F_c = P_o \,.\, fa \,.\, \left(\frac{KE_e \,.\, fx}{P_o \,.\, fa}\right)^{\frac{fx-1}{fx}}$$	(5.5)
The effective kinetic energy: $$KE_e = \frac{1}{2} M_e V_n^2$$	(5.6)
Normal Ship Velocity: $$V_n = V_{ship} \sin\alpha \cos\beta'$$	(5.6)

Effective Mass:

$$M_e = \frac{M_{ship}}{C_o} \tag{5.7}$$

Coefficients:

$$fx = 3 + 2ex \tag{5.8}$$

$$fa = \left(\frac{\tan \theta/_2}{\sin \beta' \cos^2 \beta'} \right)^{1+ex} \tag{5.9}$$

The formula for mass reduction coefficient (C_o) can be found in Daley [50]

This section investigates the ship velocity effect on the bow impact load during an ice crushing process or an ice flexural failure process. For this reason, the equation (5.4) is applied for a real ship type (PC 1) to calculate the bow impact load at different ship velocities. The calculated bow impact load is compared with the Polar Rules based bow impact load (Eq. 2.7) for a given ice thickness. Further, the ship velocity effect on the bow impact load is also considered for different ice thicknesses. Finally, the bow impact load is estimated using the Polar Rules specified parameters at different ship displacements (mass). The principal particulars of the ship and ice wedges are listed in Table 5.3.

Table 5.3 Principal particulars of ship and ice wedges for bow ice load

Parameters	Value
Polar Class	PC 1
Ship mass, M	10,000 tones
Ship block coefficient, C_b	0.768
Ship water plane coefficient, C_{pw}	0.7469
Ship mid-ship coefficient, C_m	0.934
Ship waterline angle, α	30^0
Normal ship frame angle, β'	46^0
Ice wedge angle, θ	150^0
Flexural strength of ice, σ_f	0.58 MPa

For the given ice thickness of 1.5 m, the impact load vs ship velocity curves of different models are plotted in Figure 5.11. These plotted models are the ice crushing model, velocity dependent ice flexural failure model, bow impact load model (Eq. 5.4) and Polar Rules based bow impact load model (Eq. 2.7). The ice crushing model indicates that the impact load increases very quickly with the ship velocity, whereas a gradual change is observed in the flexural failure model. For a particular ice condition, the ice crushing model represents limiting impact load at slow ship velocity. For medium to higher ship velocities, the flexural failure load is lower than the ice crushing load, and hence the flexural failure model dominates the bow impact load for this velocity range. The new bow impact load model in this figure indicates that there is a significant velocity effect in

the impact load at medium and higher ship velocities. This velocity effect is not included in the Polar Rules model.

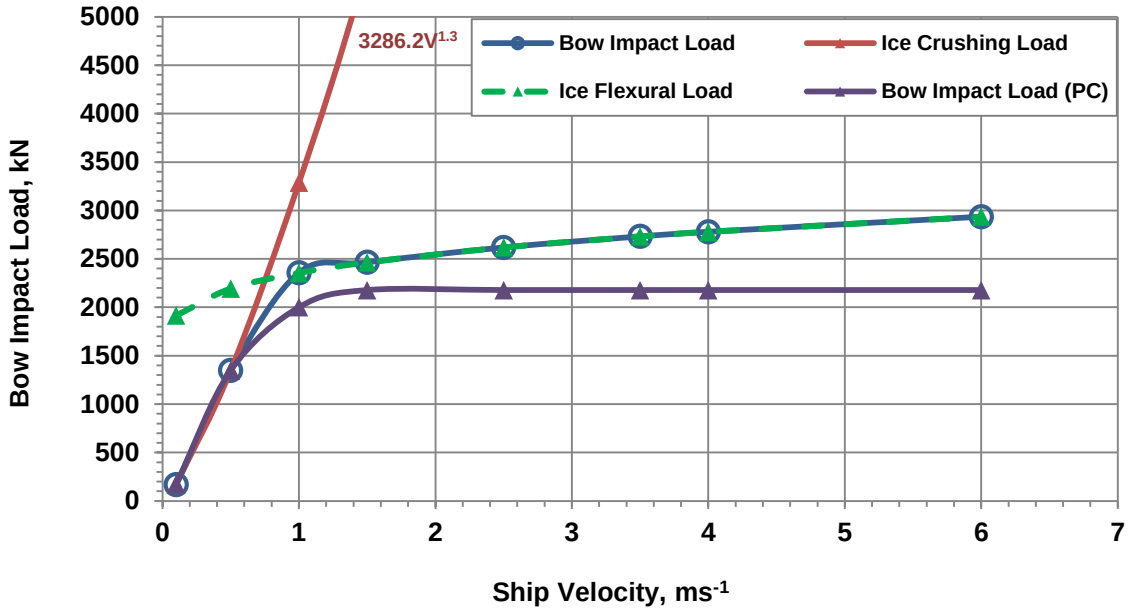

Figure 5.11 Ship velocity effect on bow impact load for an ice thickness of 1.5 m

Figure 5.12 is the result of the bow impact load model (Eq. 5.4) for a ship velocity range of 0.1 ms^{-1} to 6 ms^{-1} at different ice thicknesses. The figure indicates that the crushing failure dominates the resulting impact load for a wide range of ship velocity in the thicker ice. In addition, crushing is also a dominating criterion for the slow velocity interaction with the thinner ice. The figure also indicates that the flexure is the primary failure criterion for the thinner ice at medium to higher ship velocities.

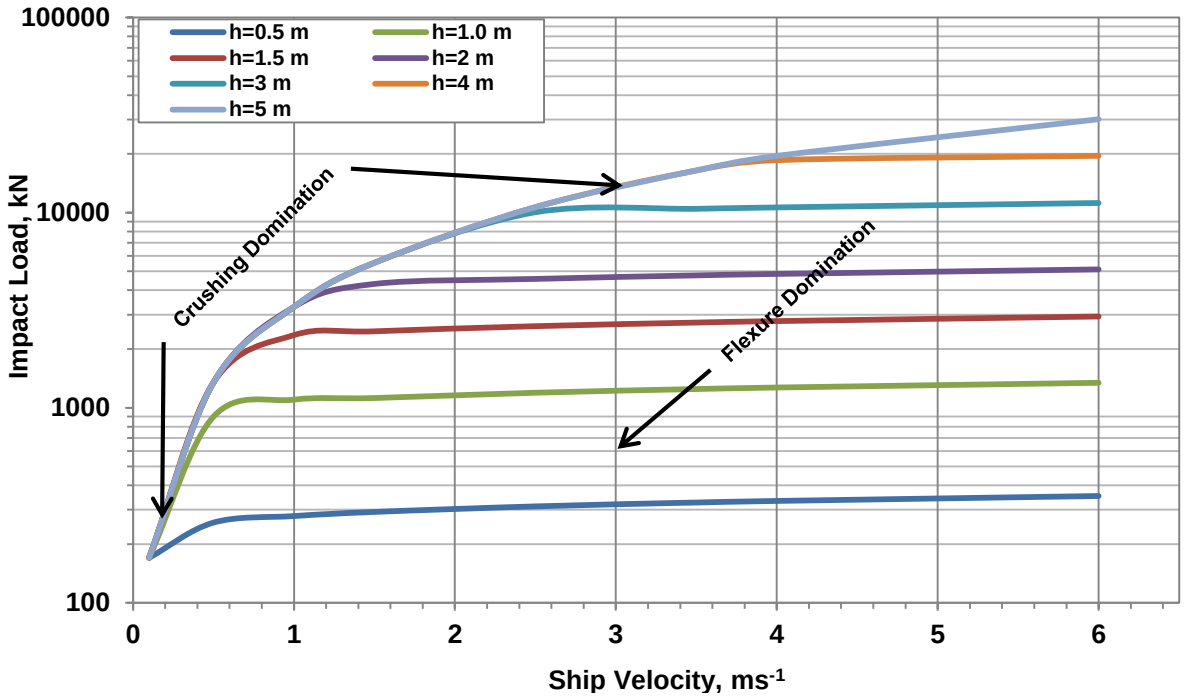

Figure 5.12 Ship velocity effect on bow impact load at different ice thicknesses

Now, the bow impact loads for the PC 1 ship at different ship velocities and displacements are estimated using the class dependent parameters such as the ice thickness (7 m) and the flexural strength (1.4 MPa). These bow impact load results are plotted in Figure 5.13 indicating the PC 1 design velocity (5.7 ms^{-1}). The figure indicates that the crushing is the only failure criterion at lower ship displacements (50 kT and 100 kT). For higher ship displacements from 150 kT to 250 kT, both the crushing and flexural failure processes contribute to the bow impact loads.

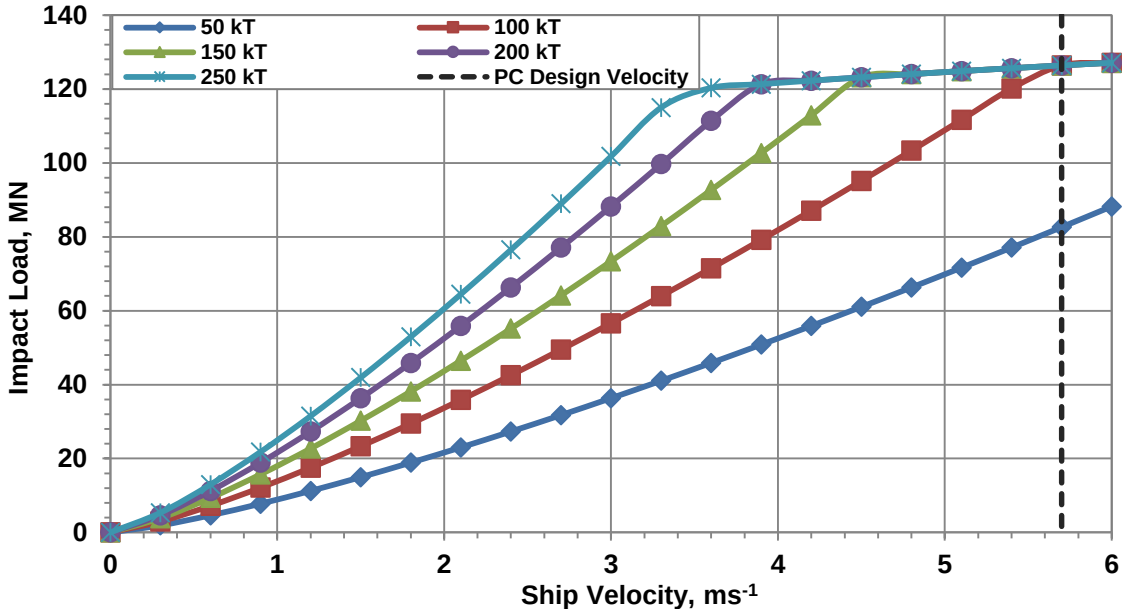

Figure 5.13 Ship velocity effect on bow impact load at different ship displacements

The above discussion indicates that the Polar Rules based bow impact load estimation method is reasonable for thicker ice operation, slow velocity interaction or for ships with lower displacement. For thinner ice at medium to higher interaction velocities or the ship with higher displacements, the Polar Rules based method may not be appropriate as their flexural failure model is insensitive to the interaction velocity. Therefore, the developed velocity dependent ice flexural failure model can help to enhance the Polar Rules based design model to account for the velocity effect.

Chapter 6

Safe Speed Methodology for Polar Ships

6.1 Introduction

This chapter presents a safe speed methodology for the Polar ships. For this purpose, an improved design ice load model is proposed based on the new velocity dependent ice flexural failure model. The improved design ice load model is used to calculate the load patch parameters. Further, the load patch parameters are employed to select the ship plate and frame dimensions as well as to develop the safe speed methodology. The safe speed methodology for the PC 5, PC 6 and PC 7 are demonstrated to examine the capability of safe speed operation in different ice conditions. Finally, a software "Safe Speed Check for Polar Ship" is developed which allows the easy prediction of ice load, the selection of plate and frame dimensions, and the determination of safe speed limit for Polar ships.

6.2 Design Ice Load Model

Design ice load model is important for a safe speed methodology. The existing PC design ice load model is based on the design scenario of glancing collision which is characterized by the average pressure uniformly distributed over the rectangular load patch [11]. This characterization of the design ice load or formulation of the rectangular load patch requires the determination of several ice load parameters such as bow impact load, line load, pressure and aspect ratio. For this purpose, the water line length of the bow region is divided into four equal sub-regions [9-11]. The required ice load parameters are calculated at the mid-position of each sub-region [11]. Figure 6.1 illustrates the methodology to estimate the design ice load parameters in the Polar Rules.

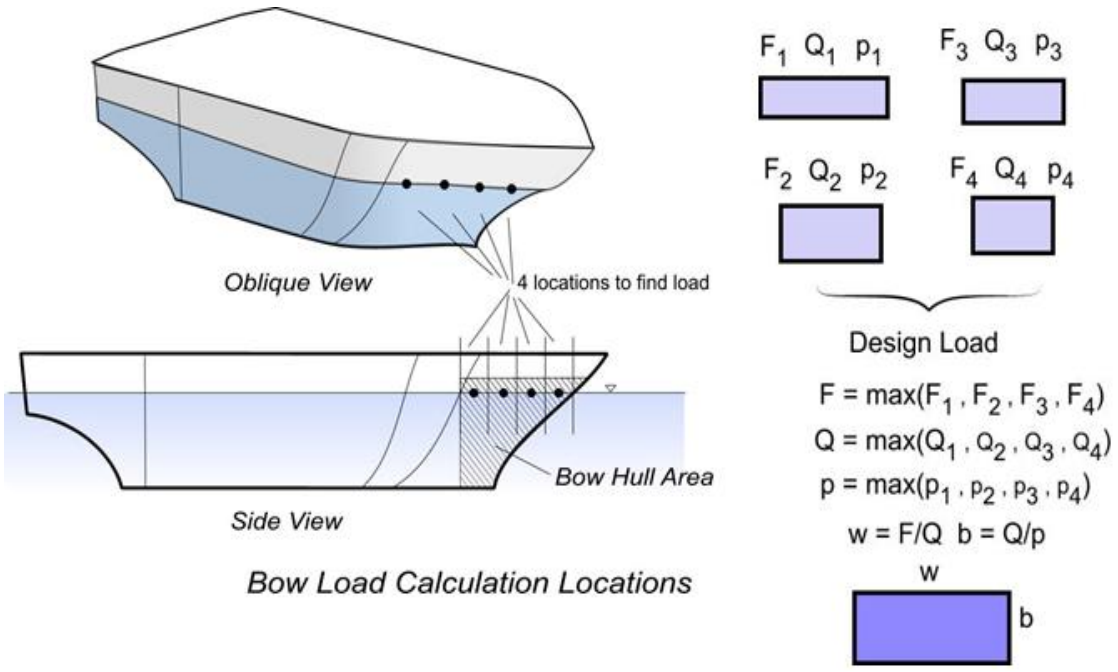

Figure 6.1 Design ice load formulation methodology in Polar Rules [9]

The magnitude of the bow impact force depends on the crushing failure and flexural failure modes of the ice wedge. Therefore, the calculation of bow impact load requires the ice crushing failure model and flexural failure model. The IACS Polar Rules specify an additional limiting value of ice failure load. According to the Polar Rules, the bow impact load cannot exceed this limiting value. The minimum of the ice crushing load, flexural failure load and limiting failure load is considered as the bow impact load at a particular bow region. Therefore, the bow impact load formula can be expressed as:

$$F_i = min\begin{Bmatrix} F_c \\ F_f \\ F_l \end{Bmatrix} \tag{6.1}$$

where, F_i is the bow impact load; F_c is the ice crushing load; F_f is the flexural failure load and F_l is the limiting ice failure load.

The ice crushing force (F_c) can be calculated from the IACS Polar crushing failure model as given in Eq. (2.7) or Eqs. given in Table 5.2. The IACS Polar Rules proposed limiting load formula in Eq. (2.7) can also be used to calculate the limiting ice failure load (F_l). However, the IACS Polar flexural failure load model in Eq. (2.7) needs an alternative to estimate the flexural failure load (F_f). This flexural failure model does not account for the velocity effect. This velocity effect influences the bow impact load and hence the design ice load model. Therefore, a modified model is presented for the bow impact load calculation which includes the velocity effect on the flexural failure. In this modified model, the Polar Rules based flexural failure model is replaced with the developed velocity dependent flexural failure model.

The modified model for the bow impact load calculation at a particular position can be expressed as:

$$F_i = min\left\{\begin{array}{c} F_c = (0.097 - 0.68(\frac{x}{L} - 0.15)^2 \frac{\alpha}{\sqrt{\beta'}} CF_c D^{0.64} \\ F_f = \frac{0.29n^{0.7}(1 + 2.57\, sin\,\alpha\, cos\,\beta'\, \theta^{0.2} Fr^{0.26})\sigma_f h^2 \theta)}{sin\,\beta'} \\ F_l = 0.6 CF_c D^{0.64} \end{array}\right\} \quad (6.2)$$

The crushing class factor (CF_c) is defined as:

$$CF_c = P_o^{0.36} V_s^{1.28} \quad (6.3)$$

The ship velocity (V_s), ice thickness (h), ice strength (σ_f), nominal ice strength (P_o) and crushing class factor in Eqs. (6.2) and (6.3) are class dependent. For a particular Polar ship, these parameters can be found from Table 6.1. Further, these parameters can be used to estimate the bow impact load for a particular location (α, β and $\frac{x}{L}$) and ship displacement (D).

Table 6.1 Polar class dependent parameters for bow load calculation [9, 10]

Polar Classes	**Vs m/s**	**Po Mpa**	**h m**	**σ_f Mpa**	**CFc**
PC 1	5.70	6.000	7.0	1.40	17.69
PC 2	4.00	4.200	6.0	1.30	9.89
PC 3	3.00	3.000	4.3	1.20	6.06
PC 4	2.50	2.450	3.5	1.10	4.50
PC 5	2.00	2.000	3.0	1.00	3.10
PC 6	1.75	1.500	2.8	0.70	2.40
PC 7	1.50	1.300	2.5	0.65	1.80

The next step after the bow impact load calculation is the estimation of load patch parameters. For calculating the load patch aspect ratio (AR_i), pressure (P_i), and line load (Q_i), Polar Rules based formulas given in the IACS [72] can be used for this purpose. These rule based formulas are given in Eqs. (6.4) to (6.7).

Load patch aspect ratio:

$$AR_i = 7.46 \sin\beta' \geq 1.3 \tag{6.4}$$

Pressure:

$$P_i = F_i^{0.22} CF_D^2 AR_i^{0.3} \tag{6.5}$$

Line load:

$$Q_i = \frac{F_i^{0.61} CF_D}{AR_i^{0.35}} \tag{6.6}$$

The patch class factor is defined as [8]:

$$CF_D = P_o^{0.389} \tag{6.7}$$

Equations (6.2) and (6.6) are applicable to the bow area. For the non-bow region, the impact force and line load can be calculated from Eqs. (6.8) and (6.10), respectively [72].

The impact load on the non-bow region is:

$$F_{nonbow} = 0.36 CF_c DF \tag{6.8}$$

The ship displacement factor is defined as:

$$DF = \begin{cases} D^{0.64} \; if \; D \leq CF_{DIS} \\ CF_{DIS}^{0.64} + 0.1(D - CF_{DIS}) \; if \; D > CF_{DIS} \end{cases} \tag{6.9}$$

where, CF_{DIS} is the displacement class factor.

The line load on the non-bow region is:

$$Q_{nonbow} = 0.639 F_{nonbow}^{0.61} CF_D \tag{6.10}$$

Equations (6.2) to (6.10) can be used to obtain the design ice load parameters and the rectangular patch load dimensions for both the bow region and non-bow region as shown in Table 6.2.

Table 6.2 Design load patch particulars in IACS Polar Rules [7, 72]

Parameters	**Bow Area**	**Non-bow Area**
Design load width	$w_{bow} = \frac{F_{bow}}{Q_{bow}}$	$w_{nonbow} = \frac{F_{nonbow}}{Q_{nonbow}}$
Design load height	$b_{bow} = \frac{Q_{bow}}{P_{bow}}$	$b_{nonbow} = \frac{w_{nonbow}}{3.6}$
Design Avg. Pressure	$P_{avgbow} = \frac{F_{bow}}{b_{bow} w_{bow}}$	$P_{avgnonbow} = \frac{F_{nonbow}}{b_{nonbow} w_{nonbow}}$

The peak pressure factor (PPF_i) in Table 2.5 can be used in the design average pressure equation to reflect the local peak pressure within the load patch. In addition, the hull area factor (HFA) in Table 2.4 is used to estimate the ice load in different hull regions. Further details of the ice load design process for the Polar ships can also be found in Daley [9], Rahman [8] and IACS [72].

6.3 Plate and Frame Design

Plastic design criterion is adopted in the IACS Polar Rules for the plating and framing requirements. This ensures better balance between the strength and safety margin against the ultimate failure of the structure for a design ice load [68, 69]. Several limit state equations were derived based on the plastic response of the plating and framing to meet the rule based design criteria [68, 69].

For plating, the limit state equations are derived based on the plate folding mechanism and by using the energy method [68]. These limit state equations specify the minimum thickness required for the shell plating to resist the design ice load. The minimum thickness requirement varies for different framing configurations and orientations. Table 6.3 contains the Polar Rules based minimum plate thickness equations for different framing configurations and orientations.

In the Polar Rules, the frame is designed to maintain the minimum shear area and section modulus [68, 69]. The limit state equations of the minimum shear area and section modulus are derived based on three possible plastic collapse mechanisms [68, 69]. These limit state equations are presented in Table 6.4 along with the limit load expressions. Perhaps, the limit load expressions are used in the design process to predict the load bearing capacity of the framing member. Detailed derivation and explanation of the limit state equations can be found in Daley [69, 73] and Daley et al. [68].

Table 6.3 Minimum plate thickness for different framing configurations [72]

Shell Plate Requirements
Minimum shell plate thickness: $$t = t_{net} + t_c$$
Transversely-framed plating ($\Omega \geq 70^0$): $$t_{net} = \frac{500s\sqrt{\frac{AF.PPF_P.P_{avg}}{R_{eH}}}}{1+\frac{s}{2b}}$$
Longitudinally-framed plating ($\Omega \leq 20^0$ and b≥s): $$t_{net} = \frac{500s\sqrt{\frac{AF.PPF_P.P_{avg}}{R_{eH}}}}{1+\frac{s}{2l}}$$
Longitudinally-framed plating ($\Omega \leq 20^0$ and b<s): $$t_{net} = \frac{500s\sqrt{\frac{AF.PPF_P.P_{avg}}{R_{eH}}\cdot\sqrt{\frac{2b}{s}-\left(\frac{b}{s}\right)^2}}}{1+\frac{s}{2l}}$$
For obliquely framed plating ($70^0 > \Omega > 20^0$), linear interpolation is used.
where, Ω is the smallest angle between waterline and framing; s is the frame spacing; R_{eH} is the minimum nominal upper yield point and *l* is the distance between frame supports. Details of the plating design can be found in IACS [72].

Table 6.4 Limit state equations in Polar Rules for framing [7, 68]

Limit State Equations
1st limit state – 3 hinge formation
Section modulus requirement: $$Z_p = \frac{P.b.s.l}{4.\sigma_y}\left(1-\frac{b}{2l}\right)\frac{1}{2+kw.\left[\sqrt{1-\left(\frac{A_o}{A_w}\right)^2}-1\right]}$$ Limit load: $$P_{limit\_1} = \frac{(2-kw)+kw\sqrt{1-48Z_{Pns}(1-kw)}}{12.Z_{pns}kw^2+1}\sigma_y Z_p \frac{4}{b.s.l.\left(1-\frac{b}{2l}\right)}$$
2nd limit state: Shear panel formation
Section modulus requirement: $$Z_p = \frac{P.b.s}{\sigma_y.(1.1+5.75.kz^{0.7})}.\left(1-\frac{b}{2l}\right).l.\left[1-\frac{A_w}{2.A_o\left(1-\frac{b}{2l}\right)}\right]$$ Limit load: $$P_{limit\_2} = \left[\frac{A_w}{\sqrt{3}}+\frac{Z_p}{l}.fz\right].\frac{\sigma_y}{b.s\left(1-\frac{b}{2l}\right)}$$
3rd Limit state: End Shear
Minimum web area: $A_o = \frac{1}{2}P.b.s.\frac{\sqrt{3}}{\sigma_y}$ Limit load: $P_{limit\_3} = \frac{2.A_o.\sigma_y}{b.s.\sqrt{3}}$ Detailed description of minimum web area (A_o), web area (A_w), flange area (A_f), flange factor (k_w), plastic modulus (Z_p) and other parameters can be found in Daley et al. [68].

The application of the limit state equations for the plating and framing design is not straight forward. This requires several assumptions and design considerations. Daley and Kendrick [12] developed an Excel spread sheet for the plate and frame design using the Polar Rules based equations. The present study utilizes the equations of this spread sheet in order to demonstrate the applicability of the modified design ice load model in the design process. Hence, detailed discussion on the application of the limit state equations for the plating and framing design are not carried out here. However, Daley [73] demonstrated that three different application methods can be useful to understand the framing design procedure. Further information on the plating and framing requirements can also be found in IACS [72].

6.4 Development of Safe Speed Methodology

This section demonstrates the safe speed methodology for different Polar class ships. For this purpose, Daley [12] developed "SAFE.speed.check" excel spread sheet is used in the present study. The SAFE.speed.check is considered as a valuable tool for the plate and frame design as well as for the safe speed analysis of the Polar ships. The SAFE.speed.check utilizes the Polar Rules based design ice load model and limit state equations. In this analysis, the Polar design ice load model is replaced with the modified design ice load model which accounts for the velocity effect in the flexural failure. The Excel-VBA code is written to determine the safe speed at a particular design point through the iteration until any of the limit state conditions is exceeded. Examples of the safe speed analysis are illustrated for the PC 5, PC 6 and PC 7 ships. Principal particulars

for the ship and structure are chosen identical to Daley and Kendrick [12] as shown in Table 6.5.

Table 6.5 Principal particulars of ship and structure for safe speed analysis

Parameters	**Value**
Ship particulars:	
Polar classes	PC 5, PC 6 and PC 7
Ship displacement	50, 000 tones
Ship block coefficient, C_b	0.768
Ship water plane coefficient, C_{pw}	0.7469
Ship mid-ship coefficient, C_m	0.934
Ship waterline angle, α	30^0
Normal ship frame angle, β'	46^0
Structure particulars:	
Frame orientation type	Transverse
Yield strength of plate and frame, $\sigma_{yp \text{ and }} \sigma_{yf}$	235 MPa
Young modulus of plate, E_p	207 GPa
Main frame span, a	2000 mm
Main frame spacing, s	350 mm
Waterline angle at contact points, α_i	30^0, 22^0, 16.8^0, 12.55^0
Normal frame angle at contact points, , β_i'	46^0, 44^0, 35^0, 26^0

The safe speed methodology is developed in three stages. At first, the bow impact loads at four different locations are calculated using Eq. (6.2). The maximum bow impact load is used to determine the design load patch parameters using Eqs. (6.4) to (6.7) and equations mentioned in Table 6.2. The calculated design load patch parameters for the PC

5, PC 6 and PC 7 are presented in Table 6.6. The table indicates that the upper Polar class (PC 5) ship needs to be designed for higher impact force and the other patch load parameters should be changed accordingly.

Table 6.6 Design load patch parameters for PC 5, PC 6 and PC 7

Patch Load Parameters	**PC 5**	**PC 6**	**PC 7**
Max. bow impact load (MN)	14.482	9.372	6.871
Aspect ratio	5.369	5.369	5.369
Line load (MN/m)	3.723	2.552	2.013
Pressure (MPa)	5.139	3.730	3.115
Load patch width (m)	3.890	3.673	3.413
Ice load patch height (m)	0.724	0.684	0.646

The load patch parameters calculated in Table 6.6 are used to design the plate and frame for the example Polar ships. The IACS Polar limit state equations in Table 6.4 and the basic rule formulas given in Daley [73] are utilized in this design process. The modified excel spread sheet and software (as discussed in section 6.5) automatically offer the optimum plate thickness and frame type based on the load patch parameters. The offered plate and frame dimensions and particulars for the PC 5, PC 6 and PC 7 are given in Table 6.7. The excel spread sheet data for the PC 5, PC 6 and PC 7 are given in Appendix C indicating detailed calculation of parameters and particulars related to the ice load patch, plate and frame design.

Table 6.7 Offered plate and frame dimensions for PC 5, PC 6 and PC 7

Plate & Frame Particulars	PC 5	PC 6	PC 7
Thickness of plate (mm)	28.00	23.50	21.50
Frame description	F 380 x 27	F 320 x 24	HP 320x16.0
Height of web (mm)	380.00	320.00	285.96
Thickness of web (mm)	27.00	25.00	16.00
Width of flange (mm)	-	-	62.00
Thickness of flange (mm)	-	-	34.04

Finally, the Polar ships with the offered plates and frames are examined to check the safe speed capability in different ice thicknesses. This involves the development of the "safe speed vs ice thickness" curves. The safe speed analysis is performed for an ice thickness range from 2.0 m to 3.5 m. Figures 6.2, 6.3 and 6.4 are the safe speed curves for the PC 5, PC 6 and PC 7, respectively.

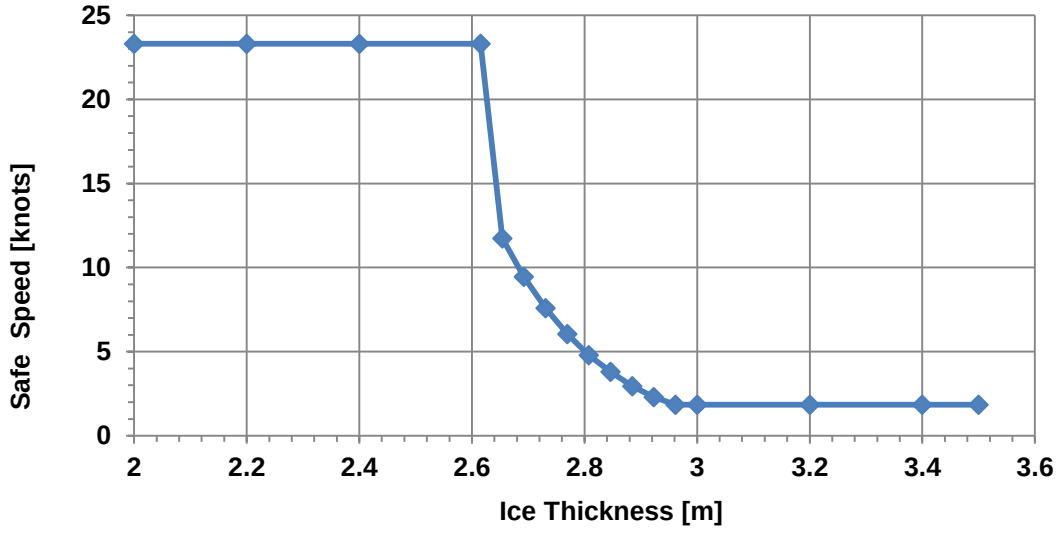

Figure 6.2 Safe speed curve for PC 5 ship

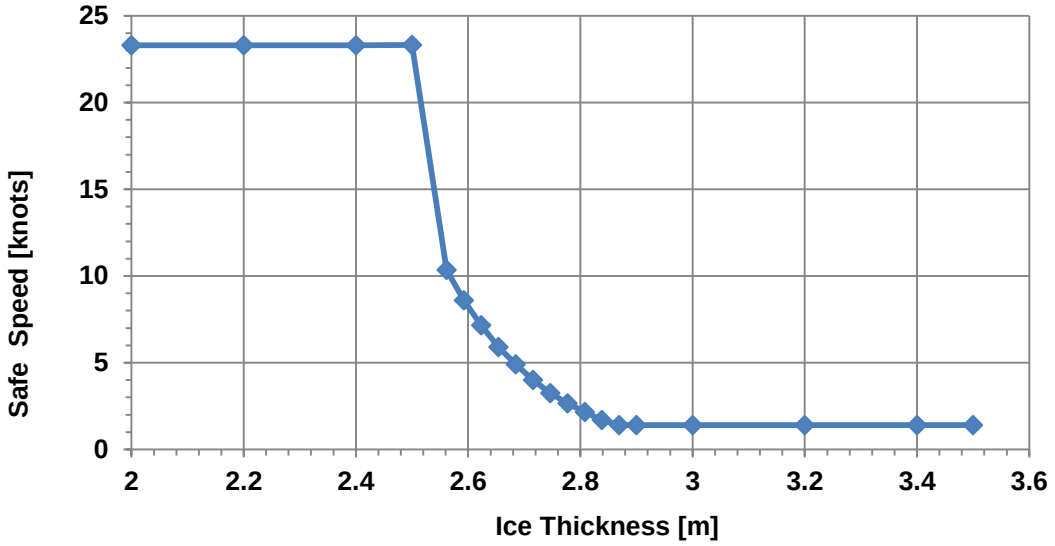

Figure 6.3 Safe speed curve for PC 6 ship

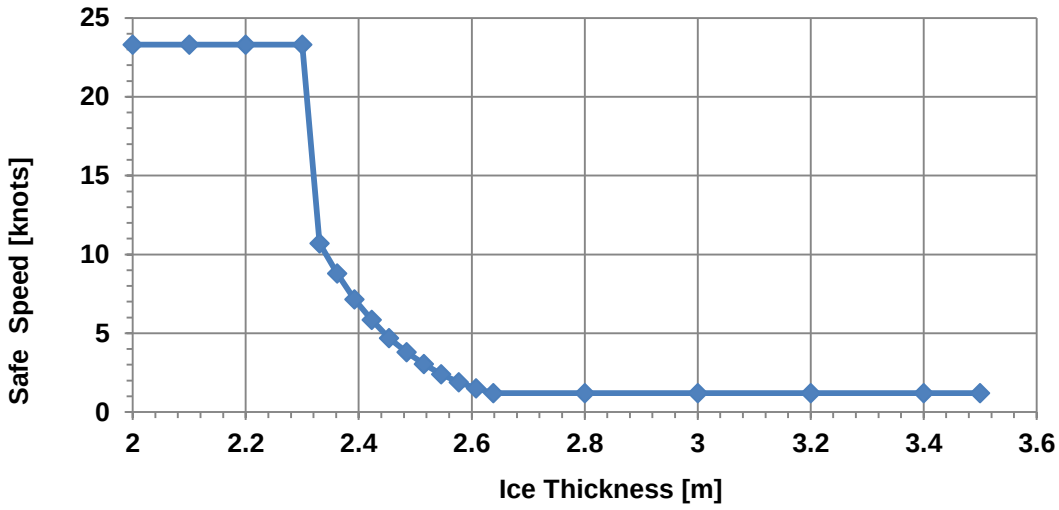

Figure 6.4 Safe speed curve for PC 7 ship

6.5 Safe Speed Check for Polar Ships-Software

The Excel-VBA software is developed based on Daley's [12] SAFE.speed.*check* spreadsheet to analyze the safe speed methodology for the Polar ships. The velocity

dependent flexural failure model is adopted into the software, and the software is named as “Safe Speed Check for Polar Ships” (Figure 6.5). In addition to safe speed analysis, the software allows easy estimation of the ice load, and plate and frame design as indicated in the main menu of the software (Figure 6.6). The software permits working in excel environment as well.

Figure 6.5 “Safe speed check for Polar ships” software

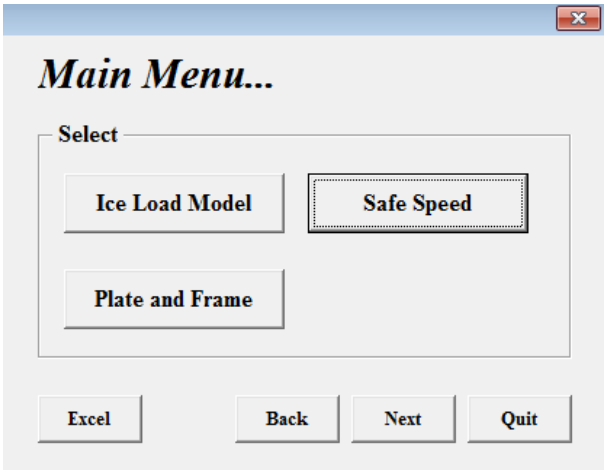

Figure 6.6 Main features of “Safe speed check for Polar ships” software

The effect of ship velocity, ship shape and ice condition can be investigated through the "Ice Load Model" option. In addition, this option can be used to estimate the design ice load parameters. On the other hand, "Plate and Frame" and "Safe Speed" options provide the optimum plate and frame design, and safe speed analysis, respectively. Applications of each option are demonstrated here with examples.

Ice Load Model Option

A 10,000 tones Polar ship (PC 7) is considered to illustrate the application of "Ice Load Model" option. This option requires several ship and ice parameters for predicting the ice load and ship velocity effect as indicated in Figure 6.7.

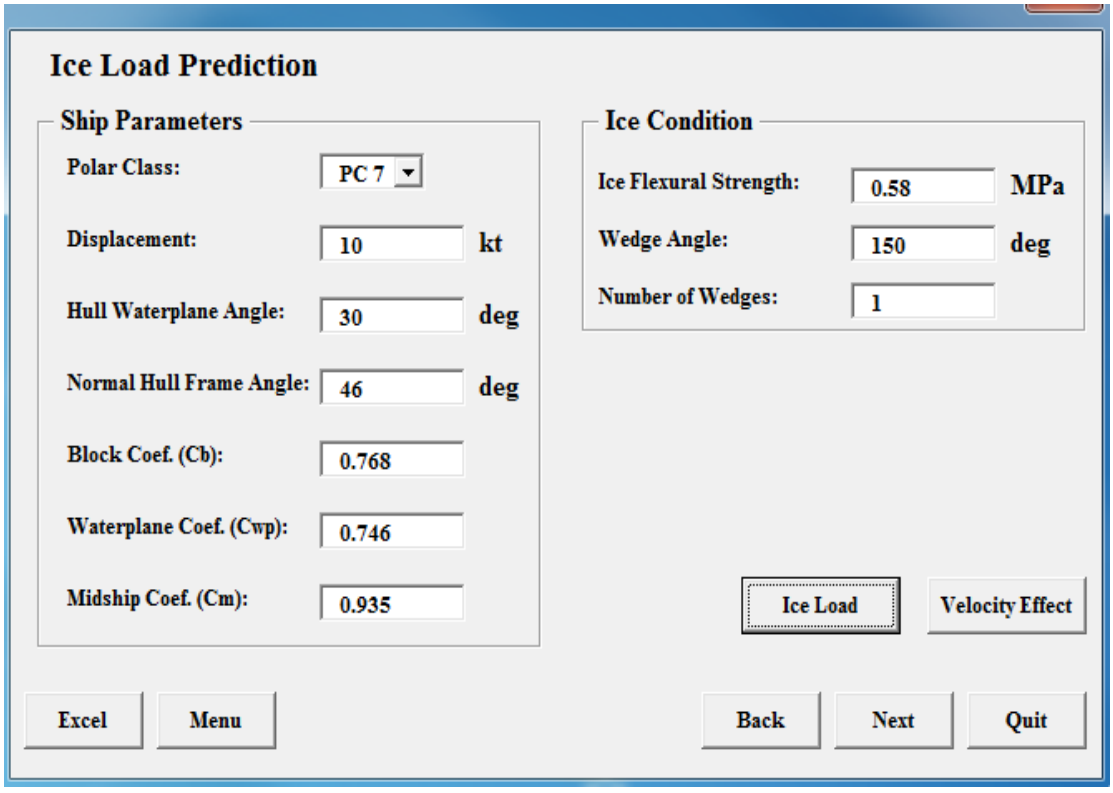

Figure 6.7 Ship and ice input parameters for ice load prediction

The above input parameters can be used to predict the bow ice load at a particular ice thickness and ship velocity (Figure 6.8). Both the IACS Polar Rules model and the modified model (Sazidy model) are utilized for this prediction. The IACS Polar Rules model provides the ice crushing load, static flexural failure load and limit bow load. The modified model allows the prediction of dynamic factor and dynamic flexural failure load in addition to the ice crushing, static flexural failure and limit bow loads. The modified model can also be used to determine the ice load patch parameters.

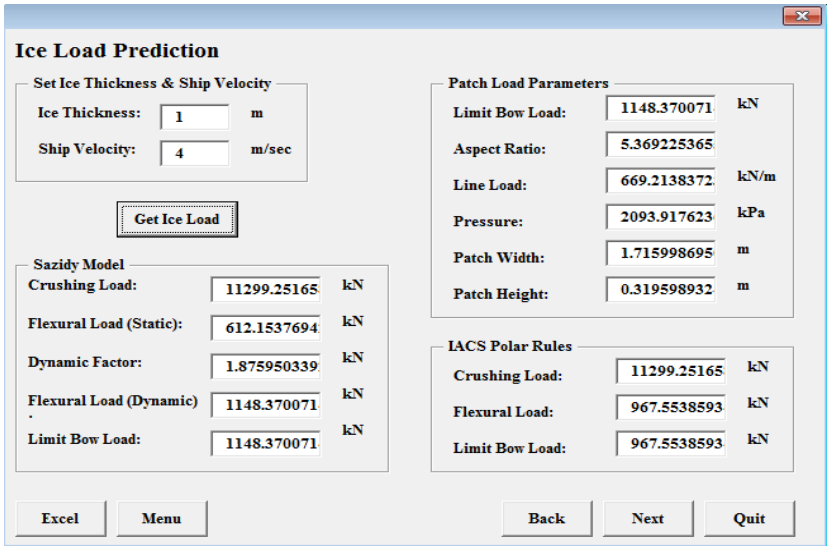

Figure 6.8 Bow ice load prediction at a particular ice thickness and ship velocity

The “Ice Load Model” option allows the investigation of ship velocity effect on the ice crushing load, ice flexural failure load and bow limit load as shown in Figures 6.9 to 6.13. The velocity effect on the ice load for a range of ice thickness can also be studied using both the Polar Rules based model and modified model (Sazidy model). Figures 6.14 and 6.15 represent the velocity effect on the bow limit load for different ice thicknesses using these two models.

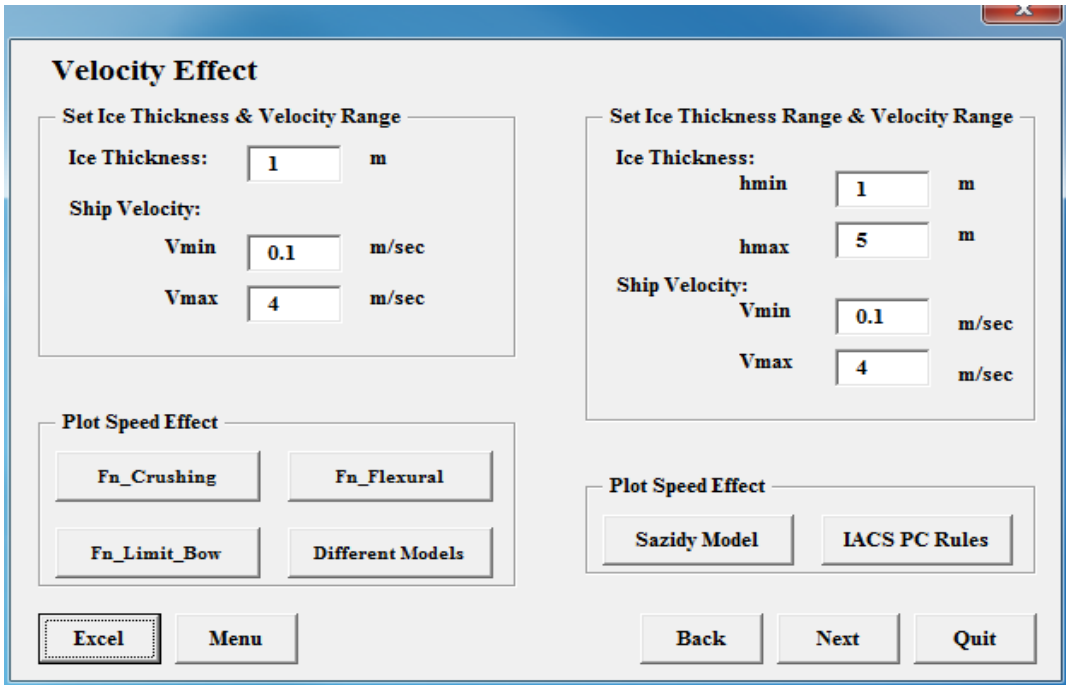

Figure 6.9 Investigation of ship velocity effect on bow ice load

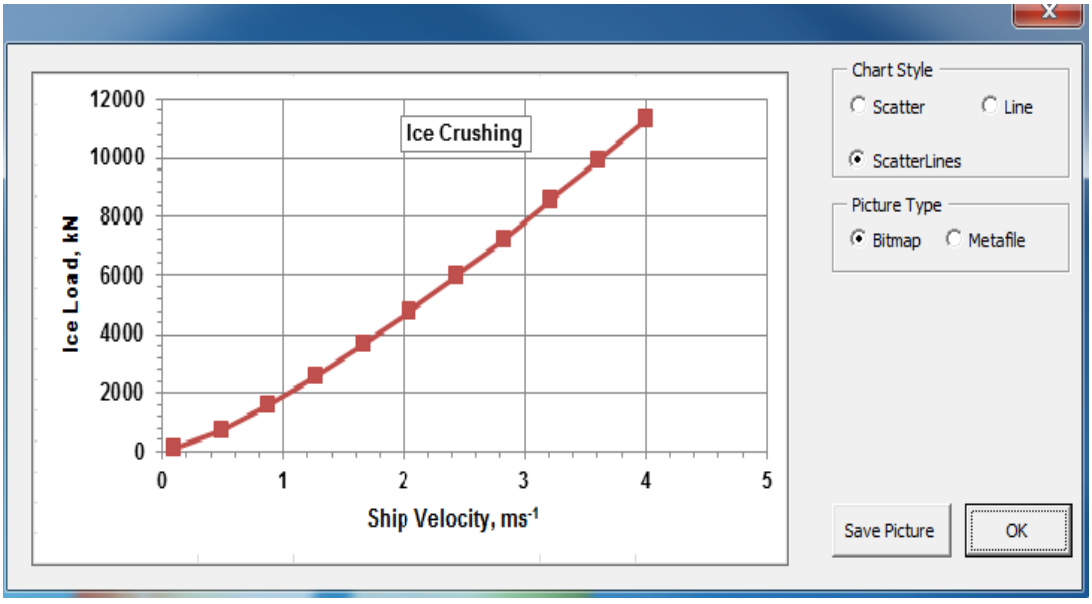

Figure 6.10 Ship velocity effect on ice crushing load at 1 m thick ice

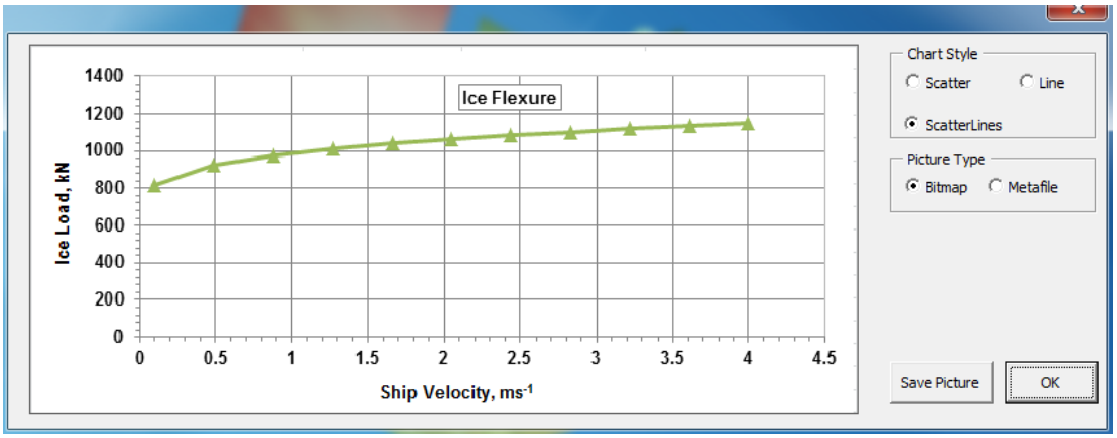

Figure 6.11 Ship velocity effect on ice flexural failure load at 1 m thick ice

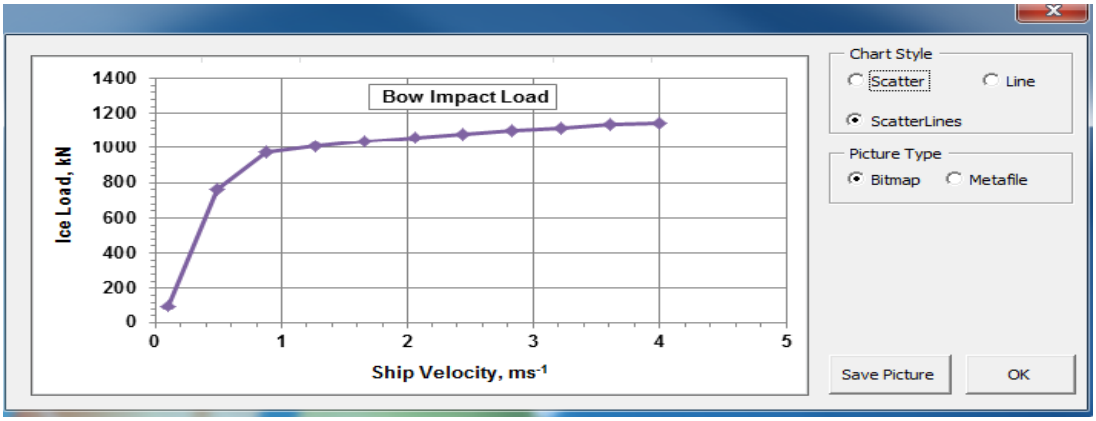

Figure 6.12 Ship velocity effect on limit bow impact load at 1 m thick ice

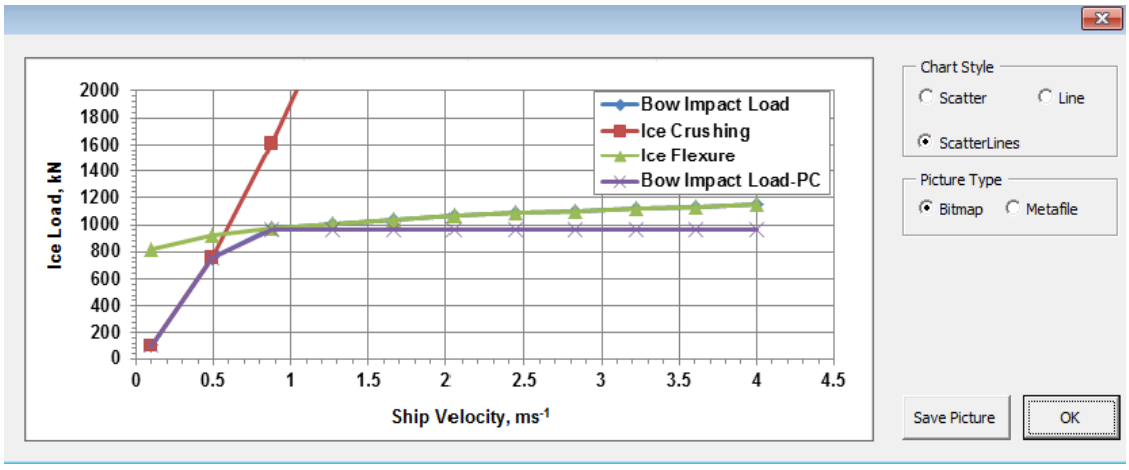

Figure 6.13 Velocity effect on ice crushing, flexural and bow ice load at 1 m thick ice

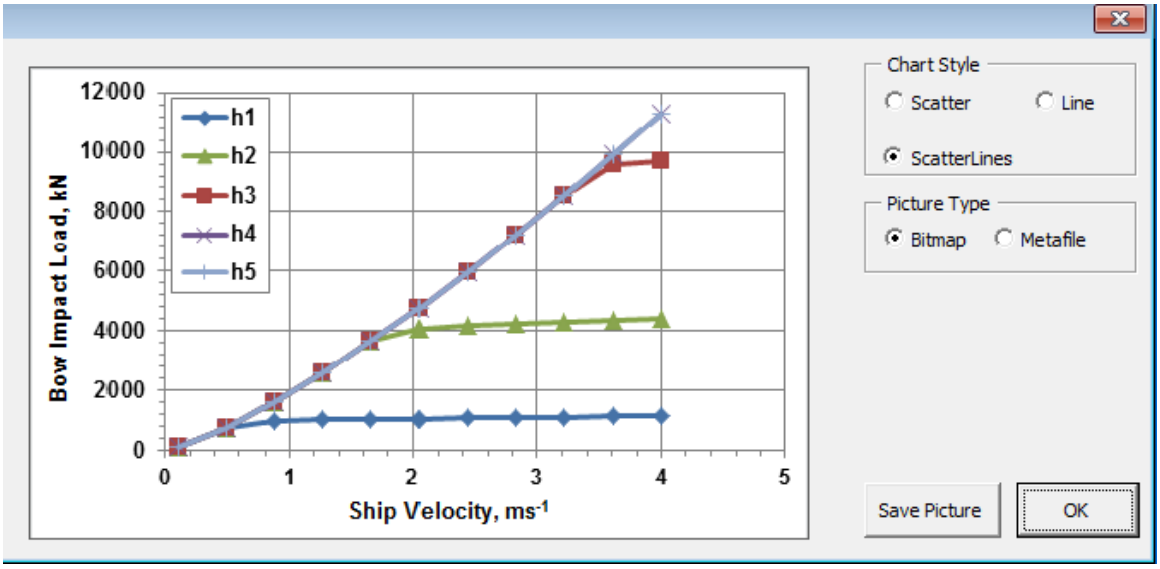

Figure 6.14 Ship velocity effect on bow impact load for ice thickness range of 1 m to 5 m (Sazidy model)

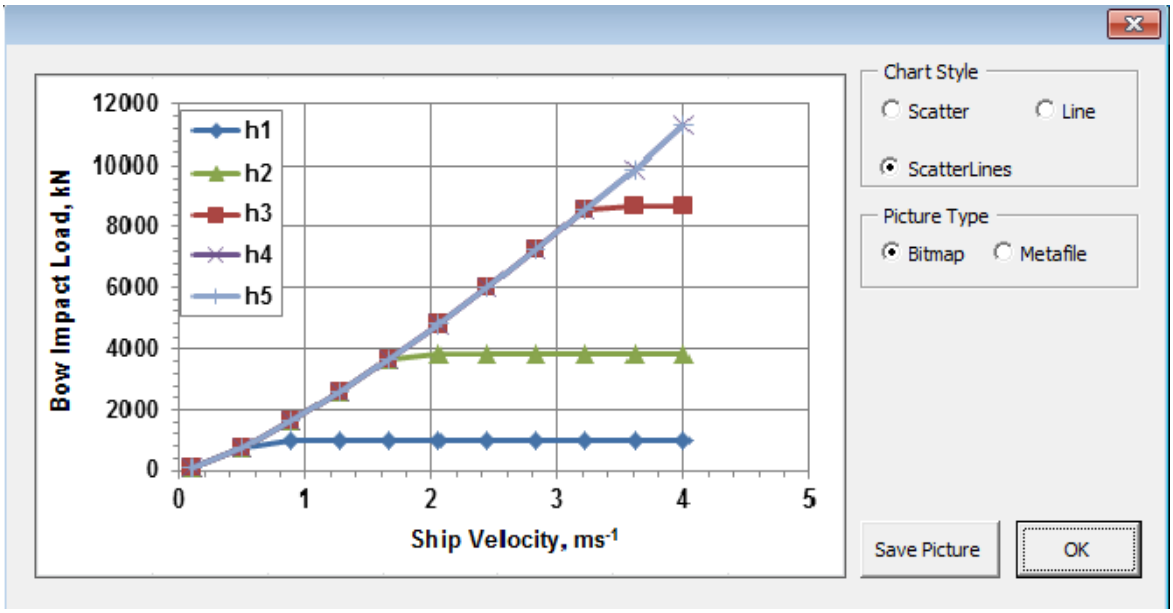

Figure 6.15 Ship velocity effect on bow impact load for ice thickness range of 1 m to 5 m (Polar Rules model)

Plate and Frame Option

This option in the software is used to design the plate and frame for the Polar ships. This design procedure needs the user to specify the contact angles at four bow locations to formulate the design ice load model. Based on this design ice load model and structural limit state equations, the software offers optimum plate thickness and frame dimensions. Figure 6.16 indicates the offered plating and framing for a 50, 000 tones PC 5 ship.

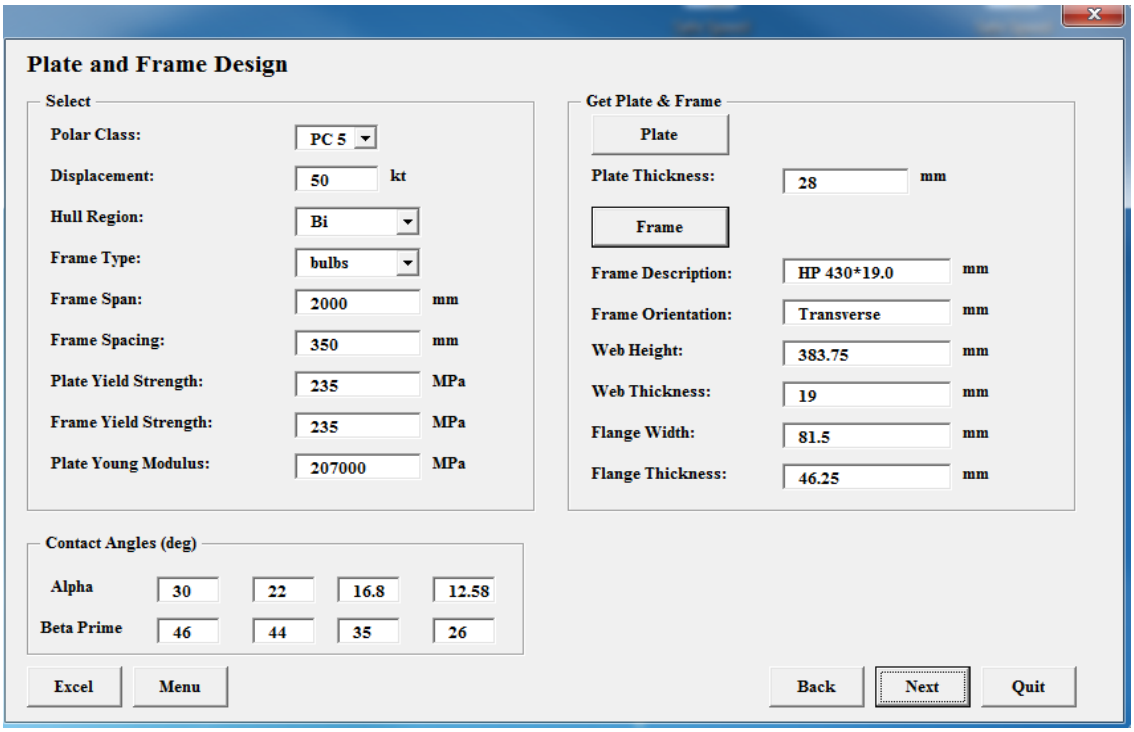

Figure 6.16 Plate and frame design for a 50,000 tones PC 5 ship

Safe Speed Option

This option is used to analyze the safe speed capabilities of different Polar class ships. Initially, the plate and frame are designed against specific design points. The designed

plate and frame are used for the safe speed analysis. The safe speed results and curves for the 50, 000 tones PC 5 ship are presented in Figures 6.17 and 6.18.

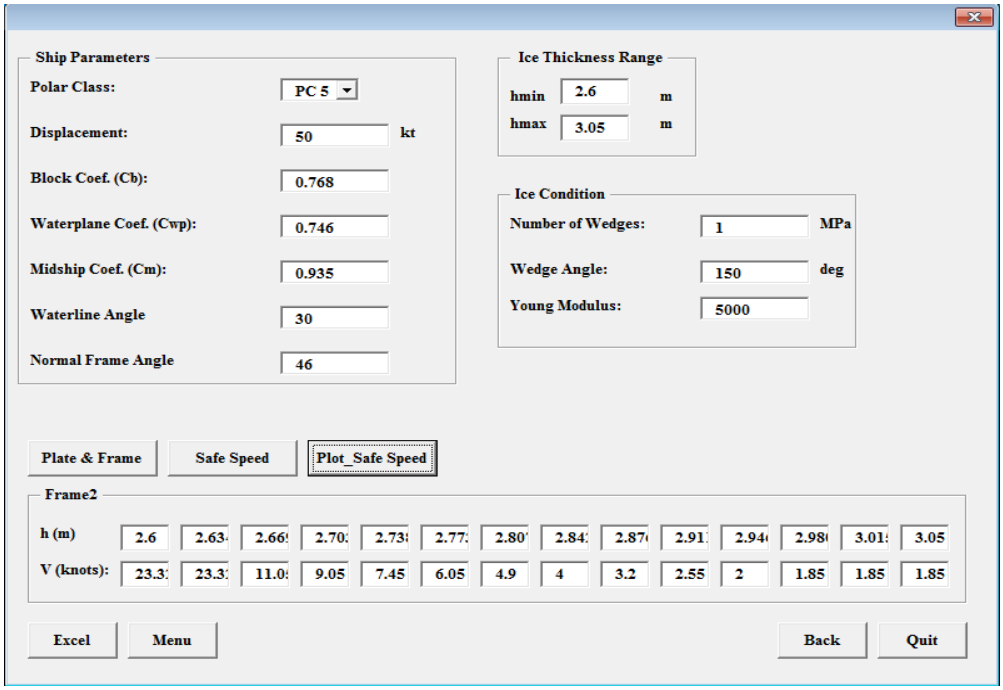

Figure 6.17 Safe speed analysis for 50,000 tones PC 5 ship

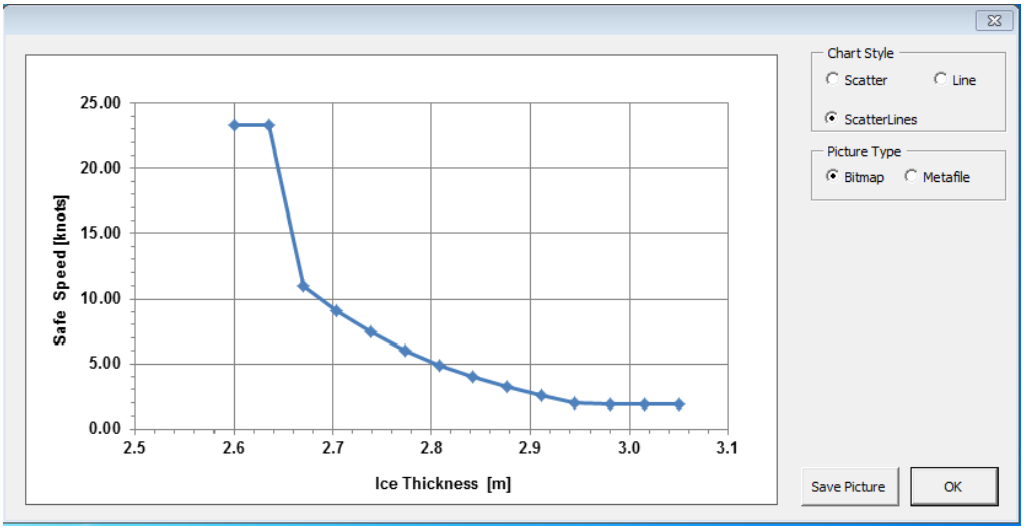

Figure 6.18 Safe speed curve for 50,000 tones PC 5 ship

Chapter 7

Summary and Recommendations

7.1 Introduction

Previous studies indicate that the safe speed methodology can be a valuable tool to ensure safe ship operation in the Polar water. The IMO, classification societies and ship industries have shown their interest towards the development of safe speed methodology. The main motivation of this present work is to help in improving the development of safe speed methodology for the Polar ships. For this purpose, a velocity dependent flexural failure model is developed and utilized to formulate the safe speed methodology for different Polar class ships. The developed model represents significant improvement of the Polar Rules based flexural failure model. The present research carries out several tasks to develop the velocity dependent flexural failure model and safe speed methodology. This chapter summarizes and evaluates these tasks. This chapter also includes original contributions of the thesis along with the limitations and some guide lines for future work.

7.2 Summary of Present Work

The following tasks are carried out to develop the velocity dependent flexural failure model and safe speed methodology:

7.2.1 Study of Ship-Ice Interaction Process

Ship-ice interaction process is important to formulate the ice load model, and hence for the Polar ship design practice and safe speed methodology. For this reason, the fundamental theories and modeling efforts are reviewed in order to identify the critical issues involved in the ship-ice interaction process. Emphasis has been placed on the current understanding of the ice failure process, ship-ice interaction process and ship-ice interaction modeling approaches. The effects of different influencing factors such as ship velocity, ship hull shape, ice condition and water foundation on the interaction process are investigated.

Most of the studies idealize the ship-ice interaction process based on the observation of model scale and full scale tests. An idealized ship-ice interaction process consists of breaking phase, rotating phase and sliding phase. The investigation of entire interaction process considering all phases is important for the global ice force and ice resistance. Studies indicate that the local peak force is responsible for the ship structural damage. The breaking phase of ship-ice interaction is sufficient to extract this local peak force. Hence, the present study considered only the breaking phase of ship-ice interaction.

The ship icebreaking process mainly involves the ice crushing and flexural failures which are influenced by the water foundation underneath of a floating ice sheet. The icebreaking pattern is important to explore this ship icebreaking process. Different idealized icebreaking patterns are used to study the icebreaking process indicating the formation of radial and circumferential cracks which produce several ice wedges or ice cusps. Many researchers suggest modeling of simple ice wedge breaking instead of full ice sheet especially for the local contact force.

Several attempts have been made to study the ship-ice interaction process analytically and numerically. The existing analytical models or numerical models using the analytical or semi-empirical approaches mainly focus on the prediction of global ice forces and ice resistance for the continuous icebreaking and maneuvering operations. Most of these models are over simplified and ignore one or more influencing parameters.

Advanced numerical techniques have also been employed to investigate the dynamic bending behavior of ice in the ship-ice interaction. Most of these models are applied to specific test conditions and cannot be used for the present investigation. Different numerical methods such as FEM, CEM, DEM and XFEM, and different numerical solvers such as Lagrangian, ALE and SPH are employed for these modeling purposes. Many of these methods and solvers have the capability to generate the bending crack initiation and propagation. However, the finite element method, with the element erosion technique and the Lagrangian solver, is efficient and hence adopted in this study.

7.2.2 Material Models of Ice and Water

Material models play a vital role in characterizing the ship icebreaking process. For this reason, three individual tests are conducted in the commercial software package LS DYNA to select the material models and parameters for the ice crushing behavior, ice flexural behavior and water foundation effect.

For the ice crushing behavior, an ice crushing test is performed in which the ice wedge is modeled as an elastic-perfectly plastic material. The material model *MAT_PLASTIC_KINEMATIC is used to represent this behavior. The compressive strength and Young's modulus of the crushing model are tuned to establish a similar pressure-area relationship suggested in the Polar Rules for PC 1.

The four point bending test is conducted at quasi-static condition to represent the flexural behavior. An isotropic elasto-plastic material model *MAT_PLASTICITY_COMPRESSION_TENSION is considered for the ice beam. The model considers different responses in compression and tension. In addition, the model accounts for the strain rate sensitivity. The Element Erosion Method is employed in which the effective plastic strain value is adjusted to get the proper bending response. The model results are compared with the theoretical bending load and crack location.

Simple foundation tests are conducted to consider the water foundation effect. In the test, the foundation is assumed as a linear elastic material, and modeled with the

*MAT_ELASTIC. The dimensions and elastic modulus are adjusted to match as close as possible to the hydrostatic pressure of water on the lower ice surface.

7.2.3 Numerical Model of Ship Icebreaking

The numerical models of ship icebreaking process are developed to explore the velocity effect on the ice flexural failure. The material models of the ice crushing, ice flexural failure and water foundation effect are incorporated into these ship icebreaking models.

The numerical models of ship icebreaking consider two collision scenarios. One is the head-on collision with a flat inclined face of the ship, and another is the shoulder collision with an R-Class icebreaking ship. For the head-on collision, two breaking conditions are considered; an ice wedge breaking and a level icebreaking. The shoulder collision is only investigated for the level icebreaking. For the ice wedge breaking, the effect of ship velocity on the breaking process is investigated for different ship angles, ice wedge angles and ice thicknesses. The level icebreaking is investigated with and without existing radial cracks for three different breaking conditions.

The model results indicate that the ice edge crushes for all breaking conditions. The circumferential bending crack initiates and propagates in the bending zone. For a particular ship frame angle, ice thickness and ice wedge; the bending crack location shifts towards the ice crushing zone at higher ship velocity. These results also indicate that the impact force, bending crack location and breaking pattern are influenced by the wedge angle, ice thickness, normal ship frame angle and ship velocity.

For the level icebreaking in both collision scenarios, the bending failure occurs close to the ice crushing zone in the absence of any radial crack. The location of the bending crack does not change significantly with the ship velocity. More realistic distributions of the bending cracks are observed in the presence of radial cracks. The distribution of bending cracks is shifted towards the ice crushing zone at higher ship velocity. The impact force increases with the ship velocity but decreases with the number of existing radial cracks.

7.2.4 Formulation of Dynamic Ice Load Models

In the absence of any suitable dynamic ice load model, a simple methodology is presented to formulate four dynamic ice load models based on the existing analytical and semi-empirical models. Two static ice load models and two dynamic factor models are selected. For the static ice load models, Kashteljan's model [29] and Daley's model [12] are considered, and modified to meet Nguyen et al.'s [32] experimental observation [8]. Daley and Kendrick [12] derived, and Lindqvist proposed [22] dynamic factor models are used in this analysis.

In addition to these four dynamic ice load models, two breaking length formulas are used to validate the numerical model results. These results indicate that the numerical models are in general agreement with the comparative models.

7.2.5 Velocity Dependent Ice Flexural Failure Model

An analytical closed form model of velocity dependent flexural failure is proposed to predict the dynamic impact load from the ship icebreaking process. The model is developed based on the numerical results of ship icebreaking process. Four factors; ship velocity, ship angle, ice thickness and ice wedge angle are considered. One factor at a time (OFAT) approach is used to establish this empirical relationship between the ship velocity and the impact force for different icebreaking conditions.

The developed velocity dependent ice flexural failure model is validated against full scale ice impact test data and against a finite element based non-linear dynamic bending load model provided by Varsta [47]. The developed model results are in good agreement with Varsta's model results as well as with the full scale test data.

Application of the velocity dependent flexural failure model to predict the bow impact load is also demonstrated for an example ship type (PC 1 ship). These bow impact loads are compared with the IACS Polar Rules based results. The bow impact load analysis indicates that there is a significant velocity effect in the impact load at medium and higher ship velocity which is ignored in the Polar Rules based model. Therefore, the developed velocity dependent flexural failure model represents a useful improvement of the current Polar Rules based model.

7.2.6 Safe Speed Methodology

Safe speed methodology for different Polar class ships such as PC 5, PC 6 and PC 7 are demonstrated to examine the capability of safe speed operation in different ice conditions. For this purpose, a modified design ice load model is proposed based on the new velocity dependent ice flexural failure model. This design ice load model is used to calculate the ice load patch parameters. The ice load patch parameters along with the Polar Rules based structural limit state equations are employed to design the plate and frame for the safe speed methodology. Finally, the Excel-VBA software "Safe Speed Check for Polar Ships" is developed which provides an easy and convenient way to predict the ice load on the ship hull, design the plate and frame, analyze the safe speed capabilities of the Polar ships.

7.3 Contributions of Present Work

The main goal of this research work is to develop a velocity dependent flexural failure model to help in improving the Polar ship design and safe speed methodology. Several tasks are carried out as mentioned in the previous section to accomplish this goal. These tasks contribute to the engineering knowledge in many ways. The contributions of this present work are addressed below:

Contribution 1: Ship-Ice Interaction Study

The literature review on ship-ice interaction process is useful to understand the basic mechanisms, and to identify the critical issues involved in the process. Discussion on the existing modeling approaches is helpful in selecting suitable modeling techniques and

methods for a particular ship-ice interaction scenario. This information provides a previously un-collated guide to modeling local contact mechanisms as well as the global ship-ice interaction.

Contribution 2: Material Model of Ice Flexural Failure

Ice flexural behavior is difficult to simulate. Studies indicate that the available numerical material models of ice flexure are not suitable to capture all important features. In most previously available cases, the models are oversimplified or follow a complicated procedure to estimate the input parameters. Some of these models are unable to simulate the bending crack initiation and propagation. In this study, a new and relatively simple methodology is presented to develop a material model of ice flexural failure, based on a four point bending test. This model allows more realistic investigation of the ice flexural behavior in the ship-ice interaction as well as the larger ice-structure interaction problem. It has proved its capability to produce the bending crack effectively which is important to represent the ice flexural behavior.

Contribution 3: Material Models of Ice crushing and Water Foundation

Previous research indicates that existing material models can be used to represent the ice crushing behavior and water foundation. However, these models are computationally inefficient when they are utilized in a large and complicated model such as ship-ice interaction model. In the present work, alternative simpler material models are developed to characterize and simulate the ice crushing and water foundation effect at lower

computational cost and with equal fidelity. These material models along with the ice flexural failure models can be used to investigate different ice interaction problems.

Contribution 4: Numerical Models of Ship Icebreaking

Numerical models of ship icebreaking are valuable tools to predict the ice impact load on the ships and offshore structures. The models developed in the present work allow a complicated ship-ice interaction process to be modeled using simple methodology and procedure. These models consider ice edge crushing, ice flexural failure and water foundation effect. The consideration of these principal mechanisms is not previously observed in published finite element models. The developed numerical models utilize an Element Erosion Method (EEM) which overcomes the difficulties of generating bending crack initiation and propagation. The models are well suited to study the dynamic ship-ice interaction process, and to investigate the effect of ship velocity, ship shape and ice condition on the icebreaking pattern.

Contribution 5: Investigation of Level Icebreaking

In this research, emphasis is placed on the modeling of ship and ice wedge breaking based on the local contact mechanism. However, a simple methodology is presented to investigate level icebreaking using the numerical models of ship icebreaking. The present work demonstrates how an existing radial crack might affect the level icebreaking pattern and icebreaking force. The methodology creates a scope for future research on the continuous icebreaking and prediction of ice resistance which involves the level icebreaking.

Contribution 6: Methodology to Formulate Dynamic Ice Load Models

Researchers and scientists always find difficulties in validating ship-ice interaction models. In general, model scale and full scale test results are utilized to validate the global ship-ice interaction models. Neither of these can characterize the local contact mechanism between the ship and ice. Analytical models are more suitable for this validation purpose. However, the existing analytical models are applicable to the static ship icebreaking conditions. In the present work, an alternative method is introduced to formulate four dynamic ice load models from existing static analytical and semi-empirical models. The models are beneficial in the absence of model test data or field test data.

Contribution 7: Velocity Dependent Flexural Failure Model

The velocity dependent flexural failure model is developed in an innovative way, using the numerical models of basic ship icebreaking mechanisms. The model is helpful to study the effect of ship velocity, ship shapes and ice conditions on the icebreaking process. This model incorporates the velocity effect in ship icebreaking and provides significantly improved load predictions when compared to the IACS Polar Rules based model, and Daley and Kendrick model [12], especially for the thinner ice and higher ship speed operation. This velocity dependent flexural failure model as well as the numerical models can be used in exploring different collision scenarios.

Contribution 8: Analysis of Bow Impact Load

Bow impact load analysis is carried out using the velocity dependent flexural failure model for the Polar class ships. This analysis incorporates and explores the ship velocity

effect on the bow impact load, which is important to formulate design load patch parameters. Improved load patch definition is useful in plate and frame design, Polar ship design practice and safe speed methodology.

Contribution 9: Safe Speed Check for Polar Ships

This software provides a safe speed methodology for different Polar class ships. This is a first implementation for Polar ships of rationally based safe operational guidance that can be used on the bridge of a vessel. In addition to the operational safe speed methodology, the software provides an easy estimation of design ice loads, and simple design of ship plates and frames that can be used at the design stage based on operational scenarios.

7.4 Limitations of Present Work

In this present work, several assumptions and simplifications are made to achieve the research objectives. In some cases, limitations need to be addressed for future refinement and improvement of the work. Some of these assumptions and major limitations are discussed below:

- The variation or influence of different ice properties such as Young modulus, density, flexural strength, compressive strength which are not considered in the development of ice material models.

- Material models of ice crushing and water foundation provide equivalent ice crushing force and hydrodynamic force, respectively. However, these models do not simulate the true crushing behavior and water foundation effect.

- Numerical models of ship icebreaking do not account for friction between the ship hull and ice.

- Numerical models are suitable to study the local contact mechanism of icebreaking phase. These models are not applicable to the global ship-ice interaction problem.

- Numerical models can also be applied to investigate the local contact between the ship and level ice. However, these models cannot be used in exploring continuous level icebreaking.

- Due to the lack of specific test data, numerical model results are validated against the existing analytical models.

- Numerical models of level icebreaking consider already existing radial cracks. These models are not able to simulate the radial crack initiation and propagation.

- The velocity dependent flexural failure model assumes that the flexural load is proportional to the flexural strength.

- Presented safe speed methodology ignores many influencing factors. This is based on only the ice crushing and ice flexural failure models. This methodology can be termed as technical safe speed.

7.5 Recommendations for Future Work

Based on above assumptions and limitations, following refinements and improvements of the work are recommended for future investigation:

- Parameter sensitivity study focusing on the ice properties such as Young modulus, density, compressive strength, flexural strength etc.
- Improvement of the ice crushing and water foundation material models for more realistic behaviors
- Refinement of the numerical models considering ship-ice friction
- Extension of the numerical models to investigate the global ship-ice interaction and continuous level icebreaking
- Development of improved numerical model to simulate the radial crack initiation and propagation. More investigation is needed to explore the effects of radial crack on the level icebreaking
- Numerical investigation of different ice collision scenarios rather than shoulder collision and head-on collision
- Improvement of the velocity dependent flexural failure model by exploring the rate sensitivity of flexural strength and crushing strength. More investigation is needed to explore the velocity effect on the ice crushing and flexural failure.
- Improvement of the developed safe speed methodology considering different influencing factors

References

[1] Arctic Council, 2009, “Arctic Marine Shipping Assessment”, *Report on Arctic Marine Shipping*.

[2] Kubat, I. and Timco, G., 2003, “Vessel Damage in the Canadian Arctic”, *Proceedings 17th International Conference on Port and Ocean Engineering under Arctic Conditions*, POAC'03, 1, pp. 203-212, 2003-06-16.

[3] Likhomanov, V., Timofeev, I. Stepanov, Kastelyan, V., Iltchuk, A., Krupina, N. and Klenov, A., 1997, “Scientific Basis and Methodology of the Development of an Ice Passport”, *Report Prepared for Arctic and Antarctic Research Institute Department of Ship Performance in Ice*, St. Petersburg, Russia.

[4] Shunying, J. and Shewen, L., 2012, “Interaction between Sea Ice/Iceberg and Ship Structures: A Review”, *Advances in Polar Science, 23:* 187-195, doi: 10.3724/SP.J.1085.2012.00187.

[5] Sawamura, J., Riska, K. and Moan, T., 2009, “Numerical Simulation of Breaking Patterns in Level Ice at Ship’s Bow”, *Proceedings of the Nineteenth (2009) International Offshore and Polar Engineering Conference,* Osaka, Japan.

[6] Daley, C. G. and Colbourne, D. B., 2012, “Arctic Ocean Engineering-Course Notes”, Memorial University of Newfoudland, St. John’s, NL, Canada.

[7] Dolny, J., Yu, H-C., Daley, C., Kendrick, A., 2013, “Developing a Technical Methodology for the Evaluation of Safe Operating Speeds in Various Ice Conditions”, *Proceedings of the 22nd International Conference on Port and Ocean Engineering under Arctic Conditions*, Espoo, Finland.

[8] Rahman, M. M., 2012, “Structural Resistance of Polar Ships and FPSO´s to Ice Loading”, *M. Sc. Thesis*, Norwegian University of Science and Technology, Department of Marine Technology, Norway.

[9] Daley, C., n.d., “IACS Requirements for Polar Class Ships Overview and Background”, www.engr.mun.ca/~cdaley/8674/L22aPolar%20Classes.ppt.

[10] Yu, H., 2008, “IACS Polar Class Requirements and Hull Structural Design Applications”,http://legacy.sname.org/sections/texas/Meetings/2008/September%20Luncheon/SNAME-Texas%20Polar%20Class%20Rules%20-%20Han%20Yu.pdf.

[11] Germanischer Lloyd, 2008, “Rules for Classification and Construction-Ship Technology”, *Report on Guidelines for the Construction of Polar Class Ships*.

[12] Daley, C. and Kendrick, A., 2011, “Safe Speed in Ice,” *Final Report*, Prepared for BMT Fleet Technology, Reference: 6931DFR.Rev00, Ottawa, ON, Canada.

[13] Lubbad, R., and Loset, S., 2010, “A Numerical Model for Real-Time Simulation of Ship-Ice Interaction,” *Journal of Cold Regions Science and Technology*, 65 (2011) 111-127.

[14] Su, B., Riska, K., and Moan, T., 2009, “A Numerical Method for the Prediction of Ship Performance in Level Ice,” *Journal of Cold Regions Science and Technology*, 60 (2010) 177-188.

[15] O’Connell, B. J., n.d., “Ice Hazard Radar”, http://www.dfo-mpo.gc.ca/Library/343422.pdf

[16] Abraham, J., 2008, “Plastic Response of Ship Structure Subjected to Ice Loading”, *Master of Engineering Thesis*, Memorial University of Newfoundland, St. John’s, NL, Canada.

[17] Hänninen, S., 2003, “Incidents and Accidents in Winter Navigation in the Baltic Sea, Winter 2002 – 2003”, *Report for Winter Navigation Research Board*, http://www.trafi.fi/filebank/a/1352716465/5666a0c12549e09d1f84c3075353d3de/10732-No_54_incidents_and_accidents_2003.pdf.

[18] Aksnes, V., 2010, "A Simplified Interaction Model for Moored Ships in Level Ice*," Journal of Cold Regions Science and Technology*, 63 (2010) 29-39.

[19] Su, B., 2013, "Maneuverability of Ships in Ice: Numerical Simulation and Comparison with Field Measurements", *Presentation for the Research Council of Norway*, http://www.cesos.ntnu.no/attachments/078_S11_Biao%20Su.pdf.

[20] Riska, K., 2011, "Ship–Ice Interaction in Ship Design: Theory and Practice", *Article on Research and Development Trend for Arctic Ship Design*, http://www.arctis-search.com/Ship-Ice+Interaction+in+Ship+Design+-+Theory+and+Practice.

[21] Liu, J., 2009, "Mathematical Modelling Ice-Hull Interaction for Real Time Simulations of Ship Maneuvering in Level ice," *Ph.D. Thesis*, Memorial University of Newfoundland, St. John's, NL, Canada.

[22] Skar, T., 2011, "Ice Induced Resistance of Ship Hulls: A Comparison of Resistance Estimated from Measurements and Analytical Formulations," *Master Thesis*, Norwegian University of Science and Technology, Norway.

[23] Jeong, S., 2014, “A Semi-Empirical Method of Ice Resistance Prediction in Level Ice”, *International Conference and Exhibition on Performance of Ships and Structures in Ice*, Alberta, Canada, ICETECH14-141-RF.

[24] Tan, X., Su, B., Riska, K., and Moan, T., 2012, “The Effect of Heave, Pitch and Roll Motions to Ice Performance of Ships”, *Proceedings of the 21st IAHR International Symposium on Ice*, Dalian, China.

[25] Erceg, S., Ehlers, S., Polach, R. F. V. B. and Leira, B., 2014, “A Numerical Model to Initiate the Icebreaking Pattern in Level Ice”, *Proceedings of the ASME 2014 33rd International Conference on Ocean, Offshore and Arctic Engineering*, California, USA, OMAE2014-23409.

[26] Myland, D. and Ehlers, S., 2014, “Theoretical Investigation on Ice Resistance Prediction Methods for Ships in Level Ice”, *Proceedings of the ASME 2014 33rd International Conference on Ocean, Offshore and Arctic Engineering*, California, USA, OMAE2014-23304.

[27] Tan, X., Riska, K., and Moan, T., 2014, “Effect of Dynamic Bending of Level Ice on Ship's Continuous-Mode Icebreaking”, *Journal of Cold Regions Science and Technology*, 106-107 (2014) 82-95.

[28] Tan, X., Su, B., Riska, K., and Moan, T., 2013, "A Six-Degrees-of-Freedom Numerical Model for Level Ice–Ship Interaction", *Journal of Cold Regions Science and Technology*, 92 (2013) 1-16.

[29] Kashteljan, V. I., Poznyak, I. I., and Ryvlin, A. Y.,1968, "Ice Resistance to Motion of A Ship", *Translation, Sudostroenie, Leningrad*, Translation by Marine Computer Application Corporation.

[30] Enkvist, E., 1972, "On the Ice Resistance Encountered by Ships Operating in the Continuous Mode of Icebreaking", *The Swedish Academy of Engineering Sciences in Finland*, Helsinki, Report No. 24, 181 pp.

[31] Kotras, T. V., Baird, A.V., and Naegle, J. W., 1983, "Predicting Ship Performance in Level Ice", *Trans. of Society of Naval Architects and Marine Engineers,* Vol.91, p. 329-349.

[32] Nguyen, D. T., Sørbø, A. H. and Sørensen, A. J., 2009, "Modelling and Control for Dynamic Positioned Vessels in Level Ice", *Proceedings of 8th Conference on Maneuvering and Control of Marine Craft*, pp. 229–236, Guarujá, Brazil.

[33] Lu, W., Lubbad, R., Loset, S., and Hoyland, K., 2012, "Cohesive Zone Method Based Simulation of Ice Wedge Bending: a Comparative Study of Element Erosion,

CEM, DEM and XFEM," *Proceedings of the 21st IAHR International Symposium on Ice*, Dalian, China.

[34] Sawamura, J., Tachibana, T., Tsuchiya, H., and Osawa, N., 2010, "Numerical Investigation for the Bending Failure of Wedge-Shaped Floating Ice", *Proceedings of the 20th IAHR International Symposium on Ice*. Lahti, Finland.

[35] Sawamura, J. Riska, K., and Moan, T., 2008, "Finite Element Analysis of Fluid-Ice Interaction during Ice Bending", *Proceedings of the 19th IAHR International Symposium on Ice*, BC, Canada.

[36] Lindqvist, G., 1989, "A Straightforward Method for Calculation of Ice Resistance of Ships", *Proceeding of the 10th International Conference on Port and Ocean Engineering under Arctic Conditions (POAC),* Lulea, Sweden, p. 722-735.

[37] Hoving, J., 2012, "Numerical Modelling of Ice & Ice-Structure Interactions", *Presentation on Arctic Battle Symposium,* Delft University of Technology, Netherlands,

[38] Daley, C. and Riska, K., 1995, "Conceptual Framework for an Ice Load Model", *Report Prepared for National Energy Board*, Calgary, Alberta, http://www.engr.mun.ca/~cdaley/Documents/concept2.pdf.

[39] Lau, M., 2006, "Discrete Element Modeling of Ship Maneuvering In Ice", *Proceedings of the 18th IAHR International Symposium on Ice*, Sapporo, Japan.

[40] Phillips, L. D., 1994, "Simulation of Ship-Ice Collision Dynamics", *Ph.D. Thesis,* Carleton Institute for Civil Engineering, Ottawa, Canada.

[41] Johnes, S. J., 2004, "Ships in Ice - A Review", *25th Symposium on Naval Hydrodynamics*, St. John's, NL, Canada.

[42] Runeberg, R., 1888/89, "On Steamers for Winter Navigation and Ice-breaking", *Proceeding of Institution of Civil Engineers*, Vol. 97, Pt. III, p. 277-301.

[43] Lewis, J. W. and Edwards, R. Y. J., 1970, "Methods for Predicting Icebreaking and Ice Resistance Characteristics of Icebreakers", *Trans. of Society of Naval Architects and Marine Engineers*, Vol.78, p. 213-249.

[44] White, R. M., 1970, "Prediction of Icebreaker Capability", *Trans. of The Royal Institution of Naval Architects (RINA),* Vol. 112, No. 2, p. 225-251.

[45] Milano, V. R, 1973, "Ship Resistance to Continuous Motion in Ice", *Trans. of Society of Naval Architects and Marine Engineers,* Vol.81.

[46] Kheisin, D. E., Likhomanov, V. A. and Kurdyumov, V. A., 1975, "Determination of Specific Breakup Energy and Contact Pressures Produced by the Impact of a Solid against Ice", *Symp. on Physical Methods in Studying Snow and Ice*, Leningrad, CRREL Translation TL539.

[47] Varsta, P., 1983, "On the Mechanics of Ice Load on Ships in level ice in the Baltic Sea", *PhD Thesis*, Technical Research Centre of Finland, Espoo, Finland.

[48] Valanto, P., 2001, "The Resistance of Ships in Level Ice", *Trans. of Society of Naval Architects and Marine Engineers*, Vol.109, p. 53-83.

[49] Liu, J., Lau, M. and Williams, F. M., 2006, "Mathematical Modeling of Ice-Hull Interaction for Ship Maneuvering in Ice Simulations", *International Conference and Exhibition on Performance of Ships and Structures in Ice*, Alberta, Canada, ICETECH06-126-RF.

[50] Daley, C., 1999, "Energy Based Ice Collision Forces," *Proceedings of the 15th International Conference on Port and Ocean Engineering under Arctic Conditions*, Helsinki University of Technology in Espoo, Finland.

[51] Kerr, A. D., 1976, "The Bearing Capacity of Floating Ice Plates Subjected to Static or Quasi-Static Loads", *Journal of Glaciology*, Vol. 17, No. 76.

[52] Zhou, L., Su, B., Riska, K., and Moan, T., 2011, "Numerical Simulation of Moored Ship in Level Ice", *Proceedings of the ASME 2011 30th International Conference on Ocean, Offshore and Arctic Engineering*, Rotterdam, Netherlands, OMAE2011-49115.

[53] Sawamura, J., Tsuchiya, H., Tachibana, T., and Osawa, N., 2010, "Numerical Modeling for Ship Maneuvering in Level Ice", *Proceedings of the 20th IAHR International Symposium on Ice*. Lahti, Finland.

[54] Ehlers, S., and Kujala, P., 2013, "Optimization-Based Material Parameter Identification for the Numerical Simulation of Sea Ice in Four-Point Bending," *Journal of Engineering for the Maritime Environment*, 0(0) 1-11.

[55] Pernas-Sanchez, J., Pedroche, D.A., Varas, D., Lopez-Puente, J. L., and Zaera, R., 2012, "Numerical Modeling of Ice Behavior under High Velocity Impacts", *Department of Continuum Mechanics and Structural Analysis,* Universidad Carlos III de Madrid, Madrid, Spain.

[56] Zong, R., 2012, "Finite Element Analysis of Ship-Ice Collision using LS-Dyna," *M. Eng. Thesis*, Memorial University of Newfoundland, St. John's, NL, Canada.

[57] Daiyan, H., and Sand, B., 2011, "Numerical Simulation of the Ice-Structure Interaction in LS-Dyna", *Proceedings of 8th European LS-DYNA Users Conference,* Strasbourg.

[58] Carney, K. S., Benson, D. J., DuBois, P., and Lee, R., 2006, "A Phenomenological High Strain Rate Model with Failure for Ice", *International Journal of Solids and Structures*, 43 (2006) 7820-7839, 2006.

[59] Gürtner, A., Bjerkas, M., Kuhnlein, W., Jochmann, P. and Konuk, I., 2009, "Numerical Simulation of Ice Action to A Lighthouse", *Proceedings of the ASME 2009 28th International Conference on Ocean, Offshore and Arctic Engineering*, Honolulu, Hawaii, OMAE2009-80164.

[60] Nevel, D. E., 1961, "The Narrow Free Infinite Wedge on Elastic Foundation", *U.S. Army Cold Regions Research and Engineering Laboratory*, Research Report 79, 24 pp.

[61] Shunying, J., Zilin, L., Chunhua, L. and Jie, S., 2013, "Discrete Element Modeling of Ice Loads on Ship Hulls in Broken Ice Fields", *Acta Oceanologica Sinica*, 32(11): 50-58, doi: 10.1007/s13131-013-0377-2.

[62] Wang, B., Yu, H. and Basu, R., 2008, "Ship and Ice Collision Modeling and Strength Evaluation of LNG Ship Structure", *Proceedings of the ASME 2008 27th International Conference on Ocean, Offshore and Arctic Engineering*, Estoril, Portugal, OMAE2008-57134.

[63] Gagnon, R. E. and Wang, J., 2012, "Numerical Simulation of a Tanker Collision with a Bergy Bit Invorporating Hydrodynamics, a Validated Ice Model and Damage to the Vessel", *Journal of Cold Regions Science and Technology*, 81 (2012) 26-35.

[64] Kim, H., 2014, "Simulation of Compressive 'Cone-Shaped' Ice Specimen Experiments using LS-DYNA", *13th LS-DYNA® International Conference*, Michigan, USA.

[65] Das, J., Polic, D., Ehlers, S. and Amdahl, J., 2014, "Numerical Simulation of an Ice Beam in Four-Point Bending using SPH", *Proceedings of the ASME 2014 33rd International Conference on Ocean, Offshore and Arctic Engineering*, California, USA, OMAE2014-23228.

[66] LS-Dyna, 2011, www.lstc.com.

[67] Akerstrom, F. B. W. C., 2012, "Ice Class Requirements on Side Shell Structures-A Comparison of Local Strength Class Requirements Regarding Plastic Design of Ice-Reinforced Side Shell Structures", *M. Sc. Thesis*, Chalmers University of Technology, Gothenburg, Sweden.

[68] Daley, C., Kendrick, A. and Appolonov, E. M., 2001, "Ships, Plating and Framing Design in the Unified Requirements for Polar Class", *Port and Ocean Engineering Under Arctic Conditions*, POAC-01. Pp. 779-791.

[69] Daley, C., 2002, “Derivation of Plastic Framing Requirements for Polar Ships”, *Journal of Marine Structures,* 15 (2002) 543-559.

[70] CNIIMF, 2007, “Ice Certificate for 70000 Dwt Arctic Shuttle Tankers”, *Report Prepared for Central Marine Research and Design Institute,* Saint-Petersburg.

[71] Makinen, E., Alekseyev, J., Frankenstein, G., Kitagawa, H., Maksutov, D., Michailidis, M., Milano, R. and Schwarz, J., 1984, “Review of Research on Modeling in of Importance to the ITTC”, *Report prepared for ITTC*, pp. 592.

[72] IACS, 2011, “Requirements Concerning Polar Class”, *Report of International Association of Classification Societies*.

[73] Daley, C. G., 2002, “Application of Plastic Framing Requirements for Polar Ships”, *Journal of Marine Structures,* 15 (2002) 533-542.

[74] Popov, Y., Faddeyev, O., Kheisin, D. and Yalovlev, A., 1967, “Strength of Ships Sailing in Ice”, *Technical Translation*, Sudostroenie Publishing House, Leningrad, , U.S. Army Foreign Science and Technology Center, FSTC-HT-23-96-68.

APPENDIX

Appendix A: LS DYNA Keyword File for Material Models

(Geometric model files are not included due to large size)

A1: Keyword File for Ice Crushing Test

```
*KEYWORD

*TITLE
Ice Crushing Test for Ship Icebreaking Analysis

$=====================Model Geometry============================

*INCLUDE
geo.k

$=====================Execution Controls ========================

*CONTROL_TERMINATION
$  endtim    endcyc     dtmin    endeng    endmas
  3.000000         0     0.000     0.000     0.000

*CONTROL_TIMESTEP
$  dtinit    tssfac      isdo    tslimt     dt2ms      lctm     erode     ms1st
    0.000  0.600000         0     0.000     0.000         0         0         0
$  dt2msf   dt2mslc     imscl
    0.000         0         0

*CONTROL_ENERGY
$     hgen      rwen    slnten     rylen
        2         2         2         2

$=====================Output Controls============================

*DATABASE_BINARY_D3PLOT
$       dt      lcdt      beam     npltc    psetid
  0.010000         0         0         0         0

*DATABASE_BINARY_D3THDT
  0.01000

*DATABASE_BINARY_INTFOR
  0.01000
```

```
*DATABASE_RCFORC
$      dt    binary      lcur      ioopt
 0.010000         0         0         0

*DATABASE_NODOUT
  0.01000

*DATABASE_GLSTAT
  0.01000

*DATABASE_MATSUM
  0.01000

*DATABASE_EXTENT_BINARY
$    neiph     neips    maxint    strflg    sigflg    epsflg    rltflg    engflg
       0         0         3         1         0         0         0         0
$   cmpflg    ieverp    beamip     dcomp      shge     stssz    n3thdt   ialemat
       0         0         0         0         0         0         0         0
$  nintsld   pkp_sen      sclp    unused     msscl     therm    iniout    iniout
       0         0     0.000         0         0         0

$======================Part Id, Section Id, Mat Id======================

*PART

P1 - Indenter
$      pid     secid       mid     eosid      hgid      grav    adpopt      tmid
         1         1         1         0         0         0         0         0

P2 – Ice Wedge
$      pid     secid       mid     eosid      hgid      grav    adpopt      tmid
         2         2         2         0         0         0         0         0

*SECTION_SHELL
$    secid    elform      shrf       nip     propt   qr/irid     icomp     setyp
         1         2    0.8330       2.0       1.0       0.0         1
$       t1        t2        t3        t4      nloc     marea
    0.37    0.37    0.37    0.37      0.0

*SECTION_SOLID
$    secid    elform       aet
         2         1         0
```

```
*MAT_RIGID
$      mid        ro         e                 pr            n        couple       m     alias
         1   7850.000   2.000E+11   0.300000     0.000     0.000     0.000
$      cmo      con1      con2
     0.000         0         0
     0.000     0.000     0.000     0.000     0.000     0.000

*MAT_PLASTIC_KINEMATIC
$      mid       rho         e                 pr               sigy       etan        beta
         2             900.0    5.00E9          0.300000    4.50E6      0.000     0.000
$     src       srp        fs               vp
     0.000     0.000   1.000E-4     0.000

$=========================Contacts==============================

*CONTACT_AUTOMATIC_NODES_TO_SURFACE
$     ssid      msid     sstyp     mstyp    sboxid    mboxid       spr       mpr
         1         2         3         3         0         0         1         1
$       fs        fd        dc        vc       vdc    penchk        bt        dt

$      sfs       sfm       sst       mst      sfst      sfmt       fsf       vsf

$================BC, IC, Body Loads and Force Field====================

*BOUNDARY_PRESCRIBED_MOTION_RIGID
$     pid       dof       vad      lcid        sf       vid     death     birth
         2         2         0         1             1.000000

*BOUNDARY_SPC_SET
$#    nsid       cid      dofx      dofy      dofz     dofrx     dofry     dofrz
         1         0         1         0         1         1         1         1

*DEFINE_CURVE
$     lcid      sidr       sfa       sfo      offa      offo    dattyp
         1
$                a1                o1
             0.000            0.5000
       100.00000            0.5000
$============================================================

*END
```

A2: Keyword File for Four Point Bending Test

```
*KEYWORD

*TITLE
Four Point Bending Test for Ship Icebreaking Analysis

$=====================Model Geometry============================

*INCLUDE
geo.k

$=====================Execution Controls ========================

*CONTROL_TERMINATION
$  endtim    endcyc     dtmin    endeng    endmas
  10.000000         0     0.000     0.000     0.000

*CONTROL_TIMESTEP
$  dtinit    tssfac      isdo    tslimt     dt2ms      lctm     erode     ms1st
    0.000  0.600000         0     0.000     0.000         0         0         0
$  dt2msf   dt2mslc     imscl
    0.000         0         0

*CONTROL_ENERGY
$     hgen      rwen    slnten     rylen
        2         2         2         2

$=====================Output Controls============================

*DATABASE_BINARY_D3PLOT
$       dt      lcdt      beam     npltc    psetid
  0.010000         0         0         0         0

*DATABASE_BINARY_D3THDT
   0.01000

*DATABASE_BINARY_INTFOR
   0.01000

*DATABASE_RCFORC
$       dt    binary      lcur     ioopt
  0.010000         0         0         0
```

```
*DATABASE_NODOUT
  0.01000

*DATABASE_GLSTAT
  0.01000

*DATABASE_MATSUM
  0.01000

*DATABASE_EXTENT_BINARY
$    neiph     neips    maxint    strflg    sigflg    epsflg    rltflg    engflg
         0         0         3         1         0         0         0         0
$   cmpflg    ieverp    beamip     dcomp      shge     stssz    n3thdt   ialemat
         0         0         0         0         0         0         0         0
$  nintsld   pkp_sen      sclp    unused     msscl     therm    iniout    iniout
         0         0     0.000         0         0         0

$======================Part Id, Section Id, Mat Id=======================
*PART

P1 – Upper Support
$      pid     secid       mid     eosid      hgid      grav    adpopt      tmid
         1         1         1         0         0         0         0         0

P2 – Lower Support
$      pid     secid       mid     eosid      hgid      grav    adpopt      tmid
         2         1         1         0         0         0         0         0

P3 – Ice Beam
$      pid     secid       mid     eosid      hgid      grav    adpopt      tmid
         3         2         2         0         0         0         0         0

*SECTION_SHELL
$    secid    elform      shrf       nip     propt   qr/irid     icomp     setyp
         1         2    0.8330       2.0       1.0       0.0         1
$       t1        t2        t3        t4      nloc     marea
    0.01    0.01    0.01    0.01     0.0

*SECTION_SOLID
$    secid    elform       aet
         2         1         0
```

```
*MAT_RIGID
$     mid        ro         e                pr           n        couple      m     alias
          1   7850.000   2.000E+11   0.300000     0.000     0.000     0.000
$     cmo      con1      con2
    0.000         0         0
    0.000     0.000     0.000     0.000     0.000     0.000

*MAT_PLASTICITY_COMPRESSION_TENSION
$     mid        ro               e                pr             c         p          fail          tdel
          2          900.000   5.0000E+9   0.300000     0.000     0.000   7.0000E-4     0.000
$   lcidc     lcidt     lcsrc     lcsrt    srflag    lcfail        ec      rpct
          1         2         3         0     0.000         0     0.000     0.000
$     pc               pt             pcutc          pcutt          pcutf
          0.0           0.00              0.00           0.00           0.00
$      k
    0.00

$=========================Contacts================================

*CONTACT_AUTOMATIC_NODES_TO_SURFACE
$     ssid      msid     sstyp     mstyp    sboxid    mboxid       spr       mpr
          3         1         3                 3         0         0         1         1
$       fs        fd        dc        vc       vdc    penchk        bt        dt

$      sfs       sfm       sst       mst      sfst      sfmt       fsf       vsf

*CONTACT_AUTOMATIC_NODES_TO_SURFACE
$     ssid      msid     sstyp     mstyp    sboxid    mboxid       spr       mpr
          3         2         3                 3         0         0         1         1
$       fs        fd        dc        vc       vdc    penchk        bt        dt

$      sfs       sfm       sst       mst      sfst      sfmt       fsf       vsf


$================BC, IC, Body Loads and Force Field====================

*BOUNDARY_PRESCRIBED_MOTION_RIGID
$     pid       dof       vad      lcid        sf       vid     death     birth
          2         3         0         4                1.000000

*BOUNDARY_SPC_SET
$    nsid       cid      dofx      dofy      dofz     dofrx     dofry     dofrz
          1         0                 1         1         1         1          1         1

*BOUNDARY_SPC_SET
```

```
$   nsid       cid      dofx      dofy      dofz     dofrx     dofry     dofrz
         2         0                 1         1         0         1          1         1

*DEFINE_CURVE
$    lcid      sidr       sfa       sfo      offa      offo    dattyp
         1
$                a1                  o1
              0.000                5.8e6
              1.00000              1.15e7

*DEFINE_CURVE
$    lcid      sidr       sfa       sfo      offa      offo    dattyp
         2
$                a1                  o1
              0.000              5.8e5
            2.00000            1.258e7

*DEFINE_CURVE
$    lcid      sidr       sfa       sfo      offa      offo    dattyp
         3
$                a1                  o1
             10e-9              0.2700
              10e-8              0.3360
             10e-7              0.41700
              10e-6              0.520
             10e-5              0.643
              10e-4              0.8000
             10e-3              1.0000
              10e-2              1.2200
              10e-1              1.520
             1.00              1.8900
              10.0              2.348
             100              2.91
              1000              3.620

*DEFINE_CURVE
$    lcid      sidr       sfa       sfo      offa      offo    dattyp
         4
$                a1                  o1
              0.000              0.0010
           100.00000              0.0010
$=============================================================

*END
```

A3: Keyword File for Water Foundation test

```
*KEYWORD

*TITLE
Water Foundation Test for Ship Icebreaking Analysis

$=====================Model Geometry============================

*INCLUDE
geo.k

$=====================Execution Controls ========================

*CONTROL_TERMINATION
$  endtim    endcyc     dtmin    endeng    endmas
  20.000000         0     0.000     0.000     0.000

*CONTROL_TIMESTEP
$  dtinit    tssfac      isdo    tslimt     dt2ms      lctm     erode     ms1st
     0.000  0.600000         0     0.000     0.000         0         0         0
$  dt2msf   dt2mslc     imscl
     0.000         0         0

*CONTROL_ENERGY
$     hgen      rwen    slnten     rylen
        2         2         2         2

$=====================Output Controls============================

*DATABASE_BINARY_D3PLOT
$       dt      lcdt      beam     npltc    psetid
  0.010000         0         0         0         0

*DATABASE_BINARY_D3THDT
   0.01000

*DATABASE_BINARY_INTFOR
   0.01000

*DATABASE_RCFORC
$       dt    binary      lcur     ioopt
  0.010000         0         0         0
```

```
*DATABASE_NODOUT
  0.01000

*DATABASE_GLSTAT
  0.01000

*DATABASE_MATSUM
  0.01000

*DATABASE_EXTENT_BINARY
$    neiph     neips    maxint    strflg    sigflg    epsflg    rltflg    engflg
         0         0         3         1         0         0         0         0
$   cmpflg    ieverp    beamip     dcomp      shge     stssz    n3thdt   ialemat
         0         0         0         0         0         0         0         0
$  nintsld   pkp_sen      sclp    unused     msscl     therm    iniout    iniout
         0         0     0.000         0         0         0

$======================Part Id, Section Id, Mat Id=======================

*PART

P1 – Ice Wedge
$      pid     secid       mid     eosid      hgid      grav    adpopt      tmid
         1         1         1         0         0         0         0         0

P2 – Water Foundation
$      pid     secid       mid     eosid      hgid      grav    adpopt      tmid
         2         1         2         0         0         0         0         0

*SECTION_SOLID
$    secid    elform       aet
         1         1         0

*MAT_RIGID
$      mid        ro         e                pr         n       couple       m     alias
         1  7850.000   2.000E+11  0.300000     0.000     0.000     0.000
$      cmo      con1      con2
     0.000         0         0
     0.000     0.000     0.000     0.000     0.000     0.000


*MAT_ELASTIC
$      mid       rho         e                 pr        da                db        k
         2    1000.0    1.363E4             0.000     0.000     0.000         0.000
```

```
$=========================Contacts==============================

*CONTACT_CONSTRAINT_NODES_TO_SURFACE
$     ssid      msid     sstyp     mstyp    sboxid    mboxid      spr      mpr
         2         1         3         3                 0         0          0         0
$       fs        fd        dc        vc       vdc    penchk        bt        dt

$      sfs       sfm       sst       mst      sfst      sfmt       fsf       vsf

*CONTACT_FORCE_TRANSDUCER_CONSTRAINT
$     ssid      msid     sstyp     mstyp    sboxid    mboxid      spr      mpr
         1         0         3         3                 0         0          0         0
$       fs        fd        dc        vc       vdc    penchk        bt        dt

$      sfs       sfm       sst       mst      sfst      sfmt       fsf       vsf


$================BC, IC, Body Loads and Force Field====================

*BOUNDARY_PRESCRIBED_MOTION_RIGID
$     pid       dof       vad      lcid        sf       vid     death     birth
         1         3         0         1             1.000000

*BOUNDARY_SPC_SET
$    nsid       cid      dofx      dofy      dofz     dofrx     dofry     dofrz
         1         0         1         1         1         1                 1         1

*BOUNDARY_SPC_SET
$    nsid       cid      dofx      dofy      dofz     dofrx     dofry     dofrz
         2         0         1         1         0         1                 1         1

*DEFINE_CURVE
$     lcid      sidr       sfa       sfo      offa      offo    dattyp
         1
$               a1                o1
             0.000            0.0100
          100.00000           0.0100
$===============================================================

*END
```

Appendix B: LS DYNA Keyword File of Ship Ice Wedge Breaking

(Geometric model files are not included due to large size)

```
*KEYWORD

*TITLE
Simple Ship Ice Wedge Breaking Analysis

$=====================Model Geometry=============================

*INCLUDE
geo.k

$=====================Execution Controls ==========================

*CONTROL_TERMINATION
$   endtim    endcyc     dtmin    endeng    endmas
  10.000000         0     0.000     0.000     0.000

*CONTROL_TIMESTEP
$   dtinit    tssfac      isdo    tslimt     dt2ms      lctm     erode     ms1st
    0.000  0.600000         0     0.000     0.000         0         0         0
$   dt2msf   dt2mslc     imscl
    0.000         0         0

*CONTROL_ENERGY
$     hgen      rwen    slnten     rylen
        2         2         2         2

$=====================Output Controls============================

*DATABASE_BINARY_D3PLOT
$       dt      lcdt      beam     npltc    psetid
  0.010000         0         0         0         0

*DATABASE_BINARY_D3THDT
  0.01000

*DATABASE_BINARY_INTFOR
  0.01000
```

```
*DATABASE_RCFORC
$      dt    binary      lcur      ioopt
 0.010000         0         0         0

*DATABASE_NODOUT
  0.01000

*DATABASE_GLSTAT
  0.01000

*DATABASE_MATSUM
  0.01000

*DATABASE_EXTENT_BINARY
$    neiph     neips    maxint    strflg    sigflg    epsflg    rltflg    engflg
         0         0         3         1         0         0         0         0
$   cmpflg    ieverp    beamip     dcomp      shge     stssz    n3thdt   ialemat
         0         0         0         0         0         0         0         0
$  nintsld   pkp_sen      sclp    unused     msscl     therm    iniout    iniout
         0         0     0.000         0         0         0

$======================Part Id, Section Id, Mat Id=======================
*PART

P1 – Ship
$      pid     secid       mid     eosid      hgid      grav    adpopt      tmid
         1         1         1         0         0         0         0                 0

P2 – Ice Crushing Edge
$      pid     secid       mid     eosid      hgid      grav    adpopt      tmid
         2         2         2         0            0         0         0                 0

P3 – Ice Bending Zone
$      pid     secid       mid     eosid      hgid      grav    adpopt      tmid
         3         2             3         0          0         0         0                 0

P4 – Water Foundation
$      pid     secid       mid     eosid      hgid      grav    adpopt      tmid
         4         2         4          0          0         0       0           0

*SECTION_SHELL
$    secid    elform      shrf       nip     propt   qr/irid     icomp     setyp
         1         2            0.8330       2.0       1.0       0.0         0             1
$       t1        t2        t3        t4      nloc     marea
```

```
   0.37    0.37    0.37    0.37      0.0

*SECTION_SOLID
$    secid    elform       aet
         2         1         0

*MAT_RIGID
$      mid        ro         e                pr            n       couple       m     alias
         1   7850.000   2.000E+11   0.300000     0.000     0.000     0.000
$      cmo      con1      con2
     0.000         0         0
     0.000     0.000     0.000     0.000     0.000     0.000

*MAT_PLASTIC_KINEMATIC
$      mid       rho         e        pr                  sigy       etan      beta
         2     900.0    5.00E9        0.300000    4.50E6      0.000     0.000
$     src       srp                   fs          vp
     0.000     0.000       1.000E-4     0.000

*MAT_PLASTICITY_COMPRESSION_TENSION
$     mid        ro              e               pr            c         p          fail          tdel
         3          900.000   5.0000E+9   0.300000     0.000     0.000   7.0000E-4     0.000
$   lcidc     lcidt     lcsrc     lcsrt    srflag    lcfail        ec       rpct
         1         2         3         0     0.000         0     0.000     0.000
$      pc               pt             pcutc          pcutt          pcutf
          0.0           0.00              0.00           0.00           0.00
$      k
     0.00

*MAT_ELASTIC
$      mid       rho         e                 pr          da              db        k
         4     1000.0     1.363E4           0.000      0.000      0.000         0.000

$=========================Contacts==============================

*CONTACT_AUTOMATIC_NODES_TO_SURFACE
$     ssid      msid     sstyp     mstyp    sboxid    mboxid       spr       mpr
         2         1         3                3         0                 0           0         0
$       fs        fd        dc        vc       vdc    penchk        bt        dt

$      sfs       sfm       sst       mst      sfst      sfmt       fsf       vsf

*CONTACT_CONSTRAINT_NODES_TO_SURFACE
$     ssid      msid     sstyp     mstyp    sboxid    mboxid       spr       mpr
```

```
      4       3              3       3       0              0          0       0
$     fs      fd      dc      vc      vdc   penchk      bt      dt

$     sfs     sfm     sst     mst     sfst    sfmt     fsf     vsf

*CONTACT_CONSTRAINT_NODES_TO_SURFACE
$    ssid    msid    sstyp   mstyp   sboxid  mboxid     spr     mpr
      4       2              3       3       0              0          0       0
$     fs      fd      dc      vc      vdc   penchk      bt      dt

$     sfs     sfm     sst     mst     sfst    sfmt     fsf     vsf


$===============BC, IC, Body Loads and Force Field===================

*BOUNDARY_PRESCRIBED_MOTION_RIGID
$    pid     dof     vad     lcid      sf      vid    death    birth
       1       2       0       4            1.000000

*BOUNDARY_SPC_SET
$   nsid     cid    dofx    dofy    dofz   dofrx   dofry   dofrz
       1       0              1       1       1       1          1       1

*BOUNDARY_SPC_SET
$   nsid     cid    dofx    dofy    dofz   dofrx   dofry   dofrz
       2       0              1       0       1       1          1       1

*DEFINE_CURVE
$    lcid     sidr      sfa      sfo     offa     offo    dattyp
       1
$              a1               o1
           0.000            5.8e6
          1.00000           1.15e7

*DEFINE_CURVE
$    lcid     sidr      sfa      sfo     offa     offo    dattyp
       2
$              a1               o1
           0.000            5.8e5
         2.00000          1.258e7

*DEFINE_CURVE
$    lcid     sidr      sfa      sfo     offa     offo    dattyp
       3
$              a1               o1
```

```
            10e-9           0.2700
             10e-8           0.3360
            10e-7           0.41700
             10e-6           0.520
            10e-5           0.643
             10e-4           0.8000
            10e-3           1.0000
             10e-2           1.2200
             10e-1           1.520
            1.00           1.8900
             10.0           2.348
            100           2.91
             1000           3.620

*DEFINE_CURVE
$    lcid      sidr       sfa       sfo      offa      offo    dattyp
         4
$               a1                 o1
             0.000              1.00
           1.00000              1.00

$=============================================================

*END
```

Appendix C: Data Sheet for Load Parameters, and Plating-Framing Particulars

C1: Spread Sheet Data for Load Parameters, and Plating-Framing Particulars (PC 5)

Vessel Particulars

			1
Item	Units	**Var**	**Value**
PC Class		Class	PC 5
Displacement	kt	Disp	50.0
Displacement Class Factor		Cfdis	70.00
Crushing Failure Class Factor		CFc	3.100
Flexural Failure Class Factor		CFf	9.000
		CFd	1.310
Load Patch Dimensions Class Factor		CFb	4.600

Offered Frame Data

Item	Units	**Var**	bow rule frame
Case Frame Number	--	FrameNum	any
Case Frame Description	--	FrameRef	F 380 x 27
Hull Region	--	HA	Bi
Hull Family	--	HF	1
Frame Orientation Angle (to waterline)	deg	OA	90°
Frame Orientation Type	--	FO	Transverse
Protective Hull Coating Used?	yes/no	Coating?	Yes
Bottom Longitudinals?	yes/no	BotLongs?	No
Load Distributing Stringers?	yes/no	LDString?	No
Water Density	t/m3	rhow	1.025
Frame Attachment Parameter	--	j	2
Yield Strength - Framing Material	MPa	Fy_f	235
Yield Strength - Plating Material	MPa	Fy_p	235
Young's Modulus of Plating Material	MPa	E_plate	207000
Main Frame Span (=web frame spacing for long'l)	mm	a	2000
Main Frame Spacing	mm	s	350
Thickness of Plate (gross)	mm	tp	28.00
Height of Web	mm	hw	380.00
Thickness of Web (gross)	mm	tw	27.00
Angle of web	deg	fiw	90.00
Width of Flange	mm	wf	0.00
Thickness of Flange (gross)	mm	tf	0.00
Flange Offset Distance	mm	bw	0

Assesment Results for Offered Frames (net)

Web Buckling Constant	--	wbc	215.8
Frame Stability Check (12.9.1)	--	frstab	**OK**
Web Thickness Min (12.9.3)	--	webmin	**OK**
Dist. to Plastc NA	mm	zna	8.5
Shell Plate Thickness - offered (net)	mm	tp	25.5
required value (12.4.2) (excl CA)	mm	t_reqd	25.1
			OK
Frame Shear Area - offered (12.5.7) (net)	cm2	Aw	98.8
required value (12.6.2 or)	cm2	At or AL	69.7
			OK
Frame Modulus - offered (12.5.8) (net)	cm3	Zp	1984.7
required value (12.6.3 or)	cm3	Zpt or ZpL	1926.3
			OK

Load Parameters

Force	MN	F	14.482
Aspect Ratio		AR	5.369
Line Load	MN/m	Q	3.723
Pressure	MPa	P	5.139
Ice Load Patch Width	m	w	3.890
Ice Load Patch Height	m	b	0.724
Average Patch Pressure	MPa	Pavg	5.139
Hull Area Factor		AF	1
Corrosion and Abrasion Allowance	mm	t_wear	2.5

Transverse Plating

Peak Pressure Factor - Plate (trans)	-	PPFpt	1.45
height of design load patch	m	bpt	0.724
Plate Thickness Required to Resist Ice Load	mm	t_net	25.1
Required Minimum Shell Plate Thickness	mm	t_min	27.599

Transverse Framing

Peak Pressure Factor - Transverse Frame	-	PPFt	1.45
Length of Loaded Portion of Span	m	LL	0.724
Required Shear Area of Transverse Frame	cm2	At	69.7
Ratio of Minimum Shear Area / Fitted Shear Area		a_1	0.705
Load Length Parameter	-	Y	0.819
Shear Parameter	-	kw	1.000
Width of Plating Acting Effectively With Frame	mm	beff	175
Sum of Plastic Moduli of Flange and Plate	cm3	z_p	34.3
Shear Parameter	-	kz	0.0173
Interaction Eq For 3H Mechanism (Sym Load)	-	A1A	0.585
Interaction Eq For Shear Mechanism (Asym Load)	-	A1B	0.374
Interaction parameter	-	A1_	0.585
Required Plastic Section Modulus of Transverse Frame	cm3	Zpt	1926.3

Longitudinal Plating (b>=s)

Peak Pressure Factor - Plate (longl)	-	PPFpl	1.78
Plate Thickness Required to Resist Ice Load	mm	t_net	31.7
Required Minimum Shell Plate Thickness	mm	t_min	34.2

Longitudinal Plating (b<s)

Plate Thickness Required to Resist Ice Load	mm	t_net	#NUM!
Required Minimum Shell Plate Thickness	mm	t_min	#NUM!

Longitudinal Framing

Peak Pressure Factor - Transverse Frame	-	PPFs	1
Length of Loaded Portion of Span	m	b_1	0.299
load height parameter	-	ko	0.855
load height parameter	m	b_2	0.350
load height parameter	-	bpri	2.070
Required Shear Area of Longitudinal Frame	cm2	AL	113.4
Ratio of Minimum Shear Area / Fitted Shear Area		a_4	1.148
Shear Parameter	-	kwl	1.000
Interaction Eq For 3H Mechanism (Sym Load)	-	A4_	1.000
Required Plastic Section Modulus of Longitudinal Frame	cm3	ZpL	3272275.4

Required Plating

ratio		angFac	0.00
Plate Thickness Required to Resist Ice Load	mm	t_reqd	25.1
Required Minimum Shell Plate Thickness	mm	t_min	27.6

Required Framing

Required Shear Area of Between Frame	cm2	A_reqd	69.7
Required Plastic Section Modulus of Longitudinal Frame	cm3	Z_reqd	1926.3

Required Web Frames

Required Shear Area of Between Frame	mm2	A_reqd	28830.1
Required Plastic Section Modulus of Longitudinal Frame	mm3	Z_reqd	10,350,646

C2: Spread Sheet Data for Load Parameters, and Plating-Framing Particulars (PC 6)

Vessel Particulars

1

Item	Units	Var	Value
PC Class		Class	PC 6
Displacement	kt	Disp	50.0
Displacement Class Factor		Cfdis	40.00
Crushing Failure Class Factor		CFc	2.400
Flexural Failure Class Factor		CFf	5.490
		CFd	1.170
Load Patch Dimensions Class Factor		CFb	3.400

Offered Frame Data

Item	Units	Var	bow rule frame
Case Frame Number	--	FrameNum	any
Case Frame Description	--	FrameRef	F 320 x 24
Hull Region	--	HA	Bi
Hull Family	--	HF	1
Frame Orientation Angle (to waterline)	deg	OA	90°
Frame Orientation Type	--	FO	Transverse
Protective Hull Coating Used?	yes/no	Coating?	Yes
Bottom Longitudinals?	yes/no	BotLongs?	No
Load Distributing Stringers?	yes/no	LDString?	No
Water Density	t/m3	rhow	1.025
Frame Attachment Parameter	--	j	2
Yield Strength - Framing Material	MPa	Fy_f	235
Yield Strength - Plating Material	MPa	Fy_p	235
Young's Modulus of Plating Material	MPa	E_plate	207000
Main Frame Span (=web frame spacing for long'l)	mm	a	2000
Main Frame Spacing	mm	s	350
Thickness of Plate (gross)	mm	tp	23.50
Height of Web	mm	hw	320.00
Thickness of Web (gross)	mm	tw	25.00
Angle of web	deg	fiw	90.00
Width of Flange	mm	wf	0.00
Thickness of Flange (gross)	mm	tf	0.00
Flange Offset Distance	mm	bw	0

Assesment Results for Offered Frames (net)

Web Buckling Constant	--	wbc	196.2
Frame Stability Check (12.9.1)	--	frstab	**OK**
Web Thickness Min (12.9.3)	--	webmin	**OK**
Dist. to Plastc NA	mm	zna	0.0
Shell Plate Thickness - offered (net)	mm	tp	21.5
required value (12.4.2) (excl CA)	mm	t_reqd	21.1

			OK
Frame Shear Area - offered (12.5.7) (net)	cm2	Aw	76.8
required value (12.6.2 or)	cm2	At or AL	47.8
			OK
Frame Modulus - offered (12.5.8) (net)	cm3	Zp	1309.7
required value (12.6.3 or)	cm3	Zpt or ZpL	1280.9
			OK

Load Parameters

Force	MN	F	9.372
Aspect Ratio		AR	5.369
Line Load	MN/m	Q	2.552
Pressure	MPa	P	3.730
Ice Load Patch Width	m	w	3.673
Ice Load Patch Height	m	b	0.684
Average Patch Pressure	MPa	Pavg	3.730
Hull Area Factor		AF	1
Corrosion and Abrasion Allowance	mm	t_wear	2

Transverse Plating

Peak Pressure Factor - Plate (trans)	-	PPFpt	1.45
height of design load patch	m	bpt	0.684
Plate Thickness Required to Resist Ice Load	mm	t_net	21.1
Required Minimum Shell Plate Thickness	mm	t_min	23.141

Transverse Framing

Peak Pressure Factor - Transverse Frame	-	PPFt	1.45
Length of Loaded Portion of Span	m	LL	0.684
Required Shear Area of Transverse Frame	cm2	At	47.8
Ratio of Minimum Shear Area / Fitted Shear Area		a_1	0.622
Load Length Parameter	-	Y	0.829
Shear Parameter	-	kw	1.000
Width of Plating Acting Effectively With Frame	mm	beff	175
Sum of Plastic Moduli of Flange and Plate	cm3	z_p	24.2
Shear Parameter	-	kz	0.0184
Interaction Eq For 3H Mechanism (Sym Load)	-	A1A	0.561
Interaction Eq For Shear Mechanism (Asym Load)	-	A1B	0.082
Interaction parameter	-	A1_	0.561
Required Plastic Section Modulus of Transverse Frame	cm3	Zpt	1280.9

Longitudinal Plating (b>=s)

Peak Pressure Factor - Plate (longl)	-	PPFpl	1.78
Plate Thickness Required to Resist Ice Load	mm	t_net	27.0
Required Minimum Shell Plate Thickness	mm	t_min	29.0

Longitudinal Plating (b<s)

Plate Thickness Required to Resist Ice Load	mm	t_net	8.8
Required Minimum Shell Plate Thickness	mm	t_min	10.8

Longitudinal Framing

Peak Pressure Factor - Transverse Frame	-	PPFs	1
Length of Loaded Portion of Span	m	b_1	0.296
load height parameter	-	ko	0.847
load height parameter	m	b_2	0.350
load height parameter	-	bpri	1.954
Required Shear Area of Longitudinal Frame	cm2	AL	81.5
Ratio of Minimum Shear Area / Fitted Shear Area		a_4	1.061
Shear Parameter	-	kwl	1.000
Interaction Eq For 3H Mechanism (Sym Load)	-	A4_	1.000
Required Plastic Section Modulus of Longitudinal Frame	cm3	ZpL	2350144.5

Required Plating

ratio		angFac	0.00
Plate Thickness Required to Resist Ice Load	mm	t_reqd	21.1
Required Minimum Shell Plate Thickness	mm	t_min	23.1

Required Framing

Required Shear Area of Between Frame	cm2	A_reqd	47.8
Required Plastic Section Modulus of Longitudinal Frame	cm3	Z_reqd	1280.9

Required Web Frames

Required Shear Area of Between Frame	mm2	A_reqd	19759.0
Required Plastic Section Modulus of Longitudinal Frame	mm3	Z_reqd	7,093,915

C3: Spread Sheet Data for Load Parameters, and Plating-Framing Particulars (PC 7)

Vessel Particulars

Item	Units	Var	Value
PC Class		Class	PC 7
Displacement	kt	Disp	50.0
Displacement Class Factor		Cfdis	22.00
Crushing Failure Class Factor		CFc	1.800
Flexural Failure Class Factor		CFf	4.060
		CFd	1.110
Load Patch Dimensions Class Factor		CFb	2.600

Offered Frame Data

Item	Units	Var	bow rule frame
Case Frame Number	--	FrameNum	any
Case Frame Description	--	FrameRef	HP 320*16.0
Hull Region	--	HA	Bi
Hull Family	--	HF	1
Frame Orientation Angle (to waterline)	deg	OA	90°
Frame Orientation Type	--	FO	Transverse
Protective Hull Coating Used?	yes/no	Coating?	Yes
Bottom Longitudinals?	yes/no	BotLongs?	No
Load Distributing Stringers?	yes/no	LDString?	No
Water Density	t/m3	rhow	1.025
Frame Attachment Parameter	--	j	2
Yield Strength - Framing Material	MPa	Fy_f	235
Yield Strength - Plating Material	MPa	Fy_p	235
Young's Modulus of Plating Material	MPa	E_plate	207000
Main Frame Span (=web frame spacing for long'l)	mm	a	2000
Main Frame Spacing	mm	s	350
Thickness of Plate (gross)	mm	tp	21.50
Height of Web	mm	hw	285.96
Thickness of Web (gross)	mm	tw	16.00
Angle of web	deg	fiw	90.00
Width of Flange	mm	wf	62.00
Thickness of Flange (gross)	mm	tf	34.04
Flange Offset Distance	mm	bw	0

Assesment Results for Offered Frames (net)

Web Buckling Constant	--	wbc	274.0
Frame Stability Check (12.9.1)	--	frstab	**OK**
Web Thickness Min (12.9.3)	--	webmin	**OK**
Dist. to Plastc NA	mm	zna	0.0
Shell Plate Thickness - offered (net)	mm	tp	19.5
required value (12.4.2) (excl CA)	mm	t_reqd	19.1

			OK
Frame Shear Area - offered (12.5.7) (net)	cm2	Aw	48.0
required value (12.6.2 or)	cm2	At or AL	37.7
			OK
Frame Modulus - offered (12.5.8) (net)	cm3	Zp	1295.7
required value (12.6.3 or)	cm3	Zpt or ZpL	1102.0
			OK

Load Parameters

Force	MN	F	6.871
Aspect Ratio		AR	5.369
Line Load	MN/m	Q	2.013
Pressure	MPa	P	3.115
Ice Load Patch Width	m	w	3.413
Ice Load Patch Height	m	b	0.646
Average Patch Pressure	MPa	Pavg	3.115
Hull Area Factor		AF	1
Corrosion and Abrasion Allowance	mm	t_wear	2

Transverse Plating

Peak Pressure Factor - Plate (trans)	-	PPFpt	1.45
height of design load patch	m	bpt	0.646
Plate Thickness Required to Resist Ice Load	mm	t_net	19.1
Required Minimum Shell Plate Thickness	mm	t_min	21.091

Transverse Framing

Peak Pressure Factor - Transverse Frame	-	PPFt	1.45
Length of Loaded Portion of Span	m	LL	0.646
Required Shear Area of Transverse Frame	cm2	At	37.7
Ratio of Minimum Shear Area / Fitted Shear Area		a_1	0.785
Load Length Parameter	-	Y	0.838
Shear Parameter	-	kw	0.548
Width of Plating Acting Effectively With Frame	mm	beff	175
Sum of Plastic Moduli of Flange and Plate	cm3	z_p	38.2
Shear Parameter	-	kz	0.0295
Interaction Eq For 3H Mechanism (Sym Load)	-	A1A	0.558
Interaction Eq For Shear Mechanism (Asym Load)	-	A1B	0.605
Interaction parameter	-	A1_	0.605
Required Plastic Section Modulus of Transverse Frame	cm3	Zpt	1102.0

Longitudinal Plating (b>=s)

Peak Pressure Factor - Plate (longl)	-	PPFpl	1.78
Plate Thickness Required to Resist Ice Load	mm	t_net	24.7
Required Minimum Shell Plate Thickness	mm	t_min	26.7

Longitudinal Plating (b<s)

Plate Thickness Required to Resist Ice Load	mm	t_net	14.3
Required Minimum Shell Plate Thickness	mm	t_min	16.3

Longitudinal Framing

Peak Pressure Factor - Transverse Frame	-	PPFs	1

Length of Loaded Portion of Span	m	b_1	0.291
load height parameter	-	ko	0.838
load height parameter	m	b_2	0.348
load height parameter	-	bpri	1.846
Required Shear Area of Longitudinal Frame	cm2	AL	66.9
Ratio of Minimum Shear Area / Fitted Shear Area		a_4	1.395
Shear Parameter	-	kwl	0.548
Interaction Eq For 3H Mechanism (Sym Load)	-	A4_	0.689
Required Plastic Section Modulus of Longitudinal Frame	cm3	ZpL	1330202.4

Required Plating

ratio		angFac	0.00
Plate Thickness Required to Resist Ice Load	mm	t_reqd	19.1
Required Minimum Shell Plate Thickness	mm	t_min	21.1

Required Framing

Required Shear Area of Between Frame	cm2	A_reqd	37.7
Required Plastic Section Modulus of Longitudinal Frame	cm3	Z_reqd	1102.0

Required Web Frames

Required Shear Area of Between Frame	mm2	A_reqd	15588.4
Required Plastic Section Modulus of Longitudinal Frame	mm3	Z_reqd	5,596,592